THE LONG-TERM MORPHOLOGICAL DEVELOPMENT OF KAKINADA BAY

Submitted by

GARIMA SHARMA

13400131002

School of Naval Architecture and Ocean Engineering

in partial fulfillment of the requirements of the Degree of Doctor of Philosophy (Ph.D) to the

INDIAN MARITIME UNIVERSITY
CHENNAI 600119
FEBRUARY

2022

INDIAN MARITIME UNIVERSITY
(A Central University, Govt. of India)
East Coast Road, Uthandi, CHENNAI- 600 119

Research Guide's Name : Dr. K.M. Sivakholundu and Dr. K.V.K.R.K. Patnaik
Designation : Professor
Department : Naval Architecture and Ocean Engineering

CERTIFICATE

We certify that the thesis titled **The Long-Term Morphological Development of Kakinada Bay** submitted for the degree of Doctor of Philosophy (Ph.D) by **Mrs. Garima Sharma** (Registration Number: **13400131002**) is the record of research work carried out by her during the period from October 2013 to February 2022 under our guidance and supervision, and that this work has not formed the basis for the award of any degree, Diploma, Associateship, Fellowship or other titles in this university or any other university or institution of Higher Learning.

We are aware of and understand the University's policy on plagiarism and we certify that the thesis submitted by above mentioned Research Scholar is her own work, except where indicated by referencing, and has not been copied from other sources or been previously submitted for award or assessment. If plagiarism related to this thesis is proved, in future, we are aware that the University will initiate disciplinary action against us.

Signature of the Co-Guide

Dr. K.V.K.R.K. Patnaik
Indian Maritime University
Visakhapatnam Campus

Signature of the Guide

Dr. K.M. Sivakholundu
Professor
Indian Maritime University
HQ, Chennai

INDIAN MARITIME UNIVERSITY
(A Central University, Govt. of India)
East Coast Road, Uthandi, CHENNAI- 600 119

DECLARATION BY THE RESEARCH SCHOLAR

I declare that the thesis titled **The Long-Term Morphological Development of Kakinada Bay** submitted by me for the degree of Doctor of Philosophy (Ph.D) is the record of research work carried out by me during the period from October 2013 to February 2022 is work has not formed the basis for the award of any degree, Diploma, Associateship, Fellowship or other titles in this university or any other university or institution of Higher Learning.

I am aware of and understand the University's policy on plagiarism and I certify that the thesis submitted by me is my own work, except where indicated by referencing, and has not been copied from other sources or been previously submitted for award or assessment. If plagiarism related to this thesis is proved, in future, I am aware that the University will initiate disciplinary action against me.

Garima

Signature of the Research Scholar
Name: Garima Sharma
Registration Number: 13400131002

ii

ACKNOWLEDGEMENTS

I begin with thanking Almighty God for Thy Blessings I am submitting my thesis. I am extremely thankful to the esteemed Indian Maritime University for giving me opportunity to carry out the research work. I thank Honorable Vice Chancellor Dr. Malini V. Shankar for her kind grace.

I express my profound gratitude to my guide Dr. K.M. Sivakholundu for his constant guidance, direction, motivation, untiring patience and greatest support. I am extremely thankful to him for his crucial feedback and pushing me overcoming the limitations and work harder to the best of my ability. I thank him immensely for all his guidance, valuable time and support.

I extremely thank my co-guide Dr. K.V.K.R.K. Patnaik for being there in this long journey since the beginning. I profusely thank him for his guidance and encouragement towards the completion of my thesis. I thank him for all his support in data collection, arranging field works and making resources available throughout my work.

I immensely thank my Doctoral Committee members Dr. B.K. Jena, Scientist G, NIOT and Professor Dr K.V.S.R. Prasad, Andhra University for their valuable guidance, support and permission for utilization of resources in NIOT lab and Andhra University lab for carrying out my research work.

I wish to express my gratitude to the following institutions for their help, resources, data and analysis:

a) Indian Maritime University, Visakhapatnam & Chennai

b) Kakinada Seaports Limited, Kakinada

c) National Institute of Ocean Technology, Chennai

d) National Centre of Coastal Research, Chennai

e) Andhra University, Visakhapatnam

I enormously thank all the esteemed members of the Academics, Library, Finance, Maintenance, Personal and IT support system and students of IMU Visakhapatnam campus for their kind help and generous support which helped me complete my research work. I whole-heartedly thank Dr. S.C. Misra, Dr. Kesavadev V.K., Dr. Niranjan Kumar Injeti, Admiral Ravi Kiran, late Mr. U.S. Ramesh, Dr. B.V.R. Rao, Mr. Ramanmurty, Mr. Ramesh Kumar, late Mr. Attili Sheshagiri Rao, Dr. Aditya Mukherjee, late Mr. Ramchandra Murty, Mrs. Sitakumari, Dr. Padmashree, , Dr. Madhu Joshi, Dr. Sirisha, Dr. RRV Suresh, Mr. Pavan, Mr. Ratnakumar, Mrs. Muthuchelvi, Mr. Vidyasagar, Mr. Pradeep, Mrs. O. Laxmi, Mr. Avinash, Mr. Premchand, Dr. Ravichandran, Mr. Harikrishnan, Mr. Krishna Prasad, Mr. Sravanan, Mr. Akbar, Mr. Shyam, Mrs. Sujata and Mr. Jaswant for their immense help, support, guidance and encouragement.

I profusely thank IMU Headquarters and IMU Chennai campus for their kind support. I thank Dr. Rajoo Balaji, Director IMU Chennai campus for his crucial help during my work. I also thank Mr. S.V. Durga Prasad for his great help.

I immensely thank Captain Jacob Satya Raju, General Manager, Kakinada Seaports Limited, Kakinada and Mr. Vijay for being very kind and benevolent during field visits for data collection.

I am deeply grateful to Mr. Rajkumar and Dr. Karunakar Kintada, Scientists, NIOT for their crucial guidance, inputs and valuable time during my work. I profusely thank them and Mrs. Shanmuga Priyaa S, Scientists, NIOT for their time to time guidance and help.

I thank Dr. R.S. Kankara, Dr. Tune Usha, Dr. V. Ranga Rao, Dr. U.S. Panda, Dr. S.K. Dash, Dr. B. Charan Kumar, Dr. Selvan, Dr. Gopinath and Dr. M. Iyyappan, NCCR, Chennai for the coastal modeling training program.

I thank proficient professor late Dr. A.V. Raman, Andhra University, Visakhapatnam for giving opportunity to participate in the field trip, data collection and utilizing laboratory facilities. I thank Dr. S. Ramakrishna Rao, Vice-Chancellor, (Retd.), Krishna University, Machilipatnam for his valuable initial counseling and support. I thank Dr. Arunjith Avaneendran for his valuable help.

At last I express my gratitude to my family and friends who were my constant support system during my research period. I thank my parents, my late father-in-law, my mother-in-law, my husband, sister and sister-in-law for their help, love and moral support. I especially thank my mother-in-law for the care extended towards my daughter during my work. I am extremely thankful to my husband for his emotional and financial support during my research period.

I dedicate this work to my sweet little daughter Zishya.

ABSTRACT

The evolution of Kakinada Bay with Coringa Mangroves at its southern shore and Kakinada Spit and Hope Island at its eastern side has occurred over the past century. This morphological development of the bay is attributed to the biophysical interactions, hydrodynamic forcing like waves, winds, tides, currents and sediment dynamics occurring inside the bay. The processes governing the short-term (decadal) and long-term (century) morphology of the bay need to be studied to develop sustainable coastal management plan for the intermediate time-scale. This study is an effort to extend the use of process based models to longer time scales to provide better understanding of the morphological development by the action of various physical processes governing alone and in combination.

This study answers the question if these long-term morphological modeling can produce the reliable results by creating nexus of two techniques 'Remote Sensing and Numerical Modeling'. The numerical modeling hindcast results are validated using remote sensing images. This study quantifies the rate of change of the shoreline of the bay using remote sensing images in the Digital Shoreline Analysis System (DSAS). The trend of erosion and accretion occurring inside the bay was obtained using indices End Point Rate (EPR), Net Shoreline Movement (NSM) and Linear Regression Rate (LRR). The rate and trend of sedimentation and erosion obtained with the satellite imageries are further used to statistically compare the transect–wise hindcast and forecast results. Thus this study demonstrates the model's ability to reproduce the long-term morphodynamic development of the bay.

This study attempts to investigate the action of physical processes on the morphological changes of the bay over a period of 100 years. For long term morphological modeling various approaches are followed like Input Reduction, Model Reduction and Acceleration techniques. Input reduction

simulates the long term morphological modeling using schematized input data like morphological tide, schematized wave which are representative sets of the entire data. Model Reduction follows the approach of giving only the most important processes in the model input. Acceleration technique approach uses the morphological acceleration factor which accelerates the morphological development by the assigned factor. Available variants of the morphological predictions have been considered for the study.

The study attempts to answer the hypothesis made to choose the appropriate approach between the two statements issued by Lesser (2009) and Roelvink (1999). The approach for adopting model reduction following the correct use of acceleration techniques as stated by Lesser (2009): "In order to use a morphological acceleration technique in a coastal situation it is essential to identify which coastal processes play a significant role in (residual) sediment transport patterns over the space and time scales of interest". The second approach following the statement given by Roelvink (1999) and quoted by Dastgheib A. (2012) as: "If you put enough of the essential physics into the model, the most important features of the morphological behavior will come out, even at the longer time scales".

The exercise was varied with different environmental forcing with three scenarios: a) Tide only following Model Reduction, b) Tide and Wave Combined, c) Tide and Wave combined action with decadal MSL changes. The planimetric and decadal volumetric changes, shoreline changes have been compared for all the three scenarios. The outcome of the morphodynamic modeling from the different sets of physical processes will help to isolate the role of each physical process that are making difference in the overall morphological changes of the bay. It aims to isolate the effect of waves by comparing two simulations one with only tide and other with both wave and tidal forcing. The study with obtained forecast results will identify the areas under erosion and accretion and

quantify the rate of shoreline changes. These results can help further in taking steps for coastal management. Thus this study gives an exemplary integration of the available techniques that can be helpful for coastal development modeling.

TABLE OF CONTENTS

LIST OF TABLES

LIST OF FIGURES

LIST OF ABBREVIATIONS

EPR	End Point Rate
NSM	Net Shoreline Movement
LRR	Linear Regression Rate
RS	Remote Sensing
GIS	Geographical Information System
DSAS	Digital Shoreline Analysis System
BSS	Brier Skill Score
NM	Numerical Modeling
MSL	Mean Sea Level
NE	North-East
SW	South-West
GEBCO	The General Bathymetric Chart of the Oceans
DGPS	Differential Global Positioning System
SWAN	Simulating WAves Nearshore
MSS	Multi Spectral Scanner
TM	Thematic Mapper
ETM+	Enhanced Thematic Mapper Plus
P	Path
R	Row
LR	Linear Regression
AOR	Average of Rates
RMSE	Root Mean Square Error
UTM	Universal Transverse Mercator

NDVI	Normalized Difference Vegetation Index
WGS	World Geodetic System
CFL	Courant-Friedrichs-Levy
Morfac	Morphological Acceleration Factor
MCA	Multi-Criteria-Analysis
NS	Nash-Sutcliffe coefficient
IPCC	International Panel of Climate Change
AR6	6^{th} Assessment Report
SSPs	Socioeconomic Pathway Scenarios

LIST OF SYMBOLS

m	Meter
s	Second
h	Hour
Km	Kilometer
E_f	Energy Flux
C	Average sound speed
μm	Micrometer
D	Water Depth below plane of reference
C	Celsius
N	North
E	East
Ha	Hectare
Sq	Square
Cm	Centimeter
Z	Depth
T	Time
Deg	Degree
f	Coriolis Parameter
$F_{x,y}$	x and y component of external forces
N/m^2	Newton per meter square
U	depth averaged velocity in x direction
V	depth averaged velocity in y direction
ρ_w	mass density of water
v	diffusion coefficient (eddy viscosity)
η	water level variation above plane of reference
g	gravity of acceleration

$\tau_{bx,y}$	x and y component of bed shear stress
Ew	Short Wave Energy
Cg	Group Velocity
q	Incidence angle with respect to the x-axis
Dw	Wave Energy Dissipation
Ws	Settling velocity of the sediment
Dh	Horizontal Eddy Diffusivity
DV	Vertical Eddy Diffusivity
Er	Erosion Rate
Dr	Deposition Rate
M	Erosion Parameter
τ_b	Bed Shear Stress
τ_{cr}	Critical Bed Shear Stress
Cb	Near Bed Sediment concentration τcr,d
$\tau_{cr,d}$	Critical Bed Shear Stress for Deposition
E_t	Total Uncertainty
E_r	Rectification Error
E_p	Pixel Error
E_{td}	Tidal Error
S_{td}	Standard Deviation
$\tan_\alpha$	Section Slope of Transect
E_{avg}	Average Uncertainty
ρ	Water density
C_g	Group Wave Celerity
Pc	Probability of occurrence
Sqrt	Square Root

CHAPTER 1

INTRODUCTION

1. Motivation of the study

1.1 Coastal Morphology

Coastal morphology is defined as the science or study of origin, evolution and natural morphodynamic processes responsible for shaping various components of the coastal zone. The coastal ecosystem comprises of shoreline between land and sea, tidal flats, wetlands, estuaries, bays, mangrove swamps, marine habitats, etc. The coastal ecosystem is subject to multiple interactions including marine and terrestrial environment, atmospheric and fluvial processes, climate change, increase in sea level, rise in temperature, altered precipitation rate and human intervention. The formation of the coastal environment largely depends on many factors like winds, waves, tides, currents, sediment dynamics, biota and changes in sea level. Coastal morphology largely acts as a precursor of the formation of the coastal ecosystem. Variation in the hydrodynamic forcing, availability of sediments brings about great morphology changes in the coastal system in a large period. The key factors affecting coastal morphology are geology, composition of sand and rock in the area, fetch of the wave, strength of the wind, tidal action, currents, shallow water processes, steepness of slopes, weather conditions, precipitation, vegetation cover and human-constructed artificial seawalls, breakwaters, etc.

Coastal morphology affects the coastal region components like Mangroves, marine species, benthic habitat, seagrass beds, coral reefs, etc. The regional coastal morphology and geomorphological settings variations lead to changes in mangrove communities, ecology and marine biodiversity. An increase in sea level and water intrusion into the land and mangrove

ecosystem, lead to the death of plants as flooding duration increases. An increase in storm intensity and degree of exposure often breaks the branches and defoliates the mangrove canopy. Coastal erosion leads to loss of biodiversity and damage to the mangrove ecosystem as the water inundation, salinity and turbidity increase. Disturbance in estuarine water quality and mineral composition leads to the death of roots and living plant cells due to water submergence in the breathing pores and loss of regeneration capacity. These geomorphological processes lead to changes in the nearby navigation, channel routing, agricultural activities, drainage system and disturb marine life. With a change in coastal morphology, there comes a change with coastal hydrodynamics. Water circulation in the coastal environment affects watershed draining. Coastal morphology changes with human-induced constructions can cause damage to near-shore marine ecosystems especially sea coral reefs, seagrass beds, smothering and shoaling of benthic habitats, etc. The impacts lead to land-filling, dredging, drainage of sediments, waste and pollutants run-off.

1.1.1 Time Scales involved in coastal morphology

Coastal morphodynamics vary with time depending upon the interaction of hydrodynamic processes, sediment dynamics and topography of the coastal region. Dividing the coastal morphodynamics into four groups as per the time scale and space span - the process can occur as instantaneous, as an event, as an engineering process and finally as a geological process. Morphodynamic changes vary from micro to mesoscale spatially and in a timespan of microseconds to Millennia. The figure 1.1 shows the temporal and spatial scale of morphodynamic processes.

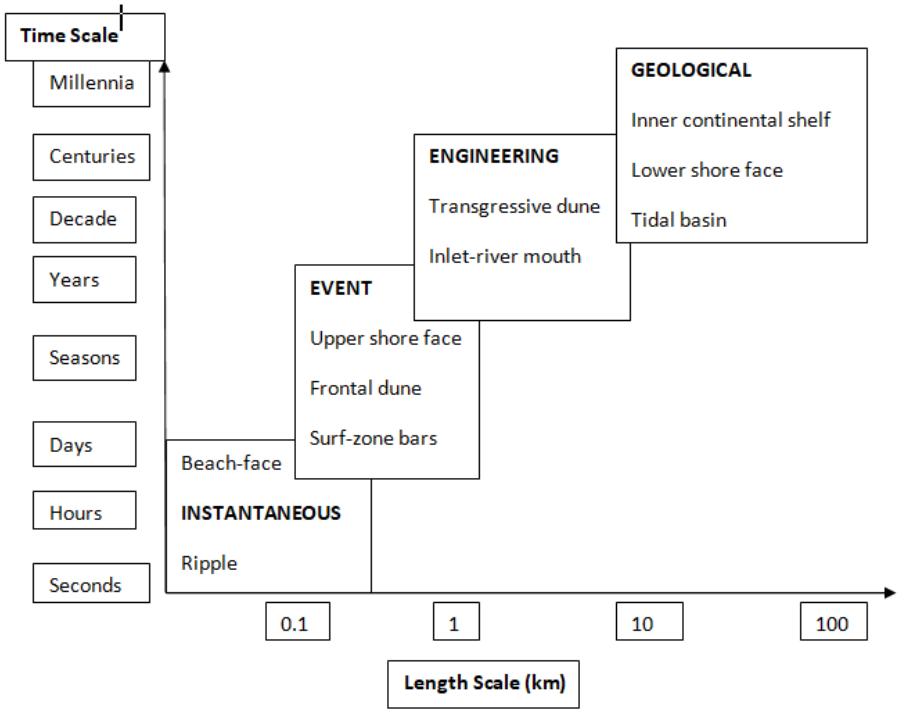

Figure 1.1. Spatial and temporal changes involved in morphological changes (Source: Cowell and Thom, 1994).

The figure 1.1 shows the four groups representing the processes occurring at the spatial and temporal scale. The processes like ripple formation and beach-face formation are instantaneous which occur in fraction of seconds to days over spatial scale around 0 to 100m. Further processes like formation of surf zone bars, frontal dunes, upper shore face formation may take time from day to years over spatial length of few meters. Next the processes which may take years to centuries are formation of river mouth inlet and transgressive dunes are categorized under engineering processes covering spatial scale from meters to kilometers. The larger time zonal morphodynamic processes are called geological morphodynamic processes like formation of tidal basins, lower shore face formation and development of inner continental shelf spreading over more than 10-100 kilometers.

There are various processes behind these morphodynamic developments which can be classified from their action over spatial and temporal scale as shown in figure 1.2.

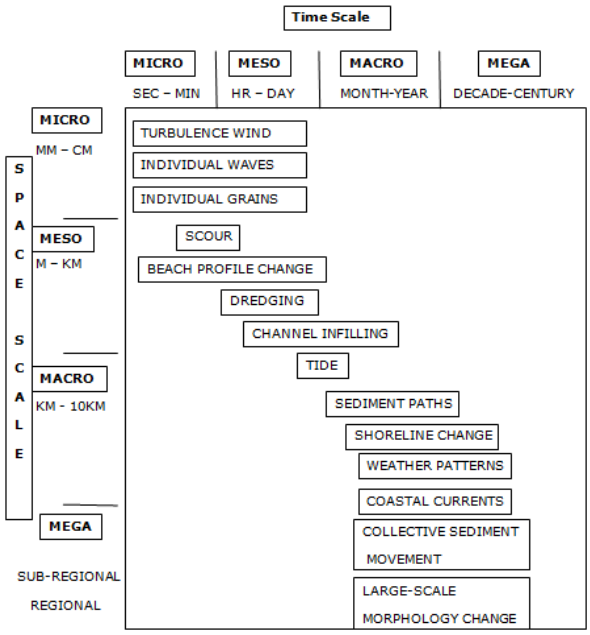

Figure 1.2. Morphological changes with respect to time and space (Source: Kraus et al., 1991).

The figure 1.2 depicts the processes occurring from micro spaces to sub-regional and regional scale and in time span of microseconds to decades and centuries. These morphological changes occurring at micro time scale and spatial scales are influenced by turbulence, winds and waves. Processes leading to scour formation, changes in beach profile, dredging, channel filling taking time period from hours to days and develop over range of meters to kilometers. Next the changes occurring over larger span of time like months to years with spatial progradation from some kilometers to 10s of kilometers are tides, change in course of sediment path, shift in shorelines, etc. The phenomena which take decades and century to occur are the changes in weather and coastal currents, collective sediment movement and large-scale morphology changes like formation of natural spits, bays, headlands, etc.

1.1.2 Processes involved

The Coastal morphology is largely dependent on various processes that influence coastal zone and ecosystem like erosion, transportation and deposition. Erosion is the phenomenon of removal of the soil by the action of waves, tides and currents, majorly due to lack of direct accumulation and induced erosion. Transportation is the phenomenon of movement of broken material and its transfer to the other place. The transfer and shift of sediment along the shore is called longshore drift acting as link between erosion and deposition. Deposition is the phenomenon of dropping of the material as the transporting forces lose energy and cease to transport. This phenomenon is responsible for creating landforms. Every coastal ecosystem is unique as it has its own balance and equilibrium of erosion, transportation and deposition. The spatial and temporal interactions of coastal ecosystem with the coastal processes lead to varying geomorphology and landforms. Other shallow water processes like shoaling, refraction, diffraction, reflection, wave breaking, nearshore currents, long shore currents, cross-shore currents, rip currents, undertow currents also affect the sediment transport significantly depending on the site conditions.

Understanding the coastal processes

Hydraulic action is one of the major processes leading to coastal erosion. It can be understood as mechanism of development of cracks in the cliff with building air compression by the action of striking waves. Due to this rock, cliffs can get eroded into particles and get dislodged and transported elsewhere. Another process responsible for coastal erosion is attrition. This is the phenomenon in which erosion occurs when rock particles break into smaller fragments and get eroded due to the continuous striking with itself and the bed. Solution is the process in which acid present in the sea dissolves rocks made of limestone. Abrasion is another phenomenon leading

to coastal erosion also called as corrosion, where waves break off the cliff and erode it. Erosion of cliff face is also affected by the pH of the sea. When pH becomes less than 7, corrosion process occurs which corrodes the cliff face gradually.

Factors involved

Waves, tides and wind are the major coastal processes leading to coastal morphology changes. Waves are caused by the action of winds over the surface of sea water. The friction between the air molecules and water molecules lead to the energy shift to water from wind. Wind is defined as the movement of air current across the earth, generally in horizontal direction. Winds are the major forces behind generation of waves. Winds often blow sediments from the land to the nearby coastlines. Waves are the major factors for transferring sediments in form of erosion either along the shore called longshore drift or normal to the shore called cross shore transport. The strength of wave depends upon the intensity of wind. With higher wind intensity and velocity, the path covered over which blows is longer, the fetch becomes larger resulting in larger waves. Waves and tides involve transfer and dissipation of enormous amount of energy capable of spectacular changes and transformation in the coastal morphology. Waves erode the coastal landforms and rocks by the phenomenon called abrasion. Waves are responsible for both accretion and erosion at the coast. Generally small waves cause sediments to move towards the coast and consequently their deposition. While the larger waves with considerably high force erode the sediments and transport them into deep water. Waves along with longshore currents are responsible for larger amount of sediments transported in the shallow regions.

Another factor contributing to coastal morphology is tide. Tides can be defined as the regular rise and fall of surface of sea water as an action of

gravitational forcing exerted by the astronomical bodies Moon and Sun. Coastal landforms are modified by the action of tides in the inlet areas and the mouth of estuaries where constriction in the coast exists for the tidal exchange. Only in such certain conditions, like existence of constrictions, the required speed for sediment transportation is generated for the tides. Tides also play an energy controlling factor when wave energy arrives at the coast. With the rise and fall of tides, there occur changes and fluctuations in the depth of water and tidal currents due to which the wave energy across the shore gets distributed.

Apart from waves, winds, tides and currents, the factors responsible for altering coastal morphology are climate and geology. Climatic factor like rainfall is the form of precipitation that brings sediment influx with stream runoffs to coast. Temperature is another factor for physical weathering of sediments of the rock cliffs at the coast especially in colder regions, where frozen water in between cracks of rocks thaw and later fragment rocks yielding sediments.

1.1.3 Quantification of Coastal Morphological changes

Coastal zones existing as intersection between land and sea are the complex systems with changes occurring at rate of hours to centuries. The coastal morphological changes over time and space need to be assessed to understand the degree of changes and further likely changes to happen over time as these changes have greater consequences on coastal habitats, ecosystems and settled communities. With rapid industrialization, urban development and human intervention in the coastal areas, climate change, rapidly increasing pressure on natural resources and changing landforms, there arises need to assess the sustainability of morphology of natural landforms. This assessment would help in building effective management plans and take steps towards planning preventive measures to sustain the

effects of morphological evolution. For quantification of morphological changes occurring over a period of time, a combination of techniques and methods can be used. The availability of high resolution remote sensing and Geographical information system, laser based surveying, numerical modeling, high-tech tools and machines for carrying our field work, real time aerial video monitoring, statistical analysis and data management tools provide a broad spectrum for analyzing the morphological changes.

Among all these methodologies Remote Sensing and Geographical Information systems are the most extensively used techniques for quantifying the morphological changes. Remote sensing is the process of acquiring information not being physically connected with the object. Using high resolution sensor satellite imageries, even small changes of erosion and accretion occurring in shorelines can be quantified. Usage of remote sensing helps in identifying regions with land cover changes, the area changed and the kind of change. With the help of two different satellite images of different time period, the change that has occurred over a period of time can be identified and quantified. The high resolution and high spatial coverage has ability to capture the rich spectral and spatial diversities in the coastal regions. Apart from providing smallest details of the region, the remote sensing data is also used in numerical models. The satellite data is often used to generate input boundary conditions of the model system, and often for validation for the numerical simulation output results.

In order to gain information for the areas which are inaccessible for human intervention to explore and gather data, remote sensing helps to understand the region better with the satellite imageries. The high resolution data helps in understanding the coastal changes occurring with time as they have high spectral information, shape and texture information of the coastal features. The data helps us to identify the coastal vegetation species, Mangroves,

aquaculture, ecosystem characteristics, etc. Thus remote sensing is a very effective method to study and quantify the coastal morphological changes.

Numerical modeling is one of the most widely applied tools for understanding the coastal morphology. Numerical modeling is the process of using mathematical model for simulating the natural processes. Numerical model mimics a real world environment in the system to predict the change. A numerical model is composed of roughly four components viz., mathematical model, numerical scheme, algorithms and interpretations. The numerical scheme converts the governing equations of mathematical model into the discrete equations which approximate the solution of the governing equations.

Numerical models quantify the morphological changes in the coastal environment using specified boundary conditions. The model predicts the development of the model region with the erosion and sedimentation processes occurring as per the model set-up and boundary conditions.

1.2 Study Area

Kakinada Bay is a shallow low-lying area spread in 132 km^2 located between 82°14’ – 82 °22’E longitude and 16°5’ -17°N latitude in the Godavari estuarine region in the East Godavari district of Andhra Pradesh (Figure 1.3). It is surrounded by naturally formed sand spit 21 km long Kakinada sand spit at the eastern side with Hope Island at its northern part protecting Kakinada Bay from high winds and wave energy. Coringa mangroves and three tributaries of Godavari River; Gaderu, Corangi and Mattlapalem are present in the southern area, Kakinada port and city in western part and bay mouth opened to the sea at the northern side (Figure 1.3) . Kakinada has a semi-arid climate with average rainfall 1040 mm per annum and average

temperature 28°Celsius. Being a large rice zone and a Special Economic Zone it holds great economic importance.

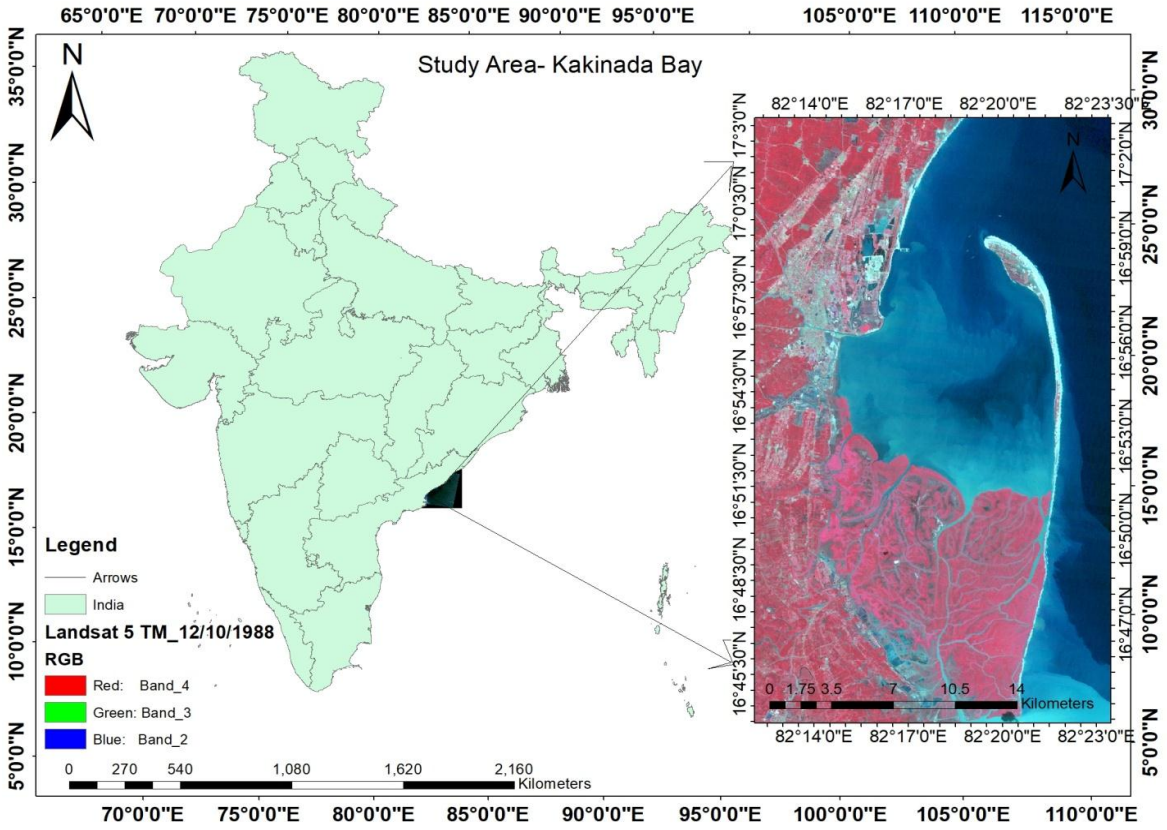

Figure 1.3. Map of Study area showing Coringa Mangroves and Kakinada Bay.

1.3 Present study

This study aims to predict the long-term progradation of Kakinada bay shoreline due to coastal processes occurring in the region. The significance of prediction of mangrove coverage due to shoreline migration over long time period is to develop efficient management and conservation plans which protect the natural environment from human led deforestation and degradation and land use and land cover changes.

Application of remote sensing for predicting mangrove coverage in future is limited. Mangrove shorelines delineated from past Remote Sensing satellite images can be helpful to predict the near-future shift in shorelines. The past shorelines give the trend of change of shoreline with areas under erosion and accretion with the help of Linear Regression model and End Point Rate (EPR). The model validation is done by matching the present satellite mangrove shoreline with the predicted shoreline by the model. The limitation of this model exists in the positional error. The non-uniform positional error at different transects of shorelines may lead to misleading prediction of shoreline. Other limitations are recognition of satellite imagery and accuracy of chosen method, consideration of ground control points for measuring shoreline position, shoreline temporal variability with time of satellite data. Often the prediction of shift in shoreline position using trend obtained by studying previous satellite imageries applied is not inclusive of the unseen or unobserved climatic or hydrological conditions occurring at the ground level. Thus spatial modeling is demanding and challenging to efficiently resolve the shoreline shift accurately. Remote sensing provides information on change in vegetation cover but the limitation exists in describing the ecological processes responsible.

The numerical modeling offers another way for predicting the morphological development of the coastal forms. Numerical simulation incorporates a model with inputs of observed field conditions to predict the future development. The forcing conditions given as input at the model boundaries can include the effects of tides, winds, waves, currents, sediments, salinity, temperature, etc. The model uses the set of equations to run the flow conditions with the input data for predicting the resultant morphodynamic form with the model set. Numerical models can help in developing management tools for development and conservation of mangrove area. Often the numerical modeling suffers some limitation for predicting the

progradation of shoreline because of complex interaction of the hydrodynamic processes associated with the complex geometry. The other limitation of numerical simulation is the lack of data incorporation for depth dependency of the vegetation characteristics as stated by Horstman et al. (2013) because of which field conditions may not be exactly represented in simulated hydrodynamics flow patterns of the area. The sensitivity of model towards the critical parameters like bed roughness, viscosity, settling velocity is very high, so applicability of a particular value over large study area becomes critical. The long-term predictions require large computational costs and time which require higher facilities, which becomes other critical requirement. The validation of model where sufficient field data is not available for calibration limits the usage of numerical simulation for such areas.

However if both the techniques (remote sensing + Numerical simulations) can be combined, then they can bring better predictions of morphological development with improved reliability. With the help of remote sensing, the satellite imageries are studied and the past development is assessed to understand the morphological evolution that has occurred. Analyzing satellite imageries and delineating the shorelines of the study area and processing them in GIS platforms provide the erosion and accretion trend. The rate of sedimentation and erosion obtained helps us to form a historical base of our study for understanding the phenomenon. The predicted shorelines from numerical simulation can be validated by superimposing them with the satellite derived shorelines to improve the overall confidence in the prediction. The amalgamation of the information obtained from remote sensing with the numerical modeling helps in predicting the future development of the coastal forms. The conjunction of remote sensing and numerical modeling simulations is beneficial as they contribute in the improving the shoreline migration prediction with better confidence.

Importance of the Present Study

The present study is an implementation of union of these two techniques. An attempt made to predict the long-term morphological development of Kakinada bay using remote sensing and geographical information system and numerical modeling using DELFT 3D package.

This study aims to predict the morphological development of Kakinada Bay. It quantifies the changes occurring at the northern boundary of Coringa mangrove of Kakinada bay as it is directly exposed to hydrodynamic forcing and establishes trend of erosion and accretion using indices of Net Shoreline Movement (NSM), End Point Rate (EPR) and Linear Regression Rate (LRR). The rate of accretion and erosion obtained will give insight into the trend of sedimentation and erosion occurring inside the bay and build a base for understanding further morphological evolution of the bay. A numerical simulation of the hydrodynamics and sedimentation in the Kakinada Bay performed for analyzing the sedimentation and erosion using numerical model package DELFT3D. For long-term morphological modeling, process based modeling is used which describes the underlying physical processes responsible for morphological changes. For reduction of computational time and effort, various approaches like Model Reduction, Input Reduction and acceleration techniques have been defined by De Vriend, 1966. The model uses morphological tide and morphological acceleration factor for reducing the long computational time and efforts, followed by validation by hindcasting and finally forecasting the long-term morphological changes of the bay. The study aims to predict the morphological development of bay for next 100 years from year 2019 to 2119, the future pro-gradation of Coringa mangrove shorelines into the bay and decadal volumetric changes in the bay using the depth averaged DELFT 3D model.

Kakinada Spit growth was initiated in late 19th century northward (Mahadevan C. and B. Prasad Rao, 1956). A bay-head delta was created by rapid filling of the calm back-barrier bay by the riverine discharge. It led to continued growth of Kakinada spit northwards with filling of finer sediments and colonization of mangroves into the vacant delta and rising floor of the bay (Murty M.R. et al., 2011).

Kakinada Bay being an enclosed bay from the three sides with only opening at the northern side with the presence of a breakwater; the action of waves inside the bay has been found to be negligible. With the negligible action of waves occurring inside the Kakinada Bay, the approach for adopting the model reduction technique by choosing only the most important physical process by eliminating action of waves from the model is adopted. As Lesser (2009) stated the right acceleration techniques usage as: "In order to use a morphological acceleration technique in a coastal situation it is essential to identify which coastal processes play a significant role in (residual) sediment transport patterns over the space and time scales of interest". While at the same time statement given by Roelvink (1999) and quoted by Dastgheib A. (2012) as: "If we put enough of the essential physics into the model, the most important features of the morphological behavior will come out, even at the longer time scales" makes this study find which approach to adopt.

This study attempts to demonstrate the essential processes and physics that are required for long-term simulation along with appropriate acceleration scheme.

This study attempts to answer the following questions:

a) To which extent the long-term morphological modeling results are reliable?

This study answers the question if these long-term morphological modeling can produce the reliable results by creating nexus of two techniques 'Remote Sensing and Numerical Modeling'. The numerical modeling hindcast results are validated using remote sensing images. This study quantifies the rate of change of the shoreline of the bay using remote sensing images in the Digital Shoreline Analysis System (DSAS). The trend of erosion and accretion occurring inside the bay was obtained using indices NSM, EPR and LRR. The rate and trend of sedimentation and erosion obtained with the satellite imageries are further used to statistically compare the transect–wise hindcast and forecast results. Thus this study demonstrates the model's ability to reproduce the qualitative long-term morphodynamic development of the bay. The process based models used for predicting long-term morphological development of the coastal regions on the spatial and temporal scales are validated and examined. Model inputs and constants are calibrated to produce the morphological results which match the real time data. The long-term morphological simulation results are validated with help of field data and satellite imageries. The reliability of the model is checked using statistical methods like Brier Skill Score (BSS).

b) Which are the most crucial hydrodynamic forcing processes in the long-term morphological development of the region?

The long-term morphological modeling uses the process-based models which use various approaches like Model reduction where physical processes to be modeled are reduced; Input reduction where the input forcing are schematized to the representative input producing results similar with the full-time data. For long-term morphological modeling it is imperative to identify and distinguish the most crucial hydrodynamic forcing for the

morphological development of the bay on larger spatial and temporal scales. This helps in understanding the result of excluding different forcing as model input over long-term morphological results of the bay. Hence prediction of the morphological development for 100 years is attempted over two sets of physical processes; one with tidal effects only and another with tides and waves.

c) Can the climate change effects on the development of bay be predicted by the long-term morphological model?

The long-term morphological models can help in examining the climate change effects like the sea-level rise. The third set of simulation represents the morphological evolution of the bay over the decadal rise in mean sea level. Since the morphological change and effect of sea level rise on the tidal bay takes long period of decades and century, this long-term modeling will certainly help in evaluating the effects of climate change (MSL rise).

1.4 Scope and Objectives of the Thesis

This study aims to predict the morphological development of Kakinada Bay. With establishment of the trend of the shoreline change and the factors responsible for the accretion and erosion, future shoreline changes and morphological development of the bay has been predicted using depth averaged Delft 3D model.

1.4.1 Objectives

The following are the objectives of this thesis:

1. Prediction of long-term morphological change of Kakinada Bay using numerical simulation studies duly validated by Remote Sensing data.
2. To identify the effects of incremental addition of environmental forcing.

1.4.2 Scope of Work

Scope of the work has been presented here for each objective defining the work to be incorporated.

1.4.2.1 Quantification of the change along the northern boundary of Coringa Mangroves using remote sensing and GIS

Coringa mangrove boundary changes to be quantified using satellite images with the help of DSAS. Delineation of Mangrove shoreline boundaries using the satellite imageries of years 1977, 1988, 2000, 2006, 2013 and 2019 for giving input in DSAS. The past shoreline of year 1977 to be taken as reference for building baseline and transects to be casted at 500m interval to assess the accretion or erosion occurred applying three statistical indices Net Shoreline Movement (NSM), End Point Rate (EPR) and Linear Regression Rate (LRR). The accretion and erosion rate obtained will give insight into the trend of sedimentation and erosion occurring inside the bay and build a base for understanding further morphological evolution of the bay.

1.4.2.2 Numerical Simulation of the hydrodynamics and sedimentation of Kakinada Bay

Mangrove shoreline propagation can be attributed to the hydrodynamic environment and sediment accumulation in the Kakinada Bay. To study the waves, tides and currents effect inside the bay on sedimentation using numerical model DELFT3D, the Flow model and Wave model to be calibrated by tuning various parameters. Validation of flow models to be done by comparing the modeled water level, currents, sediment concentrations and wave parameters with the field observations. Having studied the effect of tides, currents and waves on the occurrence of sedimentation and erosion inside the bay, factors to be incorporated in the morphological model are decided.

1.4.2.3 Prediction of long-term morphological changes of Kakinada Bay

Long-term morphological prediction of Kakinada Bay to be done by forming morphological model using model reduction method, input reduction method and morphological acceleration methods for reducing the computational time and efforts. Input reduction method to be applied forming morphological tide and morphological acceleration technique to be used by applying morphological acceleration factor. The long-term morphological simulation for 100 years was carried out with three sets of simulations for distinguishing the effect of different processes and MSL rise. First set of simulations took into account the effect of tides only, second set of simulations were carried out combining tide and waves and third set of simulations were carried out with tides and waves combined with the (estimated) change in decadal mean sea level rise. The three simulation results were compared with respect to planimetric changes, shoreline changes, Depth change and volumetric changes.

1.5 Thesis Layout

Chapter 1 includes motivation, introduction, objectives and scope of the study

Evolution of Kakinada Bay with Coringa Mangroves, Kakinada Spit and Hope Island is explained here.

Chapter 2 includes the data used and detailed literature review of application of remote sensing and GIS, modeling and observed data.

Techniques to study morphological evolution of Kakinada bay, development of sand spit, growth of mangroves and shoreline migration with help of remote sensing and GIS, modeling are explained in this chapter.

Chapter 3 includes the Quantification of shoreline change inside Kakinada Bay using Remote Sensing and GIS

Shoreline change inside Kakinada Bay is to be quantified using satellite images with the help of Digital Shoreline Analysis System (DSAS).

Chapter 4 includes Numerical Simulation of the hydrodynamics and sedimentation of Kakinada Bay

To study the action of hydrodynamic forcing inside the bay on sedimentation and erosion using numerical model DELFT3D, the Flow model and Wave model to be calibrated and validated with field observations.

Chapter 5 includes the Prediction of long-term morphological changes of Kakinada Bay

Long-term morphological changes prediction of Kakinada Bay by forming morphological model using input reduction, model reduction and morphological acceleration methods. The forecast model to be extended for next 100 years with three combination of environmental forcing – (i) Tide only, (ii) Tide + Wave, (iii) Tide + Wave + MSL variation.

Chapter 6 includes results and discussions

The statistical comparison was made for the shoreline movement obtained from numerical modeling and remote sensing. The planimetric changes, shoreline changes and volumetric results were compared for all the three scenarios: Flow alone, Flow and waves combined and Flow and waves combined with decadal rise in mean sea level.

CHAPTER 2

LITERATURE REVIEW & DATA COLLECTION

2.1 Literature review

2.1.1 Kakinada Bay

Kakinada Bay is a shallow region with area around 150km^2. It is surrounded by Kakinada spit at the eastern side, Coringa mangroves and three tributaries of Godavari River; Gaderu, Corangi and Mattlapalem in the southern area, Kakinada port and city towards the western side and the bay mouth opened to the sea at the northern side (Figure 1.3). This has extensive mud flats and Mangroves on the southern side. There are four estuaries opening into the bay, Gaderu, Corangi, Mattlapalem and Chollangi from southern side of the bay. Kakinada canal opens into the bay at the western side of the bay. Semidiurnal tides are dominant in the Kakinada bay. The development of Kakinada sand spit changes from time to time due to sediment discharges from Godavari River and due to the action of wind, wave, tides and current.

2.1.2 Characteristics of Kakinada Bay

The climatic and oceanographic conditions of the Kakinada Bay discussed below.

Waves

Predominant offshore wave directions in Kakinada region are mainly based on the monsoon variation. This region is dominated by South west monsoon during months of June-September and North east in months of October-January and fair period in months February to May. Wave heights vary from 1.0-2.5m and wave period between 5-9 seconds (Chandramohan, et al.,

1989). During North-East monsoon, wave heights vary from 0.2m to 0.8m with wave periods between 5 to 7seconds. While during South-West monsoon, significant wave heights vary between 0.4 to 1.2m, with wave periods from 6 to 9 seconds. As per the Kakinada port authorities, during the North-East monsoon (Oct.-Dec.) the wave height exceeds 2 m for 32% of the time and 58% of the waves approach from North-Northwest direction which affect the bay as it is exposed in the north and NE to direct deep water waves. During South-West monsoon, rough sea conditions prevail and wave height exceeds 2m, 68% of the time. The percentage occurrence of significant wave height for both south-west monsoon and north-east monsoon is presented in figure 2.1. However, since Kakinada Bay is protected on the eastern and southern sides by the sand spit, it remains largely unaffected.

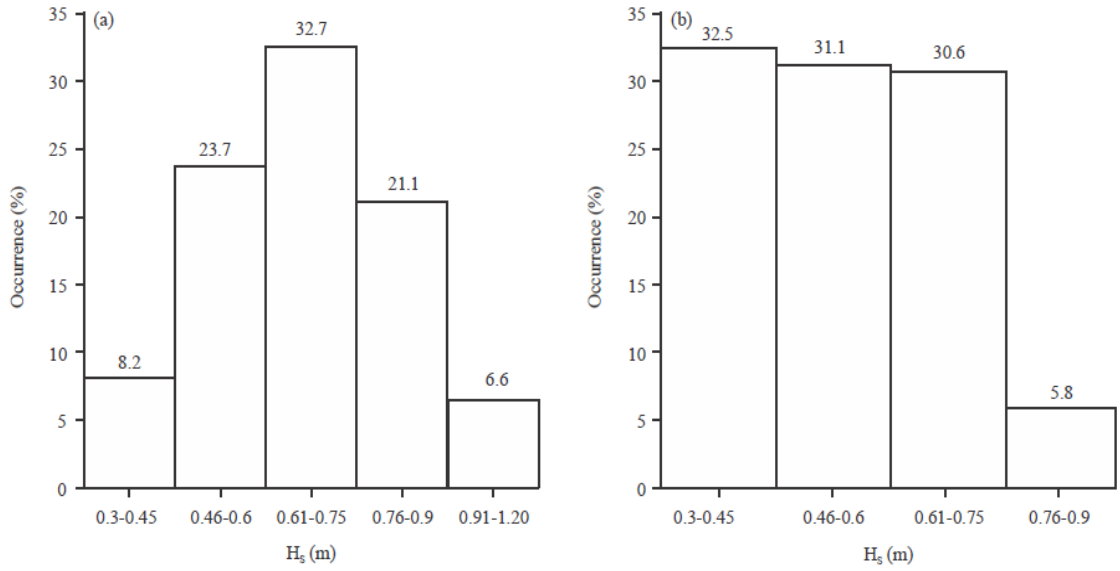

Figure 2.1. Percentage occurrence of Significant Wave Height Hs (m) for (a) South-West Monsoon and (b) North-East Monsoon. (Source: Sharmila et al., 2015).

Tides

Semidiurnal tides are dominant in the Kakinada region. Based on the Kakinada port tidal data for the year 2000 the spring tidal range is about 1.34 m and the neap tidal range is about 0.53 m (Raju N.S.N. et al., 2004). The tidal currents during neap and spring tide range from 0.15 to 0.4m.s^{-1} respectively. The tidal amplitude reaching in the mangrove area becomes quite low as mentioned by Sreenivas (1998).

Wind

As per Kakinada port data, average wind speed in this area is less than 19km.h^{-1} and the direction of the wind varies with the period of monsoon, South-westerlies prevail most of the year except October– January where north easterlies prevail during these months. During summer, the average wind speed is around 5-10km.h^{-1} but more than 15km.h^{-1} in winters. The 30 years climatic table observation from year 1931 to 1960 at Kakinada 8m above MSL is reported. It reports that the wind speed is 19km.h^{-1} in the month of May during South East-West direction. While in the month of June it is 10km.h^{-1} in South East-West Direction. The wind direction hourly time-series of Kakinada Bay is presented in figure 2.2.

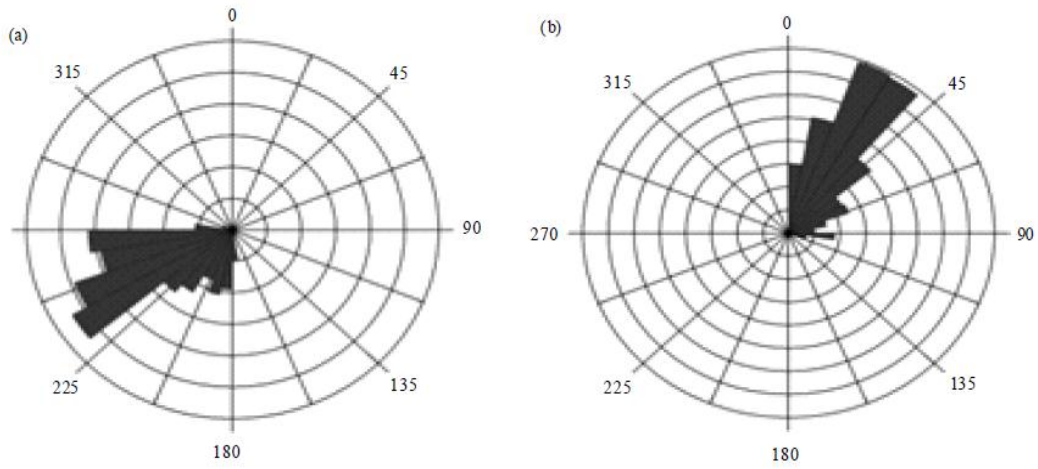

Figure 2.2. Hourly time-series of wind direction against time for (a) South-West Monsoon and (b) North-East Monsoon (Source: Sharmila et al., 2015).

Currents

Currents are indirectly determined by the large-scale circulation in the Bay of Bengal governed by the monsoon system. They are predominantly northerly during February-July while predominantly southerly during September-December. In between these periods, the direction is varying. The fully developed coastal current may reach 1m.s^{-1}. The circulation is tidal and the spring/flood and ebb/neap currents reach a maximum of 0.25 m.s^{-1}.

Climate

Kakinada climate is tropical in the nature with hot and humid weather with average relative humidity as 76%. The average rainfall is 157mm per month during June to mid-November. The South West monsoon is responsible for the major annual rainfall occurring in the region. Maximum temperature in the region ranges from 32°C–40°C while minimum temperature varies from 12°C-21°C. May and June are the hottest months of the year with temperature ranging from 38–42°C. December and January are the coolest months of the year with temperature around 18-20°C.

2.1.3 Evolution of Kakinada sand spit

Coringa Mangroves and Kakinada spit have grown significantly from 1851 as seen from British Admirality charts presented in figure 2.3. Mahadevan and B. Prasad Rao (1956) stated that the spit was not existent a hundred years ago, grew first towards the northeast of Godavari confluence and then towards northwest. They reported that at that time Kakinada Bay used to get dry during low tides. Godavari River used to discharge water through a opening towards east. Only during low tides a small sand bar used to get exposed with shape towards northerly drift. By 1864, this small bar which used to get exposed during low tides became a full-fledged sand spit, forming Godavari point. During that period this Kakinada Spit took full shape as Hope Island. Godavari point grew northwards by 1878 and river discharged its water into the Kakinada bay, instead of directly into the sea as observed in figure 2.4. They concluded that if a sand spit has to form, surplus sediment exceeding the normal limits ought to be supplying by the river to the coast.

Figure 2.3. Admirality Chart of the survey made in 1851 in the region of Godavari distributaries and Kakinada Bay.

Source: C. Mahadevan and B. Prasad Rao, Growth of the sand bar north of the Godavari Confluence, 1956.

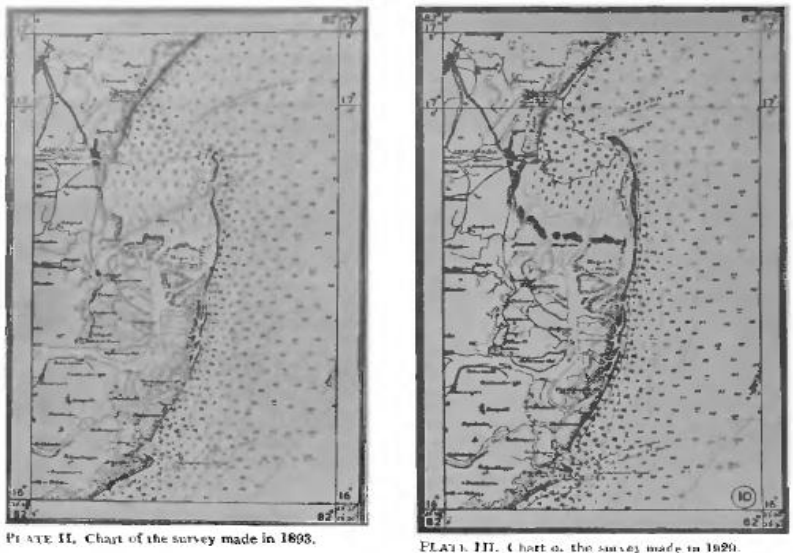

Figure 2.4. Admirality Chart of the survey made in 1893 and 1920 in the region of Godavari distributaries and Kakinada Bay.

Source: C. Mahadevan and B. Prasad Rao, Growth of the sand bar north of the Godavari Confluence, 1956.

By the action of wind, wave and current, sediments brought by river discharges get deposited and form new landforms like Mangrove area and Kakinada Spit. Morphodynamics of Coringa Mangroves and Kakinada Spit initiated in late 19th century had grown progressively northward as stated by Mahadevan and Prasad Rao, 1956. In the initial growth years of the spit, it had even deflected the course of Gautami distributary to be parallel to the coast. A bay head delta was created by rapid filling of the relatively calm back barrier bay by the riverine discharge stated by Nagesawara Rao, 2006. Bayhead shoreline advanced northwards by at least three km in last 40 years. Over extension of Gautami river course parallel to the coast cut the Kakinada Spit to find a short route to Bay of Bengal. The Kakinada spit had continued to grow northwards with filling of finer sediments and colonization of mangroves occurred in the delta and rising floor of the bay (Nageswara Rao, 2006) (figure 2.5).

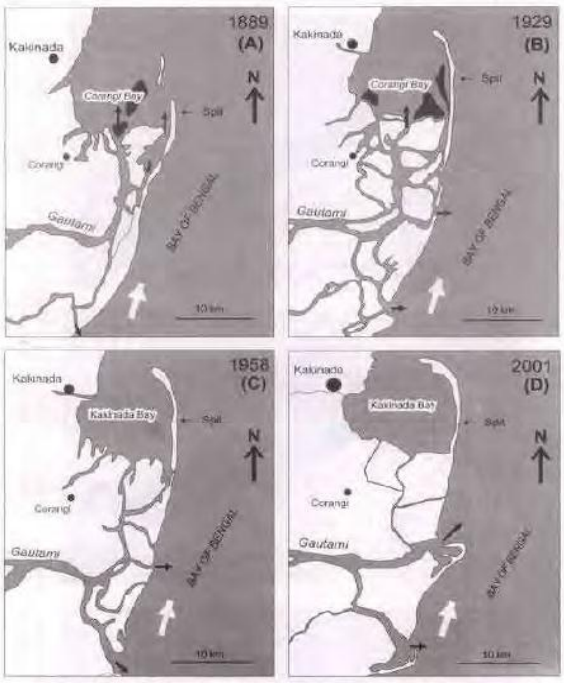

Figure 2.5. Growth stages in Kakinada Spit towards northeast of Godavari delta. Black arrows indicate location of main discharges of rivers and white arrows show the direction of net littoral drift.

Source: Nagesawara Rao et al., Sedimentation Processes and asymmetric development of the Godavari Delta, India, 2005.

The Kakinada sand spit has undergone morphological changes with a rapid rate of growth of sand spit since from the year 1851 extending its length around 18 km. The hydrographic study reveals that the Bay has been undergoing rapid siltation. Due to this creeks land has elevated with deposition of silt during peak monsoon. With land elevation, the tidal flushing becomes weak and only the marginal areas support mangroves (Ramasubramanian & Ravishankar, 2004).

2.1.4 Coringa Mangroves

Mangroves are trees, shrubs, palms, epiphytes and ferns, which together called as the marine tidal forest of tropical and subtropical latitudes influenced by tides (Tomlinson, 1986). Mangrove ecosystems are adapted to the harsh environmental conditions of hypersaline, soft-bottomed anaerobic mud and frequently inundated conditions. They absorb the strong wave forces especially during the cyclones. They also prevent erosion caused by waves, holding soil strongly with the roots. Mangroves also called as natural sinks as they also neutralize sediment runoff from natural and anthropogenic activities.

Coringa Mangroves are located in the southern part of Kakinada Bay named after River Corangi situated at 16°44’ to 16°53’N latitude and 82°14’ to 82°22’E longitude. Coringa mangroves receive freshwater from the Gaderu, Corangi and Mattlapalem rivers, which are tributaries of the Godavari Gautami River. The area of Coringa reserve forests is 3156hectares with around 15 species of Mangroves mainly *Avicennia, Excoecaria, Rhizophora, Sonneratia, Bruguiera, Xylocarpus, Ceriops,* etc. Coringa Mangroves are the second largest mangroves in India’s Eastern coast with large diversity of mangrove species, threatened flora and fauna. The Coringa mangrove region has significant economic significance, as it acts as the reproducing zones for fish and other marine resources.

Coringa mangroves are like living grooves building up sediments, stabilizing the ground and fixing mudbanks. As stated by K. Thulsi Rao (2013), it is estimated that there is an annual sedimentation rate ranging from 1 and 8mm in mangrove areas that are expanding in land area, promoting accretion.

Coringa Mangroves hold great importance with their significance in environment protection and ecosystem balancing. These have been investigated as a highly important ecological repository of resources and protect from coastal calamities (Chandra Mohan et al., 1997; Satyanarayana, 1997, Rönnbäck et al., 2003). They are highly productive intertidal wetland ecosystems that exist as woody halophytes in coastal areas with less wave energy which helps in sediment accumulation (Alongi, 2002). They absorb the strong wave forces, especially during cyclones. They also prevent erosion caused by waves, holding soil strongly with the roots. Mangroves are also called natural sinks as they also neutralize sediment runoff from natural and anthropogenic activities. Coringa Mangroves are valuable wetland ecosystems supporting huge biodiversity of flora and fauna providing tidal control, shoreline stabilization, and barrier against cyclones. Recognizing the biodiversity significance of Coringa mangroves, government has declared it as protected area.

However, there has been a degradation of mangroves owing to the conversion of mangrove area into aquaculture, agriculture and industrial practices etc., which is a serious environmental concern and needs continuous monitoring.

The Coringa mangrove area is mainly influenced by its surrounding oceanographic and hydrological conditions. The Coringa mangrove area bordered by Kakinada bay in the north and in south by the Godavari River, which are mainly important for growth, stability and survival of the Coringa

mangrove area. Hence it is crucial to understand the morphological conditions of the Kakinada bay.

2.1.5 Shoreline Migration

Shorelines are borders between the land and the sea which keep varying as a result of hydrodynamic factors like tides, currents, waves, availability of sediments, sea level rise, etc. Mangroves are the halophytic plants growing in the confluence of land and sea, protecting coastal erosion with the help of their complex root system (Pandey and Nayak, 2013). They accumulate sediments and form mudflats (Cook et al., 2004; Jickells & Rae, 1997; Sanders et al., 2010) evolving with the action of hydrodynamic forcing with time. Long-term shoreline and morphological changes occur with gradients in sediment transport involving movement of sand by the action of waves and currents. This long-term net sediment movement leads to sediment gain or sediment loss which makes either shoreline movement towards sea (accretion) or towards land leading to erosion. Quantitative shoreline migration is important for understanding morphodynamic processes in coastal region.

Studying extent of shoreline change in past decades using RS and GIS helps in understanding how they have been changing owing to various attributes like hydrodynamic processes, sediment dynamics. Timely, accurate and periodic information of natural resources help in sustainable management with the help of either ground surveys; which are very time consuming, uneconomical and laborious and often not useful for inaccessible areas. Remote sensing has emerged as a powerful tool for surveying and getting information of such areas along with synoptic and temporal coverage of large area.

Remote sensing is defined as acquiring information, identification and delineation of various objects from distance without being in physical contact

and GIS is geographical information system, a tool to process information acquired by remote sensing which digitizes processes and analyzes the spatial information and converts them into readable format. Remote sensing measures electromagnetic energy emerging from sun, which gets reflected, scattered by objects on the surface of earth. Different objects reflect different amount of energy referred as their spectral signatures which are used to identify and differentiate them. Ramasubramanian R. et al., (2006) analysed Godavari Mangroves using remote sensing approach describing the changes occurred in the mangrove region between 1986 and 2001 by the action of waves and floods. During this period 586 ha of new mangrove area accreted with alluvium sedimentation from the Godavari estuaries' runoff.

The tidal asymmetry and water movement in Kakinada Bay and mangrove creeks is affected by the tidal circulation (Rao et al., 2003). The existence of deep tidal channels was attributed to ebb-flood tidal asymmetry. The presence of dense vegetation including mangroves in the swamp area around the tidal channels and waterways led to the flow retardation led to sediment entrapment. Flood current at Coringa and Gaderu River was low around 30–40 cm sec^{-1} while ebb strength was around 50–70 cm sec^{-1}. They mentioned that a large mudflat with an area of 12 km^2 in the southern side of the bay opposite to Coringa and Gaderu Rivers with mean depth less than 1m was exposed almost during every low tide which led to the significant lowering of the flow. They attributed this phenomenon responsible for sediment granulometry change after the flow of River Godavari shifted in 1970s. They informed the levels of silt and clay with diameter less than 63mm at the Kakinada Bay and Coringa Mangrove adjacent since 1958-1963. The study for Kakinada Bay and Coringa mangroves waterways by Raut et al., (2005) confirmed the complicated circulation hypothesis inside mangrove creeks led by Wolanski et al., (1992) which leads to the formation

of new sediment transport regimes which would alter the incoming tidal water properties.

Mangrove shoreline is considered as a prominent geoindicator in coastal changes (Souza Filho et al., 2006). It stabilizes coastal sediments, preventing coastal erosion. Shorelines keep changing with time, either landward migration because of erosion or towards seawards by the action of hydrodynamic forcing. RS and GIS are important tools for studying the spatial and temporal changes of Mangroves boundary changes and coastal dynamics (Woodroffe, 1995; Wilton and Saintilan, 2000; Satyanarayana et al., 2011). It helps in studying all the inaccessible regions and provides a platform to understand the trend of shoreline changing attributed to erosion and accretion patterns. These changes in Mangrove boundary and shoreline are brought by action of winds, waves and currents, which move unconsolidated sediments (Mazda et al., 2002, Morton et al., 2004)

Some studies have been done combining hydrodynamics and sediment transport for understanding the quantitative morphological changes along the mangrove shorelines. E. Hortsman, 2012 studied bio-physical (mangrove-morphodynamics, mangrove-hydrodynamics) interactions and reported that the mangroves act as ecosystem engineer by facilitating and enhancing sediment deposition. Balke et al., (2011) stated that colonization and establishment of mangroves are affected by the short-term hydrodynamics and morphodynamics. Woodroffe, (1982) and Thom, (1967) reported mangroves as opportunistic colonizers. Friess et al., (2012) stated the requirement of understanding the bio-physical linkages of mangroves for their better survival and functioning.

2.1.6 Factors affecting shoreline migration

Shoreline stability is affected by various coastal processes like wind, waves, tides, currents, nutrients, sediments, sediment transport including erosion

and deposition acting as threshold, beyond which changes occur in coast. Sediment transport leads to erosion and accretion by accumulation or washing off of sediments lead to change in shoreline. The development and growth of Coringa mangroves has been largely affected by hydrodynamic forcing and sediment transport occurring in Kakinada Bay. Growth of Mangroves in Kakinada Bay due to formation of sand bar is attributed to the suitable hydrodynamic forcing and frequency of tidal inundation. In order to root and grow amply, the seedlings need low energy environments for accumulation of suspended sediments. Friess, D.A. and Oliver, G.J.H., (2013) attributed physical stressors like temperature, variation in salinity of water, light, nutrients, availability of fresh water etc. for the growth of mangroves. Hydrodynamic forcing along with water circulation, tidal oscillations and sedimentation is largely responsible for mangrove ecosystem formation (Massel et al., 1999; Wolanski, 1995; Furukawa et al., 1997).

Toorman, (2001) suggested that numerical modeling is the most suitable technique for studying hydrodynamics and sediment transport in coastal region. Furukawa et al., (1997) stated that mangroves trap maximum suspended sediments in the stagnant mangrove zones with low energy. Dispersal of the bottom sediment is affected by the variation in low and high frequency velocities during turbulent flow. Mangrove vegetation offers resistance to the wave, flow and bottom friction. The significant wave heights reduce with enhanced mangrove coverage (Quartel et al., 2007). The results from the mangrove numerical modeling performed by Awang Nor (2010) state that mangroves reduce wave heights and current velocities and lead to enhanced sedimentation.

In order to inhabit and to reproduce and regenerate new trees, mangroves depend on these sediments. Simultaneously, they feed and protect marine life and terrestrial animals by providing nutrients and shelters. Mangroves protect the coastal environment from natural calamities and disasters.

2.17 Long-Term Morphological Development- approaches for evaluation

In order to predict the long-term morphological evolution of the coastal forms, various approaches are available. The most widely used tools are remote sensing, statistical methods, numerical modeling, etc. The characteristics with advantages and limitations for some approaches are presented here.

2.17.1 Remote Sensing

Remote sensing is the tool to monitor the multi-temporal changes over large spatial area. It provides cost-effective and time saving data with relatively accurate information. Remote sensing and GIS is broadly used to analyze the changes in mangrove areas which can help in better coastal planning and management. Remote sensing technique is useful especially for inaccessible area where physical monitoring is difficult. It helps in supervising the mangrove restoration programs (Selvam et al., 2003). It proves as an essential technique for planning land-cover and land use. They are widely used for studying changes in geomorphology of coastal areas especially for the areas with absence of field surveys. They are cost-effective and reduce manual error.

Remote sensing images have been widely used to quantify the past changes in shoreline. Satellite images have extensively used for studying shoreline changes using GIS in India. DSAS is a useful GIS tool to analyze trend of accretion and erosion of shorelines using satellite images. It assesses the position of shoreline geometry studying satellite imageries from past and present. DSAS is an application tool for computing statistics to study the trend of change of shoreline positions and its timely development. It evaluates the historical change analysis of coastal areas, analyses shoreline geometry by delineating shorelines from satellite imageries and aerial

photographs. It is also used for predicting the pattern of shoreline behavior in future using the trend of historical rate of change assuming the similar course of climatic and geographical conditions leading to the happened course of events. It analyzes the long-term and short-term shoreline development.

These models use empirical methods towards calculating shoreline position geometry changes occurred due to coastal erosion processes. For calculating the change in shoreline, several shorelines are delineated from satellite images, historical charts, etc. The shoreline change rate is evaluated by calculating the distance between each shoreline for a given time period. Dolan et al., (1991) described many ways of measure rate of change of shoreline like Transect Based method, EPR, LRR and Average of Rates. These statistical methods calculate rate of change of shoreline by calculating the distance between the shorelines over a particular period of time given as change in meters per year along transects. Transect based method use transects casted at right angles at the shorelines divided into several segments. The rate of change is calculated at these transects.

Net Shoreline Movement (NSM): NSM denotes the total distance between the oldest and most recent shorelines calculated for all transects. It is the total movement of between the two shoreline positions and is considered as the measure of the end point of the change.

NSM= Distance (m) between the oldest and the recent shoreline.

End Point Rate (EPR): EPR is the method which divides the shoreline movement distance by the time between the most recent and the oldest shoreline (Fletcher, C.H., 2012). EPR usage benefit is the computational simplicity as minimum only two shorelines are required. Fenster et al., 1993 stated that EPR model is the best way to predict the shoreline development

for future as it is based on observed periodical rate of change of shoreline position.

EPR= NSM/Time between oldest and most recent shoreline

Linear Regression Rate (LRR): LRR is the slope of the line determined by fitting a least-squares regression line to all the shoreline points for each transect. A linear regression rate-of-change statistic can be determined by fitting a least-squares regression line to all shoreline points for a transect. The regression line is placed so that the sum of the squared residuals (determined by squaring the offset distance of each data point from the regression line and adding the squared residuals together) is minimized. The linear regression rate is the slope of the line (Himmelstoss, E.A., et al., 2018).

Dolan et al., (1991) mentioned useful features of LRR method as it is easily employable, entirely computational including all the input data irrespective of the accuracy and trend change and calculating the change rate applied on the accepted statistical concepts.

Nayak S., 2002; Chandrasekar et al., 2013; Kankara et al., 2015; Mageshwaran T. et al., 2015 have studied long-term changes in shoreline. Joesidawati M.I. and Suntoyo (2016) compared shoreline changes combining two coastlines and five shorelines of beach Tuban using EPR, NSM and LRR. They found merging of two shorelines with different times gave detailed result over shoreline retreat with average EPR as 15.25m.y^{-1} and NSM as 650.11m. Mary et al.,(2017) studied mangrove shoreline changes for Krishna and Godavari Delta with shoreline stretches of 65 and 59 km respectively, for a period of 37 years and assessed overall erosion rate as 1.5m.y^{-1} and 2 m.y^{-1}, respectively. They attributed overall erosion of mangrove shoreline for Krishna Delta and Godavari Delta to coastal erosion, decreased sediment discharge from rivers and stated that there had been

decline in mangrove extent due to over exploitation of natural resources and anthropogenic activities like aquaculture.

Tran Thi, V. et al., (2004) used the edge of mangrove forest as the shoreline indicator and NDVI for delineating mangrove shoreline. They quantified mangrove shoreline changes for 58 years in Vietnam sampling 1129 transects and concluded that the mean erosion Linear Regression Rate at the eastern sea side of Thailand Gulf was 33.24m.y^{-1} and average accretion rate was 40.65m.y^{-1}. They attributed erosion and mangrove loss to natural changes, deforestation and reduction in sediment supply. Alemayehu et al., (2014) assessed shoreline changes in Watamu area of Kenya using NSM, EPR and Weighted Linear Regression (WLR) tools of Digital Shoreline Analysis System. They divided 9.8km shoreline into 245 transects with 40m space in between them. They reported mean shoreline changes of EPR and NSM as 0.7m.yr^{-1} and -30.3m.yr^{-1}, respectively. Their EPR and NSM results concluded that around 64.4% of shoreline was undergoing erosion while accretion had taken place for rest 35.5% of shoreline. They attributed erosion to the anthropogenic activities.

Mukhopadhyay A. et al., (2012) analyzed and predicted shoreline accretion and erosion development for 142km long coastline for Puri district in Orissa. They used landsat images to delineate shoreline and used EPR to calculate the shoreline changes and predict the short term and future long-term shoreline development prediction. They concluded that Puri coast is suffering erosion and their short term EPR results matched with the satellite data. Their long-term prediction of future shoreline matched the past shoreline movement scenario. They also concluded that cross validation helps to predict the model results with better accuracy.

Elbagory I.A. et al., (2019) quantified shoreline changes using Landsat images in Alexandria, Egypt from year 2000 to 2016. Their study analyzed

accretion occurring at most of the shorelines at a rate from 1 to 20m.y^{-1}. They used shoreline prediction model from year 2016 to year 2050 using Linear Regression Rate and predicted shoreline development accretion occurring between 5-60m.

Barman N.K. et al., (2015) used shoreline trends for future prediction of Balasore shoreline in Orissa, India. They calculated short-term and long-term rate of shoreline movement for 38years from 1975 to 2013 for a shoreline of 67km dividing it into 67transects. They validated their model by comparing the shoreline prediction results with the shoreline of year 2015. They found positional error varying from -4.82m to 212.41m attributing to the effects of coastal hazards. They brought out the limitations of the method as high positional model error occurring due to some natural geological events and coastal hazards and tropical cyclones. Even if the error is found at one or two transects, the overall model error increases.

Frederick A.A. (2011) studied the factors responsible for shoreline erosion and determined the rate of shoreline change for Accra situated in Ghana between 1990 and 2010 using Landsat satellite imageries. They divided entire shoreline into 435 transects with 100m spacing and each transect length of 3800m. They used EPR and LRR for determining the rate of shoreline change and found out the similar results as erosion occurring at rate of -12.34m.y^{-1} and -12.2m.y^{-1} respectively. They found out that in entire shoreline there was no point where accretion had taken place, whole shoreline was getting eroded. They stated that unlike EPR, LRR doesn't consider years of the shorelines incorporated, while the EPR incorporates the changes occurred between the shorelines along with the transect analysis generated data. They informed the major reasons responsible for entire shoreline subjected to shoreline as sand mining, presence of hard rocky structures and climatic conditions affecting shoreline like winds, tides and waves.

Oyedotun T.D.T. (2014) described DSAS as an important tool for studying shoreline geometry changes. Author mentioned the statistical methods NSM, EPR, LRR, Shoreline Change Envelope (SCE) and Weighted Linear Regression Rate (WLRR) derived from DSAS for comparison of shoreline change over time. Author pointed out the limitation of this method to be unable to determine the morphodynamics forcing while calculating the rate of change, but at the same time coined out the benefit of being an effective tool for determining the historical and temporal geometry changes of the shorelines. DSAS cannot indicate the forcing responsible for the observed changes is coastal areas. Author summarized the effective benefits as identification of accretion and erosion occurring in coastal areas and their significant mapping and measurement at all historical time scales like annual, decadal and more. It yields important information on the morphodynamics of coastal shoreline with shift in shoreline position and geometry and their planimetric properties variations.

Kannan R. et al., (2016) detected shoreline changes of Visakhapatnam coast from year 1989 to 2015 studying temporal changes for 5-10 years difference using Linear Regression Rate and End Point Rate. They studied coastline of 135km dividing into total 576 transects with a spacing of 200m and estimated the geomorphological shoreline shift of the shoreline position. They found around 74.6km of shoreline was subjected to average accretion rate of $1.08 m.y^{-1}$ while another 38.4km shoreline was undergoing erosion at rate of $1.4 m.y^{-1}$. They identified region with utmost erosion at the northern side of Bheemunipatnam with a rate of $-22.39 m.y^{-1}$ occurred due to Hudhud cyclone in October 2014. They identified maximum accretion occurring from the period 2012 to 2015 at the northern side of Visakhapatnam Port and southern side of Gangavaram Port at a rate of $30.25 m.y^{-1}$.

NSM and EPR were used to analyze shoreline changes in Ghana Coast from year 1974 to 2012 by Jonah F.E. et al., (2016) observing huge erosion

occurring from 1974 to 2005 than from 2005 to 2012. They attributed beach erosion to the anthropogenic activities like beach and sand mining because of which the high tides and storm water hitting the scarps toe of the lowered beach level and further leading to beach recession. They stated that continued monitoring of shoreline dynamics is essential and recommended the future studies interlinking the land use pattern, anthropogenic activities and coastal processes and dynamics together in the coastal areas. They recommended the combined activities for better coastal planning and investments in coastal constructions.

Many studies have been carried out assessing the shoreline changes using DSAS and indices like EPR, NSM and LRR. The authors and researchers have concluded these methods as the best way to understand the trend of shoreline dynamics and identification of erosion and accretion areas in the shoreline positions. The spatial and temporal rate of shoreline growth or recession can be easily studied using this application with help of RS and GIS. The high resolution multi-temporal imageries are very effective in delineation of coastal shorelines and identify the regions susceptible to erosion hazard. The information obtained is highly beneficial for the coastal managers, decision makers and policy makers for the better steps to be taken for effective management of coastal region.

The recommendations regarding combining the studies assessing the change in coastal shorelines and land use and land cover changes with coastal processes and hydrodynamics governing these changes in the coastal area is adapted in this study. This study is a comprehensive study making use of the available satellite imageries for quantifying the rate of erosion and accretion occurring in the Kakinada Bay and using the results for validating the forecast model of numerical morphodynamic model for simulating the hydrodynamics leading to the morphological development of the bay using numerical modeling.

2.17.2 Numerical Model Approach

Numerical method can be defined as a set of combination of a large number of mathematical equations representing a real world situation working on digital platform for finding an approximate solution to the physical process problem. Coastal morphological models combine waves, tides, currents, winds and sediment dynamics for a coastal area with updated bathymetry for simulating the geomorphological changes of the region for longer time period. Process based morphological model for studying coastal landform changes and development of coastal structures implements empirical observations into mathematical equations related to morphodynamic control processes like winds, waves, tides and currents responsible for sediment transport. In these numerical modes, hydrodynamic flow calculations are done leading to change in the sea bed which gets dynamically updated at each computational time step and further calculations are done with the updated bathymetry.

The morphological models are used to simulate and predict the long-term morphological evolution of the coastal areas with scales ranging from decades to centuries. The computational time, facility and effort required to simulate the model for such long time period is very high and unrealistic. In order to reduce the long computational time and resources, there arises need to develop some methods to overcome these limitations of these morphological models. The two general techniques used majorly for the efficient use of morphological model are the Input Schematization and speeding up of the sediment transport rates. De Vriend et al., (1993) described three technical methods to accelerate the long-term morphological modeling. First method is Input Reduction Method which uses the approach of representing the smaller-scale processes with the reduced representative inputs. The second method is Model reduction method which uses the approach for model itself reformulating excluding the smaller-scale

processes. The third method is behaviour-oriented modeling which is based on the approach of using modeling for only interested phenomenon without describing the underlying processes.

Latteux B. (1995) discussed techniques for reduction of computational cost of long-term morphological modeling for tidal current situations. He stated the need of developing huge computation required for producing the accurate simulation composed of long-term simulation representing the slow evolution of bed and the short time step to meet the faster changes in hydrodynamics along with the numerical stability of the flow model. He devised ways for reducing the computational cost as input reduction method which selects the representative set of tides for reducing the number of natural situations; and increasing the morphological time step in order to run the simulation faster. He utilized astronomical tides for input reduction as their nature is deterministic and can be predicted with time evolution. He mentioned characteristics for using either a single tide as the representative tide or a set of representative tides for morphodynamics if it produces the same intensity and direction of flood-ebb and residual transport as that of the sum of the transports for each tidal class, weighed by its frequency of occurrence representing average actual transport which will have similar effects as that of the actual set of natural tides. He investigated and developed the methods for increasing the morphological time step with their adequacy depending on the kind of case; using extrapolation method for the bed case where changes occur at around same place while for the propagative cases, lengthened tide or expansion method to be preferred.

Lesser G.R. (2009) described two techniques for reduction of high computational time and efforts for morphological modeling. He used Input reduction method and acceleration techniques. Input reduction method uses the representative tidal inputs which represents the average condition for morphology capturing accurate important residual sediment transport. He

explained the interaction of tidal components M_2, O_1 and K_1 for morphological studies with their implications on residual sediment transport. Hoitink et al., (2003) discussed that tidal constituents M_2, O_1, K_1 are linear combinations of two astronomical frequencies and the phenomenon of their combination generates a neap-spring cycle of 13.66 days. After forming morphological tide with the representative tidal constituents M_2, O_1, K_1, he devised a scaling factor to multiply the M_2 constituent. The scaling factor was applied to overcome the limitation of the simplified tide for not satisfying the requirement for creating the similar residual sediment transport as the full tide (Lesser, 2009). He added the importance of preserving the tidal energy in the simplified tide. This scaling factor can also be called as the amplification factor as it brings energy levels high for the requisite point overstating the M_2, O_1 and K_1 interaction residual. Lesser stated that morphological acceleration factor overcomes the time scale difference with hydrodynamic and morphodynamic scale evolution. It is multiplied with the hydrodynamic forcing sediment fluxes to and from the bed. He added that usage of acceleration factor helps to achieve morphodynamic simulation by running simulation only for a fraction of the hydrodynamic time scale.

The limitations and strengths of the morfac approach was investigated by Ranasinghe R. et al., (2011) using the long-term numerical morphological model using DELFT 3D. They presented two outcomes of their study based on the Morfac approach dependencies to the forcing conditions and model parameters and secondly proposed the application of Courant-Friedrichs-Levy (CFL) condition for determination of the critical Morfac. They suggested rigorous and methodically assessed approach for determination of critical Morfac value for coastal modeling. They carried out comprehensive investigation program for checking validation and limitation of Morfac approach for higher time scales and developing an effective criterion for

determination of critical Morfac using DELFT 3D and X-BEACH. The modeling program focused relationship between Morfac and various other factors like hydrodynamic forcing, size of grid and time step, simulation time period with other critical model tuning parameters, etc. They concluded their observations based on the unidirectional flow defining critical morfac as the highest morfac value which gives the most trusted morphodynamic development with strong dependencies on the size of the grid and Froude number but not directly affected by the Courant number. They gave criterion $CFL_{MF}<0.05$ as safe estimate of critical Morfac value. They used Brier Skill Score for choosing the critical Morfac as measure of model performance indicating BSS value 1 as best match for the simulated bed levels obtained from the benchmark simulation with Morfac 1 and simulation with higher Morfac value.

Michiel A.F. Knaapen and Joustra R. (2012) studied usability of Morfac approach, reduction of the computational time and loss of accuracy by multiplying it with the evolution and time factor leading model jump forward in time with rapid water level changes, altering the hydrodynamics. They performed two tests using morphological model for stationary currents using a trench flume experiment and tidal current using large ranges of morphological factors and compared model results with observed bathymetry with and without morphological acceleration factor using root mean square error (RMSE), bias and the Brier Skill Score (BSS). They found that BSS reduced very slightly from Morfac 1 to 130 in case of stationary current and with higher Morfac value model became unstable. They reported that the Bias result showed that the errors increased with increase in Morfac value. In case of tidal current, they found that results could only be compared after completion of N number of spring-neap tidal cycle; hence they limited their study using factor 5, 10 and 20. Their reported results showed that usage of morphological factor changed the model results where

Brier Skill Score reduced with increase in Morfac and Bias increased with increase in Morfac value. They concluded that usage of Morfac values reduced the computational time but at the same time additional errors get introduced in prediction thereby reducing the model performance.`

Various methods for long-term morphological modeling like input reduction method, tide schematization technique, morphological acceleration factor, tide-averaging, increase in morphological time-step, etc were reviewed by Zeinali S. et al., (2014). They stated the need of developing technique for coupling the short term functions of hydrodynamics and sediment dynamics for simulating the long-term morphological changes. They studied practical methods to reduce the computational time and efforts in morphological models. They stated that using input reduction method, representative tide can be formed for the input tide which represents the full tidal cycle. They discussed the application of morphological acceleration factor for faster computations for simulating the long-term morphological development.

Deltares carried out project for establishing the morphological model for the Rhine-Meuse Delta using Delft 3D for simulating the tides and seasonal river-discharge variations. They used morphological tide using representative tide and multiplying it with scaling factor 1.1 to obtain correction for spring-neap cycle. They explained the need for morphological acceleration factor (morfac) for scaling up the morphological changes to the rate with crucial effect on the flow. Morfac which is discharge dependent constant reduces the simulation flow by multiplying with the computed sediment transport rates. They used morphological acceleration factor 51 simulating whole year with fourteen tidal cycles.

While optimizing the input value of the acceleration factor, there arises need to set an upper scale of the value of Morfac as a function of model geometry and time step for the schematized tidal flow. Reyns J. et al., (2014) chose a

model geometry representing a flume with bar morphology. With shoaling contracting the flow in the vertical, higher sediment transportation occurs and limits the critical value of Morfac. They varied morfac value from 1 to 700 in series of short sediment transport simulations considering the simulation with Morfac 1 as benchmark simulation. The critical morfac value was considered as the highest value which resulted in the similar morphology as resulted by the benchmark simulation with morfac 1 at the same morphological time. The number of tidal cycles is considered as the time unit and output is presented at the end of the hydrodynamic tidal cycles. As Morfac is applied in the simulations, morphological simulation results are applicable and can be compared only at the end of tidal cycles of simulations (Roelvink, 2006, Roelvink and Reniers, 2012). Accuracy of the applied Morfac in morphological simulation results was determined using BSS which indicates the correspondence of modeled bathymetry obtained with the higher Morfac value with the benchmark simulation run with morfac 1. They quoted BSS value greater than 0.5 sufficiently accurate for the complicated cases while 0.99 as cut off score for the lowest Morfac value for their experimental idealized case.

The hindcasting morphodynamic behavior was studied by Dam G. et al., (2015) for the Western Scheldt estuary. They simulated two different time periods of 110 years and 65 years and compared results with the bathymetric maps. The process based model FINEL2D was used with the unstructured triangular grid giving seaward astronomical tidal boundaries 40km away from the coastline taking influence of only tidal effects ignoring wave action. They used Morfac value 24.75 for speeding up the morphological simulations with one neap-spring cycle representing a morphodynamic year. They calibrated model using water level at the tidal stations and validated model for tidal currents in both the channels and inter-tidal areas with good correlation between the simulated model results

and the field data. They used BSS for comparison and concluded that the model results getting better with time were independent of the initial bed level. They explained the reasoning for low initial BSS value as model takes time to adjust the bathymetry with model parameter settings, processes and boundary conditions. Roelvink and Reniers (2012) described a method to obtain and verify the morphological tide by performing an analysis on the sediment transport during a spring neap cycle.

Moerman E. (2011) investigated methods and morphological modeling approaches using DELFT 3D. He applied Input reduction method using morphological tide and acceleration method using morphological acceleration factor to reduce the computational time. He formed the harmonic water level boundary conditions using morphological tide with tidal constituents M_2, O_1 and K_1 multiplying them with scaling factor 1.08 for tidal energy preservation. They calibrated the morphological model simulating five years of change and compared the development by comparing the erosion and sedimentation results of the river mouth computing bed elevation differences. During calibration it was found that the model was over-predicting the results, hence after several trial-and error pragmatic methods, he concluded that using no scaling factor gave more desirable morphological results. The morphological acceleration factor was given for each successive tide of different offshore wave boundary conditions. They used BSS for analyzing model results by comparing the modeled and measured bed level changes with initial bed level.

Van der Werf et al., (2015) described process based model formation for Scheldt estuary using DELFT 3D for predicting the morphological development of the mouth on account of natural processes and human interferences. They developed high resolution model for hindcast simulation from year 1985-2011 construction of Zeebrugge harbour studying effects of tides, currents, waves, winds and river discharge for the hard non-erodible

bed layers. In order to reduce the computational time, they split model domain into five online-coupled domains using domain decomposition. They used morphological acceleration factor 104 to reduce the computational timing in which simulation of one spring and neap cycle of 14 days resulted into morphological changes for 4 years. At the same time they used Mormerge technique where wave effects were efficiently included by running different wave conditions in parallel, sharing same bathymetry updated every time step. They compared the bed level changes obtained by computations using different morfac values. They computed the volumetric changes and concluded that with time, differences became smaller.

To accelerate the morphological model, two approaches Morfac and Mormerge were tested by Wilmink R.J.A. (2015). He developed morphological model for predicting 10years of morphological development for uniform sandy coastal and offshore area of Ijmuiden using DELFT 3D. He used input reduction method forming morphological tide composed of harmonic tide of two consecutive tidal cycles. He schematized waves using Optimum selection method. The simulation results were compared with the reference simulation comparing the reduced and non-reduced input conditions using performance indicators Nash-Sutcliffe coefficient (NS) and BSS with the resultant value as 0.98 and 0.958 respectively. The resultant ten yearly morphological developments showed similarity with the observed morphological development. They compared Morfac and Mormerge using Multi-Criteria-Analysis (MCA) and found very little differences obtained in simulation results using morfac and Mormerge. They concluded Morfac performing better when climate with two and six waves used while Mormerge performed better in case of ten wave classes used.

George D.A. et al., (2006) modeled restoration feasibility of Deschutes estuary by the action of tidal and storm processes using DELFT 3D. They extracted twelve tidal constituents as dominant contributors to tide

representing the tidal height of the model boundary. For river schematization and reducing the computational time and effort, they mentioned need of input reduction technique for representing full year tide. They formed harmonic morphological tide using tidal constituents M_2 multiplying it with scaling factor 1.1 and accelerated simulations using morfac. They developed models for simulating high tidal heights and flood events and validated the hydrodynamics and salinity simulation results. They observed similar patterns of erosion and deposition occurred at the restored estuary with some localized differences.

Stark J. (2012) used domain decomposition method creating three coupled orthogonal curvilinear grids decomposing model into sea, estuarine and river domains as it decreases the computational time. The model boundary was surrounded by four open boundaries where sea domain was forced with water level boundaries forcing harmonic tidal constituents M_2 and C_1; the north and south end of model were forced with Neumann boundaries imposing an alongshore water level gradient making possible for internally generated currents to propagate out of the model undisturbed. The model boundary was closed with no movement of sand or water passing through them. He used tidal schematization for long-term morphological simulation using input reduction method applying morphological tide for reducing the computational time taking into the account the condition of morphological tide leading to the pattern of residual sediment transport similar to that that represented by a total spring neap tidal cycle. Author followed Lesser (2009) work and applied scaling factor 1.0 to M_2 constituent only adjusting time period of total tide as 1490 minutes and a period of 745 minutes for M_2. To speed up the morphodynamic simulation, variable morphological acceleration factor were used with the wave climate schematization.

Various long-term morphological studies have been performed using input reduction method and acceleration method for reducing the computational

efforts, time and money. The reduction of water level model boundary conditions using morphological tide formed with tidal constituents M_2 and C_1, where C_1 is composed of O_1 and K_1 have been widely used and implemented for long-term morphological simulations. For tidal energy preservation, the tidal constituent M_2 has been multiplied with scaling factor for amplification. At the same time morphological acceleration factor has been used to multiply the hydrodynamic forcing sediment fluxed to and from the bed for overcoming the time scale difference with hydrodynamic scales and morphodynamic scale development. Morphological acceleration factor has been considerably used for reducing the large computational time. Brier Skill Score has been used for evaluating the morphological model results which compares the modeled bathymetry obtained with the higher Morfac value with the benchmark simulation run with morfac 1. The accelerated and non-accelerated morphological simulation bathymetry results were compared and the resultant BSS values showed if the model performed well.

Sahu A. (2019) studied shoreline response to tidal storms and sea level rise using numerical modeling. Flow wave coupled model was developed using Delft 3D and validated the model with insitu water level and wave data. The model output was given as input in the XBeach model and computed shoreline response along the beach and validated with field surveys. The effect of relative sea level rise on beach erosion for projected for years 2020, 2030 and 2070 and was found that consistent beach erosion occurred due to relative sea level rise.

Valchev et al., (2018) formed and validated Delft3D Flow and Wave coupled model. They used XBeach for further implementing a coastal forecasting system for Varna Beach in Bulgaria. The system formed with coupled wave and flow interactions with sea level rise effect and change in coastal morphology helped in improved understanding of the effect of storm effects on the long-term shoreline evolution.

Enriquez A.R. et al., (2016) assessed impacts of sea level rise and waves on shoreline migration on the Balearic Islands in Western Mediterranean. They chose combination of SWAN – SWASH models to reproduce the shoreline variability within a reasonable accuracy. They projected shoreline changes under climate scenarios of sea level and wave climate with major assumption that the morphology of the beach will not change in the future. They assumed that both the beach shape and the profile will be the same under the climate conditions at the end of the century. They demonstrated that the changes in beach profiles play minor role in shoreline changes due to waves and sea level rise.

Van der Wegen, M. (2013) studied effect of sea level rise on tidal basin morphodynamics using numerical modeling. It was found that the sea level rise rate led to the disappearance of the intertidal area and basin shifted to sediment import system from sediment exporting. This led to disturbance in the tidal propagation balance developing tidal asymmetry with emergence of M_4 overtide and sediment transport shift. The effect of waves was identified as sediment supply due to littoral drift towards the mouth of the basin which later may get transported into the basin.

With the reported benefits and limitations and the discussed conclusion of various long-term morphological simulation studies carried out with techniques implemented for reducing the high computational time and efforts, this study shall perform long-term morphodynamic development simulations using the two widely accepted and implemented techniques - Input Reduction Method and the Morphological Acceleration Method forming reduced morphological tide and choosing morphological acceleration factor respectively.

2.2 Data Collection

To assess the shoreline migration and predict the morphological development of the bay, various data sets of study area were prepared for giving input in the model.

2.2.1 Bathymetry

Kakinada Bay bathymetry was obtained from field work, C-Map data and GEBCO data. Bathymetry Survey was done for Kakinada Bay in April 2016 using Single Beam Echosounder interfaced with a Digital Global Positioning System connected to the on a fishing trawling boat attached with Heave sensor which helps for correction of the boat's roll, pitch and roll. Single beam echosounder is the mostly used Sonar systems indicating water depth. It works on the principle of measuring time taken by a pulse traveling from the sonar transducer to the surface of the bottom of the sea and again back up to the sonar transducer.

$$Z=t*c/2 \quad (1)$$

Where Z = depth, t = time between signal transmission and reception, c = average speed of sound.

Before starting the bathymetry survey, the grid with transects was made with coordinate information for the route to be followed for the data collection. This grid data with the coordinates of transects was fed into the HYPACK data collection software which helped the boat in following the planned track. Water depth soundings were provided by the variable frequency transducer and the coordinates of the depth points were obtained from the DGPS that was connected to the transducer with a serial cable and an antenna. The data was recorded with the information comprising of date, time, latitude, longitude and depth. The depth is given by the equation 1.

Tidal corrections were made and data was converted to xyz format, uploaded in Delft 3D and interpolated to get the Depth file.

2.2.2 Water Sample Collection

Water samples were collected using NINSKIN bottle sampler for suspended sediment analysis. A Niskin Bottle is device used for water sample collection at a specific depth. Niskin bottle was used to collect one liter of seawater sample at surface and the near bottom. It is a plastic cylinder with lids at both the ends connected by an elastic cord cable. Water sample collected by lowering the open bottle into the water on a wire until it reaches the required depth and then a weighted trigger called as messenger gets the bottle closed through a small weight encircling the drop line of the sampler when sent down the cable. For all the locations, 1litre of sample was collected.

2.2.3 Suspended Sediment Concentration

The collected water samples were used to analyze the suspended sediment concentration at various locations of the bay. The suspended sediment concentration was analysed by collecting the sediments in the filter. The analysis was done using Gravimetric method after filtration. For the filtration purpose Whatmann filtration papers were used which are glass microfiber filter with a nominal pore size of 0.45µm. The filter paper was weighed first and a well-mixed seawater sample was poured into the crucible. Thereafter with the help of weighed standard Whatmann filter paper, it was filtered. In order to accelerate the filtration process, a vacuum pump was connected to the crucible using a pipe which accelerated the suction speed to fasten the process. After filtering the water sample, the filter paper was dried at 103-105°C for one hour in an oven to a constant weight. After the filter papers got completely dried, they were weighed and the initial weight of the filter

paper was subtracted from the oven-dried filter paper with sample weight. Thus suspended sediment was quantified in grams per liter of sample.

2.2.5 Data obtained from institutes

The observed tide, wave and current data was obtained from Kakinada Seaports Ltd. for the month of September 2011 (Table 2.1) (Figure 2.6).

Table 2.1. Data Collection

S.No.	Parameter	Location	Period	Source
1	Tide	16°58.588'N 82°16.994 E	September 2011	Kakinada Seaports
2	Wave	16°23.400'N 82° 55.200'E	September 2011	Kakinada Seaports
3	Current	16°58.800'N 82° 18.899'E	September 2011	Kakinada Seaports
4	Sediment	Kakinada Bay	February 2015	Field Work

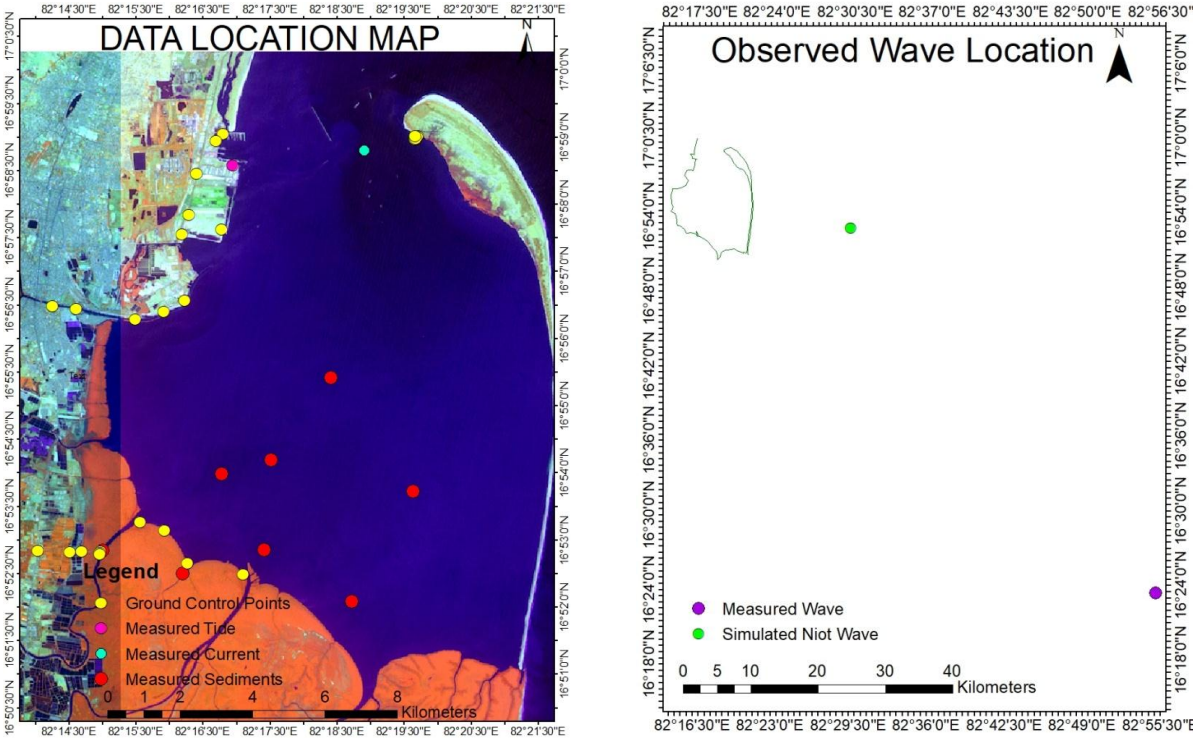

Figure 2.6. Measured Tide, Waves, Current, suspended sediment concentration and ground control points locations for validation.

2.3 Satellite Data Collection

The landsat images were chosen for the study as they are freely widely available for good spatial coverage with higher resolution and provide mostly cloud free images for long span of time. Landsat images for years 1977, 1988, 2000, 2013 and 2019 were used to analyze decadal shoreline changes as shown in table 2.2. These four years were chosen for study to analyze decadal progression of mangroves towards the sea. A suite of Landsat images including a Landsat Multi Spectral Scanner (MSS) data (1977), a Landsat Thematic Mapper (TM) image (1988) and Landsat Enhanced TM Plus (ETM+) image (2000) were obtained from landsat.org. Landsat 8 (Operational Land Imager, OLI) image (2013 and 2019) were obtained from Earthexplorer website. There are seven spectral bands in Landsat TM data with a spatial resolution of 30 m for bands 1–5 and 7. There are nine

spectral bands in Landsat 8 with 30m resolution for band numbers 1–7 and 9. Cloud cover was less than 10% for these images. All the images were obtained at the similar tidal phase to reduce the tidal errors. The landsat images were selected with acquisition time at low tide time period of sea level so that the maximum coastal zone gets exposed and mangrove boundaries could be determined and extracted accurately as much possible. For reducing the tide-influenced errors, the tidal conditions at image acquisition time were noted down as suggested by Reshma, K.N. and Murali, R.M. (2018). Although Mangroves are evergreen and are known to be not highly different in their phenology during different times and seasons of the year as reported by Nair S. (2017); images were selected picking up the best image without cloud coverage from the period of months of October-March which are months of late winters and early spring as they play critical roles in mangrove mapping. These cold months increase the phenology signatures of mangroves; hence the accuracy of mangrove mapping increases as reported by Li, H. et al., (2019).

Table 2.2 Details of multi-temporal satellite data products, acquisition date and time and the tidal condition

S.No	Satellite	No. of Spectral Bands	Path/ Row	Acquisition Date	Acquisition Time	Resolution (m)	Tidal Height (m)
1	Landsat MSS	4	P 152 R48	08/01/1977	04:40:00	60	0.23
2	Landsat 5 TM	7	P 141 R48	12/10/1988	04:40:00	30	0.16
3	Landsat 7 ETM+	8	P 141 R 48	08/12/2000	04:40:00	30	0.38
4	Landsat 8	9	P 141 R48	21/03/2013	04:40:00	30	0.27
5	Landsat 8	9	P 141 R48	27/03/2019	04:40:00	30	0.28

CHAPTER 3

QUANTIFICATION OF SHORELINE CHANGE INSIDE KAKINADA BAY USING REMOTE SENSING AND GIS

3.1 Digital Shoreline Analysis System

In order to study the progression and regression rates of mangrove shoreline and its movement, the analysis of rate of change of shoreline was computed in the Digital Shoreline Analysis System 4.3 (DSAS), developed by the USGS as an ArcGIS extension. DSAS computes the rate of change statistics of shoreline using multiple historic shorelines in GIS with respect to the baseline position at user specific intervals (Thieler, E.R., 2009). DSAS is an effective tool that helps in Historical Trend analysis for examining the present and past mangrove shoreline position measuring the changes at the casted transects from a defined baseline as it incorporates an identified attribute position at different time periods.

3.2 Methodology

3.2.1 Shoreline Extraction

The Landsat MSS, TM and ETM+ imageries obtained for 1977, 1988, 2000 and 2019 were subjected to correction for the geometric errors using the reference image of 2013 Landsat 8 (OLI) in ArcGIS. Geometric rectification is done to remove errors as remotely sensed coordinates vary from image to image due to earth's rotation and panoramic distortions during acquisition of images (Elnabwy, M.T. et al., 2020). The process removes the geometric anomalies and corrects the coordinates of images with the correct ground coordinates with the pixel location. All images were corrected using 10 ground control points, selected from different features during ground

truthing exercise at Kakinada Spit, Kakinada Port, Kakinada Channel and Coringa Mangroves (Figure 2.6). Total root mean square error (RMSE) was below 1 pixel during rectification of images. Resampling of the geometrically rectified images was carried out using Cubic convolution method registering all images to the 30m pixel size taking year 2013 as base image. These imageries were projected to the Universal Transverse Mercator system (UTM) WGS datum-1984 projection zone 44N.

Mangrove shoreline was digitized using the seaward mangrove forest edge as the shoreline indicator. The closed canopy forest cover was used as the border for distinguishing mangroves from the mudflats and sea (V. Tran Trih., 2014). The Normalized Difference Vegetation Index (NDVI) was used for differentiating vegetation from land and the sea. NDVI is considered as one of the best extensively used feature for quick and easy detection of the living green vegetation cover from other land features. The border pixels differentiating between vegetation, land and sea were delineated as mangrove shoreline.

3.2.2 Shoreline Database Preparation

All shorelines were compiled in the GIS geodatabase with 5 attribute fields which include Object ID (a distinct number for each transect), shape (poly line), shape length, ID, and date (year). All shorelines were appended into a single shape file. A baseline which is a reference datum used in DSAS model was casted offshore and parallel to the general orientation of shorelines. It is the initial point to cast transects at closest intersection using simple baseline cast method, crossing the shorelines and providing change over time. 41 transects were casted at 500m length interval at right angles from shoreline stretch of 20.5km (Figure 3.1). In order to calculate the rate of erosion and accretion three mostly used statistical indices EPR, NSM and LRR were employed for a period of 43 years.

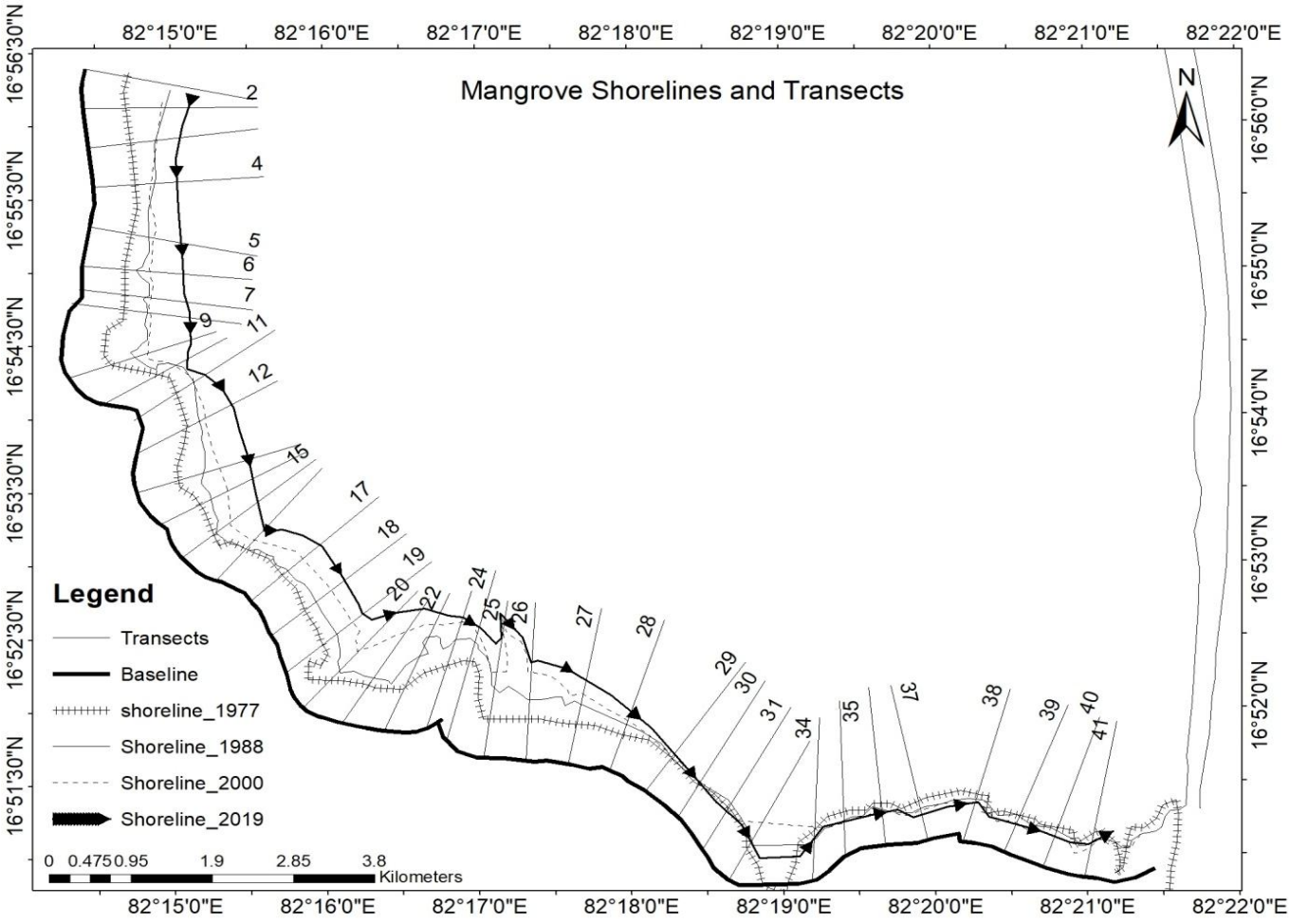

Figure 3.1. Mangrove Shorelines and Transects casted for the study

3.3 Estimates from Digital Shoreline Analysis System- EPR, NSM, LRR

The shoreline migration trend has been successfully studied using the statistical parameters EPR, NSM and LRR.

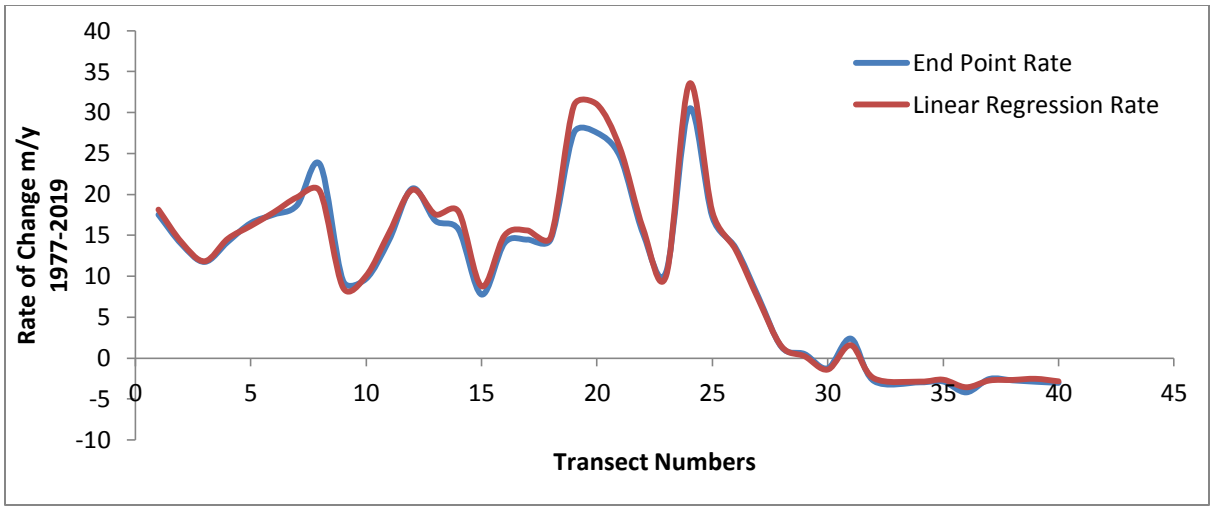

Figure 3.2. Shoreline change rate for the period 1977-2019.

The shoreline rate changes are compared for EPR and LRR. The trend differences between indices EPR and LRR is shown in figure 3.2. It indicates the consistent variations in the rate of accretion and erosion of the shoreline. Accretion zones are demarcated in the figure from transects 1-29. The shoreline is receding at transect 30 and from 32-41 transects. The average accretion rate is found to be 14.98m.y^{-1} while the erosion rate has been found as -2.8m.y^{-1}. Transects 30 and 31 have been relatively stable and very less shoreline change has occurred in this area with the lowest shoreline index values.

Figure 3.2 illustrates that Coringa mangrove shoreline has accreted in general over the period of 36 years. The major area accreted is at transect 25 with the end point rate at 30.46m.y^{-1} and linear regression rate at 33.51m.y^{-1}, while the region with the least accretion is at transect 30 with the end point rate at 0.49m.y^{-1} and linear regression rate at 0.22m.y^{-1}. EPR and LRR with maximum erosion are at transect number 37 at -4.19m.y^{-1} and -3.56m.y^{-1} respectively. The average accretion rate of EPR and LRR for the whole shoreline stretch is 14.98m.y^{-1} and 15.50m.y^{-1} respectively while the average erosion rate of EPR and LRR is -2.8m.y^{-1} and -2.63m.y^{-1}

respectively. Thus it has been found that there has been pro-gradation of mangrove shoreline towards the sea for a major part of the shoreline at high shoreline change rates as shown in table 3.2.

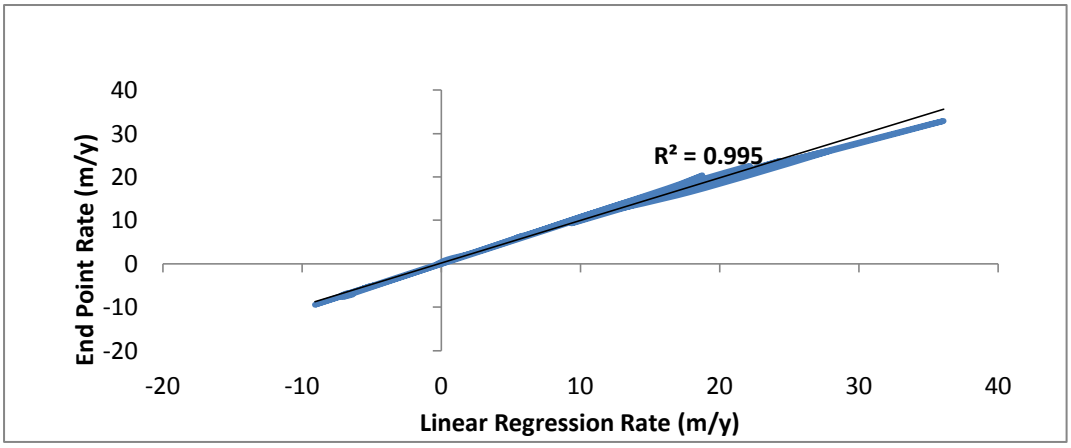

Figure 3.3. Shoreline change rates (End Point Rate and Linear Regression Rate)

The mangrove shoreline change rate obtained by the statistical methods EPR and LRR is very similar throughout the study area. The comparison of EPR and LRR results as shown in figure 3.3 presents the R^2 value for the period 1977-2019 as 0.995 which is highly correlated. The graph infers that the dependent and independent variables are in good correlation.

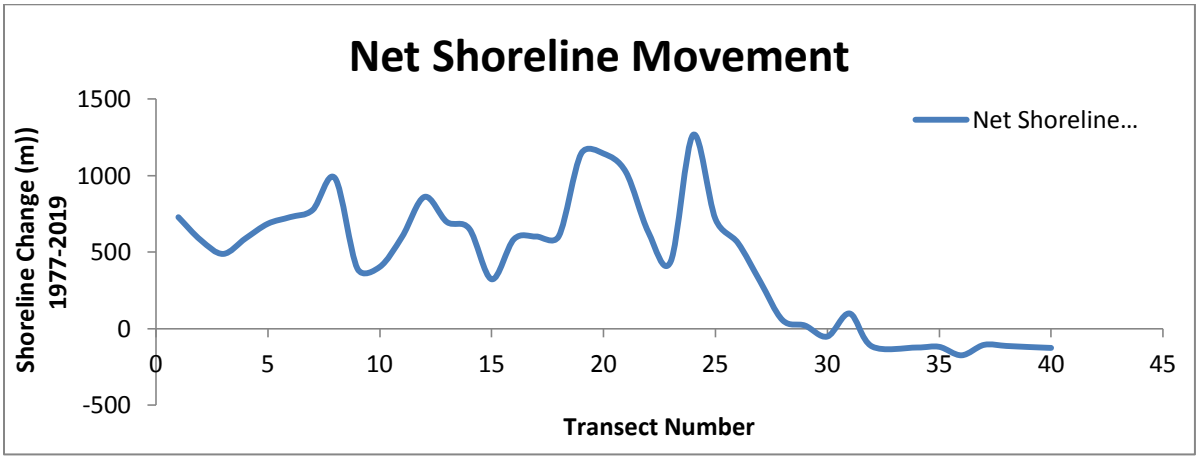

Figure 3.4. Shoreline change at each transect was expressed by the Net Shoreline Movement (NSM) for period 1977-2019.

The average accretion rate for the period was found to be 14. 98m.y^{-1} (EPR), 15.5m.y^{-1} (LRR), and erosion rate was -2.8m.y^{-1} (EPR) and -2.63m.y^{-1} (LRR).

The mangrove shoreline movement in the study period has changed differently in the bay dividing it into two different zones of accretion and erosion. The results have shown the mangrove shoreline movement significantly accreting from the western side of the bay till half of the southern side of the bay. While thereafter, the shoreline has undergone a recession for the other half of the southern part of bay reaching the spit. Mangroves have undergone significant progradation at the western side of the bay with maximum movement over transects 9, 20 and 21 with a distance of 983.41, 1144.22 and 1144.57m respectively (Figure 3.4). At the southern portion of the bay, maximum distance accreted by mangrove shoreline is 1266.55m at transect 25. The different behavior of two different parts of the mangrove shoreline stretch undergoing accretion and erosion in the western and the eastern side of the bay observed in the entire period is presented in table 3.2. The results indicate the hydrodynamic forcing leading to the sediment deposition at the western part of the bay.

Table 3.1. Overall Shoreline Changes from year 1977-2019

Shoreline Statistics	Erosion	Accretion
Average End Point Rate (m.y^{-1})	-2.8	14.98
Average Linear Regression Rate (m.y^{-1})	-2.63	15.50
Average Net Shoreline Movement (m)	-116.57	622.5

Table 3.1 shows that the mangrove shoreline stretch is significantly prograding with the high rates of shoreline accretion, while quite less shoreline stretch has receded at a very less rate of shoreline erosion.

Table 3.2 Shoreline change rate comparison between the Western and South-Eastern part of the bay from year 1977-2019

Statistics	Western Part of the Bay	South-Eastern Part of the Bay
Number of Transects	25	15
Number of Transects undergoing Erosion	0	11
Number of Transects undergoing Accretion	25	4
Mean Shoreline Change ($m.y^{-1}$)	16.96	1.41
Erosion Rate ($m.y^{-1}$)	0	-2.8
Accretion Rate ($m.y^{-1}$)	16.96	7.06
Maximum Erosion Rate ($m.y^{-1}$)	0	-4.19
Minimum Erosion Rate ($m.y^{-1}$)	0	-1.24
Maximum Accretion Rate ($m.y^{-1}$)	30.46	17.23
Minimum Accretion Rate ($m.y^{-1}$)	7.76	-1.24

The overall results presented in table 3.2 show that there has been significant accretion in the southwest of the Bay, while there was some erosion of mangrove shoreline towards the southern end of Kakinada spit. 25 transects are considered in the western side of the bay, where all transects have undergone accretion with the highest rate of $30.46m.y^{-1}$ at transect number 25. Rest 15 transects at the south-eastern part of the bay have been relatively stable and some have been under erosion with the maximum erosion occurred at transect 37 with an average erosion rate -$4.19m.y^{-1}$. Very less accretion has occurred in the south-eastern part with the highest accretion rate of $17.23m.y^{-1}$ at transect 26 and least accretion rate of $0.49m.y^{-1}$ at transect 30.

CHAPTER 4

NUMERICAL SIMULATION OF THE HYDRODYNAMICS AND SEDIMENTATION OF KAKINADA BAY

4.1 Numerical Modeling

To study the hydrodynamics and sedimentation inside the bay, process based model has been set up using Delft 3D. Deltares and Delft University of Technology developed Delft3D modeling system. It provides computation of hydrodynamics in coastal areas. Delft 3D is a computational fluid dynamics model that helps in hydrodynamic, sediment dynamics, wave dynamics study.

4.1.1 Numerical Grid

Delft 3D uses the orthogonal curvilinear or rectangular grid in horizontal plane to compute Delft3D equations. Delft 3D uses Arakawa C-grid for discretization of hydrodynamics variables like water level and velocities (u and v). The water level points are defined in the cell centre while the components of velocity are perpendicular to the faces of the grid cell.

Five components Bed level point (zb), water level points (ζ), velocity points in horizontal and vertical directions (u and v), suspended and bed level transport rates in both vertical and horizontal directions. Water level points are locations for computation of water depth, sediment concentration and sediment transport rates. The staggering becomes important when specifying the boundary conditions and interpreting the results. The spatial arrangement of variables of the Delft 3D model in horizontal plane is presented in figure 4.1.

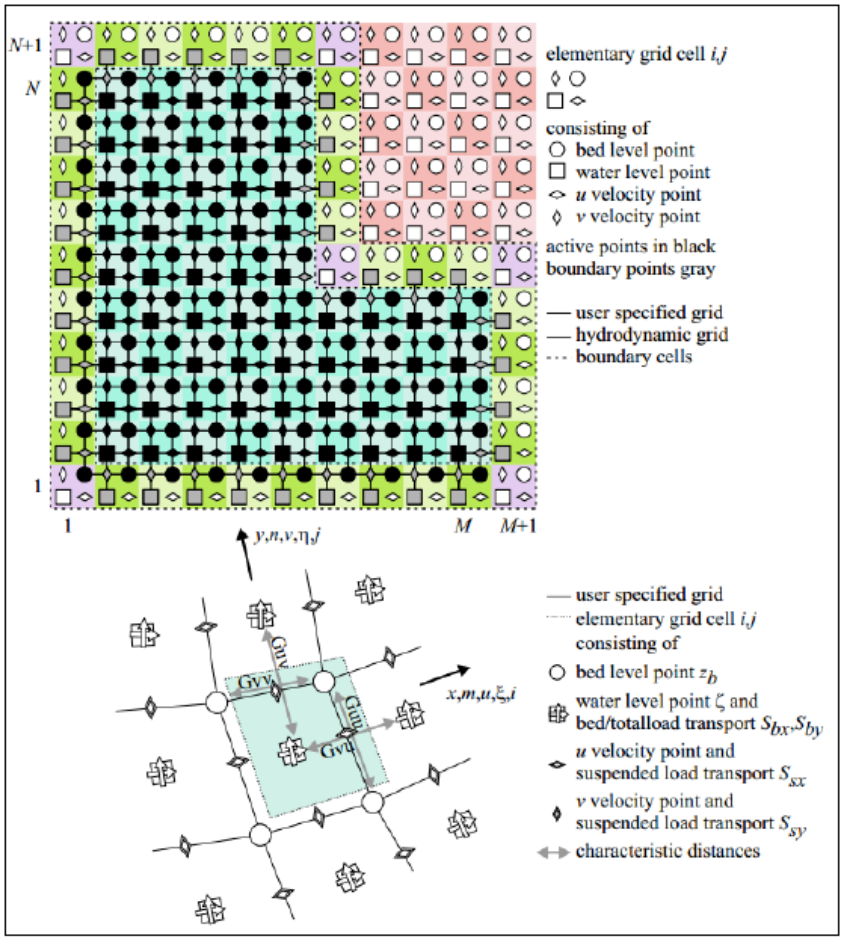

Figure 4.1. Spatial arrangement of variables of the Delft 3D model in horizontal plane. (Source: Jagers, 2003).

Modeling approach followed in Delft 3D is the calculation of the hydrodynamic flow on a boundary fitted grid to which bathymetry, initial conditions and boundary conditions are applied. Sediment transport is calculated using the flow and wave model with the applied sediment transport formula. The morphological development of the model is dependent on the sediment transport. The processes of flow, waves, sediment transport and updation of morphological development are all executed at every time step according to the 'online' approach (Roelvink, 2006, Figure 4.2)

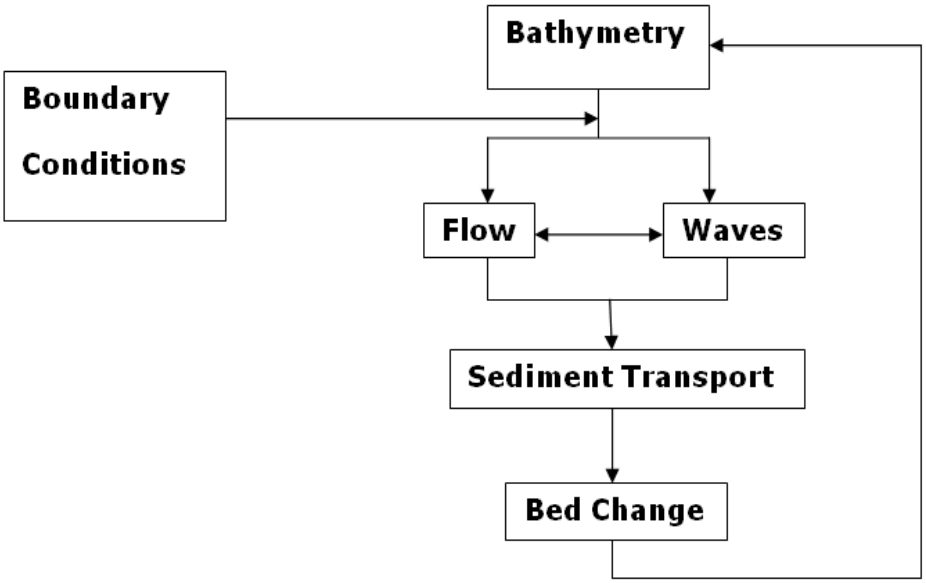

Figure 4.2. Overview of Delft 3D calculation steps (Source: Roelvink, 2006)

Delft3D-FLOW and WAVE modules are used in this study. Delft 3D Flow module is the main component of Delft 3D package. Delft3D-FLOW simulates the non-steady flow, sediment transport and morphology (Lesser et al., 2004, Deltares, 2010a).It simultaneously computes and updates the flow hydrodynamics, sediment transport and morphological changes along with the calculation of salinity, heat and tracer, etc. Delft 3D-Flow includes many processes like waves, tides, wind, density driven flows, salinity and temperature gradient stratification, atmospheric pressure changes, drying and flooding events, etc. (Lesser et al., 2004). Delft3D-WAVE simulates the short waves evolution with the application of SWAN-model (Booij et al., 1999). The action of tidal and meteorological forcing on the boundary fitted grid is calculated by computing the non-steady flow and transport process (Deltares, 2011a). This numerical model solves the unsteady shallow-water equations based on finite differences computing the continuity equation, horizontal momentum equations and transport equation.

Delft 3D Model

Delft 3D package is comprised of various models like Flow model, Wave model as described here.

4.1.2 Flow Model

Delft 3D Flow model calculates non-steady flow by action of wind, wave and tides composed of horizontal momentum equations, continuity equations in 2-D depth-averaged dimension. The horizontal momentum equations are represented as Eq. 2 and 3:

$$\frac{\partial U}{\partial t} + U\frac{\partial U}{\partial x} + V\frac{\partial U}{\partial y} + g\frac{\partial \eta}{\partial x} - fV + \frac{\tau_{bx}}{\rho_{w(d+\eta)}} - \frac{F_x}{\rho_{w(d+\eta)}} - v\left(\frac{\partial^2 U}{\partial x^2} + \frac{\partial^2 U}{\partial y^2}\right) = 0 \quad (2)$$

$$\frac{\partial V}{\partial t} + U\frac{\partial V}{\partial x} + V\frac{\partial V}{\partial y} + g\frac{\partial \eta}{\partial x} + fV + \frac{\tau_{by}}{\rho_{w(d+\eta)}} - \frac{F_y}{\rho_{w(d+\eta)}} - v\left(\frac{\partial^2 V}{\partial x^2} + \frac{\partial^2 V}{\partial y^2}\right) = 0 \quad (3)$$

where U, V are depth averaged velocity ($m.s^{-1}$), g is the acceleration due to gravity ($m.s^{-2}$), d is the water depth below the reference plane (m), f is the Coriolis Parameter ($1.s^{-1}$), $F_{x,y}$ is the x and y component of external forces ($N.m^{-2}$), ρ_w is mass density of water ($kg.m^{-3}$), v is diffusion coefficient (eddy viscosity) ($m^2.s^{-1}$), η is water level variation above plane of reference (m) and $\tau_{bx,y}$ is x and y component of bed shear stress ($N.m^{-2}$).

The depth averaged continuity equation is represented below as Eq. 4:

$$\frac{\partial \eta}{\partial t} + \frac{\partial [d+\eta]U}{\partial x} + \frac{\partial [d+\eta]V}{\partial y} = 0 \quad (4)$$

These equations are computed on a finite difference grid along with the boundary conditions of water level and horizontal velocities.

4.1.3 Delft 3D SWAN model

Delft 3D SWAN model is used here which is a stand-alone application used to simulate wind-generated waves in coastal areas. SWAN stands for Simulating WAves Nearshore. The Delft3D WAVE module (SWAN - **S**imulating **WA**ves **N**earshore) simulates the evolution of random short-crested waves in water bodies like tidal inlets, estuaries among others. SWAN model is fully spectral in frequencies and directions and the wave computations are absolutely stable (Deltares, 2011b).

The short wave energy, Ew is computed by the energy flux balances using Eq. 5.

$$\frac{\partial \mathrm{Ew}}{\partial \mathrm{t}} + \frac{\partial \mathrm{EwCgcos}(\theta)}{\partial \mathrm{x}} + \frac{\partial \mathrm{EwCgcos}(\theta)}{\partial \mathrm{y}} = -\mathrm{Dw} \qquad (5)$$

Where cg is the group velocity, ϴ is the angle of incidence of x-axis, x is the cross-shore distance, y is alongshore distance, and Dw is dissipation of wave energy.

4.1.4 Sediment Transport

The Delft 3D sediment transport module computes suspended load transport of cohesive sediments and both bed load and suspended load transport of both cohesive and non-cohesive sediments (figure 4.4).

Sediments are classified as mud, sand and silt fractions where mud is classified as cohesive bed load transport, sand is classified as non-cohesive bed load and suspended load transport and silt is classified as transition between cohesive and non-cohesive sediments (Deltares, 2014) shown in figure 4.3.

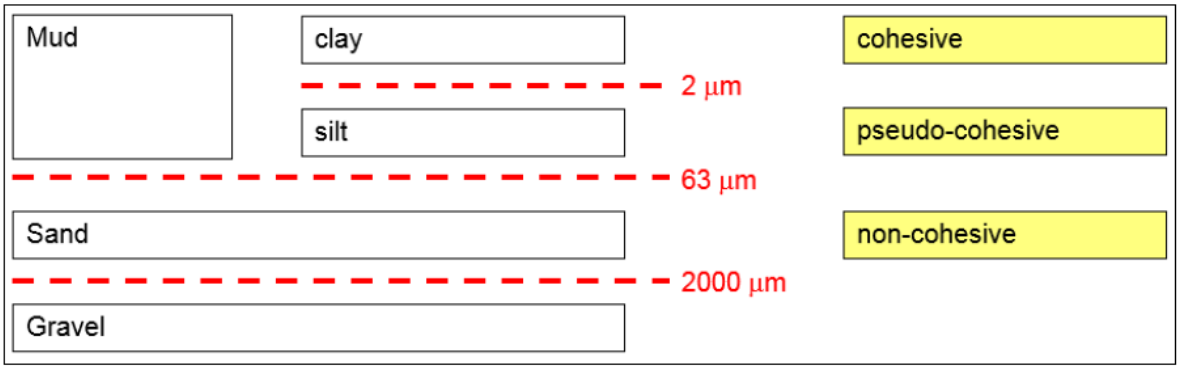

Figure 4.3. Sediment Classification in Delft 3D (Source: Deltares, 2014).

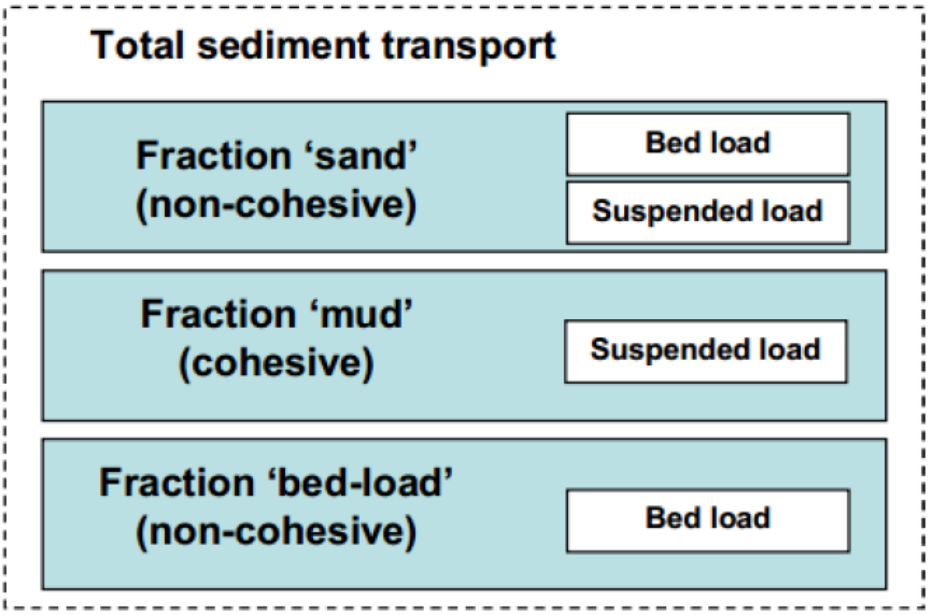

Figure 4.4. Classification of Sediment Transport modes in Delft 3D (Source: Deltares, 2013).

Advection-diffusion equation is used to calculate suspended sediment transport as suggested by Deltares (2012) presented in Eq. 6:

$$\frac{\partial c}{\partial t}+\frac{\partial uc}{\partial x}+\frac{\partial vc}{\partial y}+\frac{\partial (w-ws)c}{\partial z}=\frac{\partial}{\partial x}\left(DH\frac{\partial c}{\partial x}\right)+\frac{\partial}{\partial y}\left(DH\frac{\partial c}{\partial y}\right)+\frac{\partial}{\partial z}\left(DV\frac{\partial c}{\partial z}\right) \quad (6)$$

Where c is suspended sediment concentration ($kg.m^{-3}$); u, v and w are velocity components in x, y and z directions respectively ($m.s^{-1}$); w_s is the

settling velocity of the sediment ($m.s^{-1}$), and Dh and DV are horizontal and vertical eddy diffusivity ($m^2.s^{-1}$).

Partheniades-Krone formulations are used to calculate erosion (Er) and deposition rates (Dr) ($kg.m^{-2}.s^{-1}$) for cohesive sediments as shown in Eq. 7 and 8:

$$Er=M(\frac{\tau b}{\tau cr,e}-1) \text{for } \tau b > \tau cr,e \text{(else} Er=0) \quad (7)$$

$$Dr= w_s c_b(1-\frac{\tau b}{\tau cr,d}) \text{ for } \tau b < \tau_{cr,d} \text{ (else } Dr=0) \quad (8)$$

Where M denotes the erosion parameter ($kg.m^{-2}.s^{-1}$), τb is bed shear stress ($N.m^{-2}$), τ_{cr} is critical bed shear stress for initiation of the erosion ($N.m^{-2}$), Cb is the near bed sediment concentration ($kg.m^{-3}$) and $\tau_{cr,d}$ is the critical bed shear stress for deposition ($N.m^{-2}$). At the simulation end, time-integrated deposition and erosion rates are subtracted to calculate the net deposition representing the morphological changes.

Settling velocity Ws is calculated using Eq. 9:

$$Ws = \frac{(S-1)g\,(dsphere)^2}{18v} \quad (9)$$

Where S is the relative density obtained using Eq. 10:

$$S= \rho s/\rho \quad (10)$$

Where, ρs is sediment density, ρ is the fluid density, g is the acceleration due to gravity, ν is the kinematic viscosity coefficient and dsphere is the equivalent spherical settling diameter.

Critical bed shear stress $\tau b, cr$ is calculated using Eq. 11:

$$\tau b, cr = (\rho s - \rho)\, g\, d50 \text{ } cr \quad (11)$$

where, θ_{cr} is the critical Shield's parameter for incipient motion of sediments.

4.2 DELFT 3D Model Description & Set Up

For hydrodynamic modeling, the working domain is composed of data groups like grid, bathymetry and thin dams. Grid formation is the initial and the most crucial step which uses the grid generator program of Delft3D modeling suite called RGFGRID which helps in generating a grid using either Cartesian or spherical co-ordinates of the requisite resolution. In this study grid for hydrodynamics and wave modeling was set up using the Cartesian coordinate system in the horizontal. The grid represented the study area by curvilinear orthogonal grid (M*N) in horizontal plane using 433 * 487 grid cells with grid size dx and dy 10m and 40 m near bay shoreline and Kakinada Spit and 58m and 60m in the bay respectively as shown in figure 4.5. The grid size was chosen ensuring the feasible computational time and effort taken for the large morphodynamic simulations covering the whole area of Kakinada Bay and the outer sea. Grid criteria was maintained by keeping orthogonality of grid less than 0.4, aspect ratio between 1 to 2 and smoothness less than 0.1. The bathymetry of the study area is presented in figure 4.6.

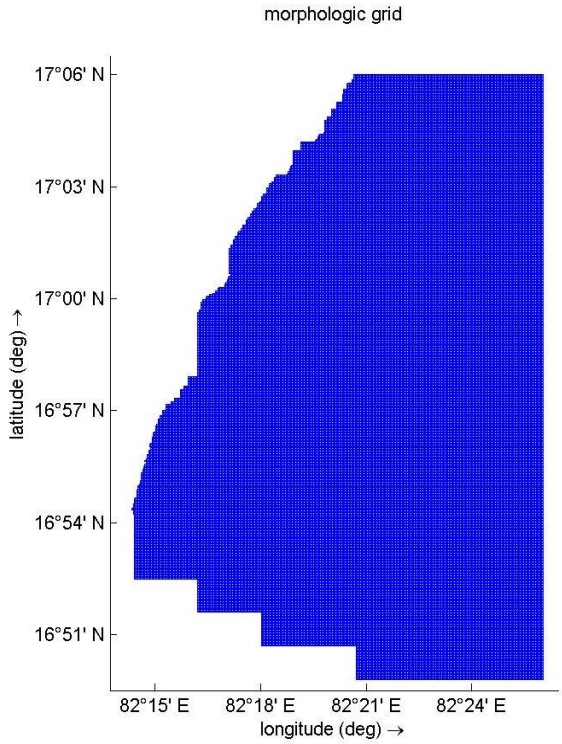

Figure 4.5. The computational grid for the Flow and Wave model.

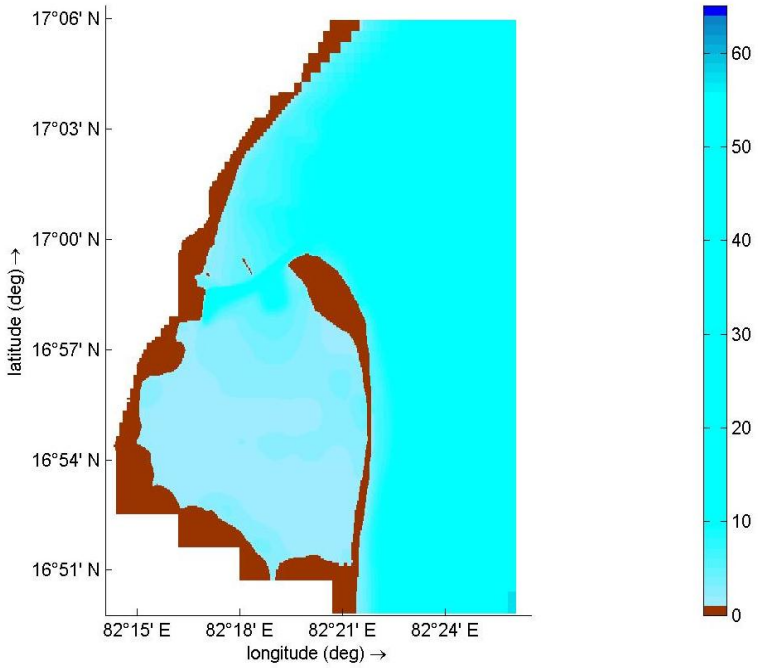

Figure 4.6. Interpolated Bathymetry of Flow and Wave model.

With Cartesian coordinate system, the latitude and orientation of the model grid was specified which helps in determination of Coriolis force of that location. The number of layers was set to 1 for the depth averaged computation.

Bathymetry of the study area was non-uniform and space varying obtained by combining the echo sounding measurements and the available bathymetric charts and data for the most elaborate depth data bringing them to the same reference level. The depth values of the grid were interpolated using volume preserving triangulation interpolation method with the help of QUICKIN program to obtain bathymetry resembling the natural bathymetry closely with equality of averaged bathymetric features. In order to reduce the noise and the wave frequency disturbances, the bottom gradients were smoothened.

Thin dams are the infinitely thin objects defined at the velocity points prohibiting the exchange of flow between the two adjacent computational cells which represent small obstacles like breakwater or dam. Time frame defines the date and time of the start and end of the simulation. Time step used in the simulation was 0.5 minutes based upon the Courant number maintaining the model stability.

The data group provides option for specifying the processes and their initial conditions and the boundaries which influence the hydrodynamic simulations. The transportation process of suspended cohesive sediments was selected as the factor given as input for updating the bathymetry. Initial conditions at the beginning of the simulation were specified into the model for computations to start at. The optimum initial values depend on the boundary conditions and the timing of the start of the simulation. A uniform value of 0.02Kg.m^{-3} was given as initial sediment condition.

Boundary condition for the model was defined with their location and type with all inputs affecting the simulation. Boundary conditions for water level variations due to tides have been imposed at the offshore model. Astronomical water level forcing was given as boundary from the three offshore open boundaries (North, East and South). The astronomical tides are generated from the gravitational effect of Earth, Sun and Moon without any atmospheric influence.

The astronomic tidal forcing at the model boundaries for the initial calibration is defined by thirteen (13) astronomical tidal constituents (M_2, S_2, N_2, K_2, K_1, O_1, P_1, Q_1, MF, MM, M_4, MS_4 and MN_4. The astronomical water level boundary condition is computed using eq 4.1.

$$z_s(t) \quad A_o + \sum_{i=1}^{n} Ai \cos(2\Pi fi - \varphi i) \qquad (4.1)$$

where, $z_s(t)$ is water elevation (m), A_o is mean value of water elevation time-series (m), A_i is the amplitude of the i^{th} constituent (m), f_i is the frequency of the i^{th} constituent (m) and φi is phase of the i^{th} constituent.

The open boundaries were kept far to prevent the boundary effects. Hence the size of study area was kept 25km by 30km. The tidal prediction of water level at the model boundary was derived from the Global Ocean Tide Model. The suspended sediment concentration taken as boundary concentration was based on the measurements made on the field site and taking reference from the literature review. The bed material sediments were cohesive and silty clay bed.

4.3 Numerical stability

Courant number indicates the numerical stability of Delft 3D flow model which should be equal or less than 1. This criterion is fulfilled by specifying the hydrodynamic time step of the flow model. It defines relation between the propagation speed and the time step. The total computational time is

determined by the time step. The Courant number criterion is presented in Eq 4.2 (Deltares, 2014).

$$\mathrm{CFL} = \frac{\Delta t\sqrt{gH}}{\min\{\Delta x,\Delta y\}} \quad \rightarrow \quad \Delta t < \frac{10 * \min\{\Delta x,\Delta y\}}{\sqrt{gH}} \tag{4.2}$$

Where, Δt is time step (s), g the acceleration due to gravity ($m.s^{-2}$), H is the maximum water depth (m) and min $\{\Delta x, \Delta y\}$ is the smallest grid size (m). A time step of 30seconds is given as input in this study. The courant number obtained was 0.8.

Small courant number can be obtained by either decreasing time step or increasing the grid size.

4.4 Model Calibration and Validation

In order for a model to represent an original field, various parameters like bed roughness, eddy viscosity, eddy diffusivity, etc were defined with a certain value that would represent the actual field. For this various simulations were performed by giving various values for tuning these parameters so that the obtained flow model results are in well agreement with the data obtained by field work. This procedure is termed as Model calibration.

4.4.1 Calibration-Resolving unknown model parameters

Various physical parameter constants were defined for the model. The hydrodynamic constants like acceleration due to gravity and water density were defined as $9.81 m.s^{-2}$ and $1000 Kg.m^{-3}$ respectively. The calibration parameters like Bottom roughness, eddy viscosity and diffusivity were varied in the calibration simulation runs according to their potential ranges for the best sought agreement with the local observed tidal level, current velocities and suspended sediment concentrations. Each of the calibration simulation was for a period of 14days. The accuracy of the computed water level and

current velocities with respect to the observed data was expressed through the R^2 and RMSE values.

Chezy coefficient and Horizontal Eddy Viscosity and Diffusivity were used to finely tune and calibrate the current and tidal phase. Chezy bed roughness formulation is a hydraulic bed roughness parameter which parameterises the energy dissipation at the seabed for formulating the bottom boundary closure. The horizontal Eddy Viscosity is a spatially variant but time constant parameter which closes the 2-D momentum equations which can damp the variance in modeled flows. Increased viscosity values reduce the modeled amplitude of maximum flows and tidal elevations.

For the calibrated hydrodynamic model, the best agreement obtained for uniform Chezy's bottom roughness coefficient was 74 in horizontal direction 'U' and 71 in vertical direction 'V'. The calibrated values for both horizontal eddy diffusivity and viscosity were $1m^2.s^{-1}$. Figures 4.8 and 4.9 shows the computed water levels and current velocities generally agree well with the observed field data.

4.4.2 Model Validation

In order to develop confidence in the model, simulation results were validated by comparing with the observed data.

4.4.2.1 Flow Model

The Delft3D flow model was calibrated for period of 15 days from 15th August 2011 to 30th August 2011. The modeled water levels were compared with the in-situ observation results (Figure 4.7). Hydrodynamic simulations were run with the astronomical tidal constituents forced at the open boundaries.

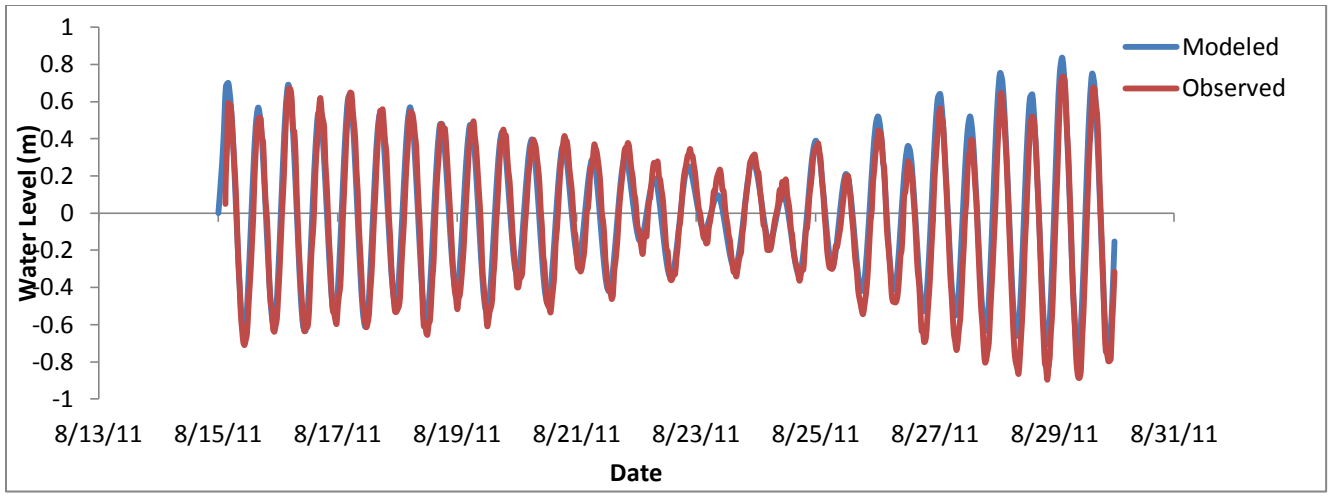

Figure 4.7. Calibration of Flow model by comparing the observed and modeled water levels at the Tide Gauge of Kakinada Port from 15th August to 30th August 2011.

The figure shows that the model was well calibrated. Water levels were compared for modeled and observed data. The Regression Coefficient value was found to be 0.9578. Once model was calibrated, simulation was performed for validating the model.

The validation simulation began on 25th August 2011 and ran for 36days till 30th September 2011 with a time step of 30s. The initial 5days were for reducing the numerical instabilities for the initial model adjustment period.

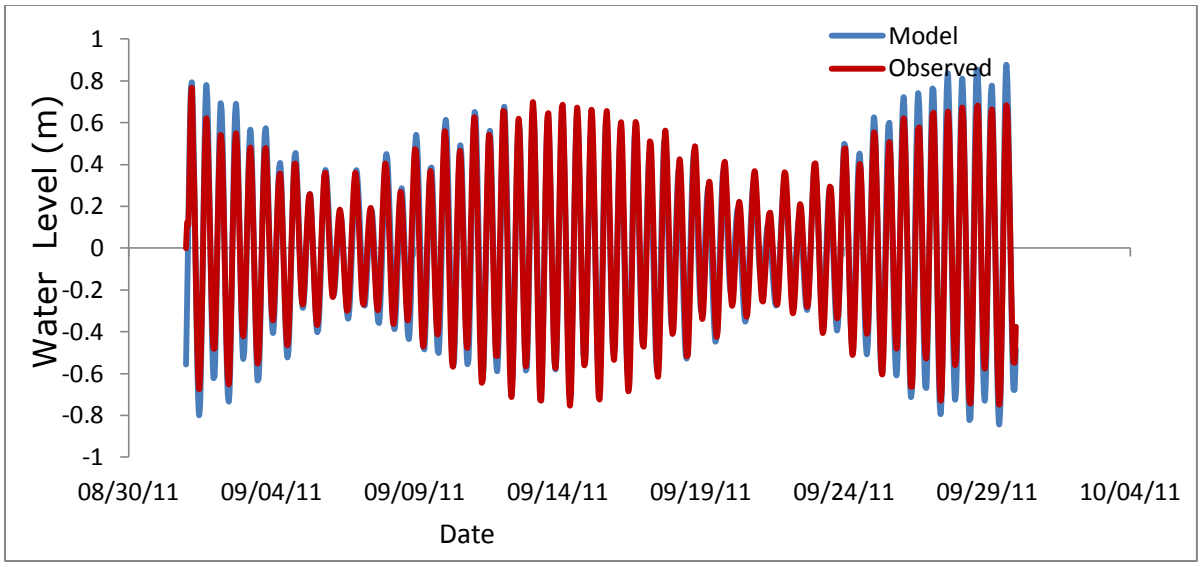

Figure 4.8. Observed and modeled water levels at the Tide Gauge of Kakinada Port from 1st September to 30th September 2011

Figure 4.8 shows the comparison between the observed and modeled water level for month of September 2011 at the tide gauge location of Kakinada Port. The regression coefficient R^2 value obtained after comparison was 0.945 and the Root Mean Square Error value was 0.091m.

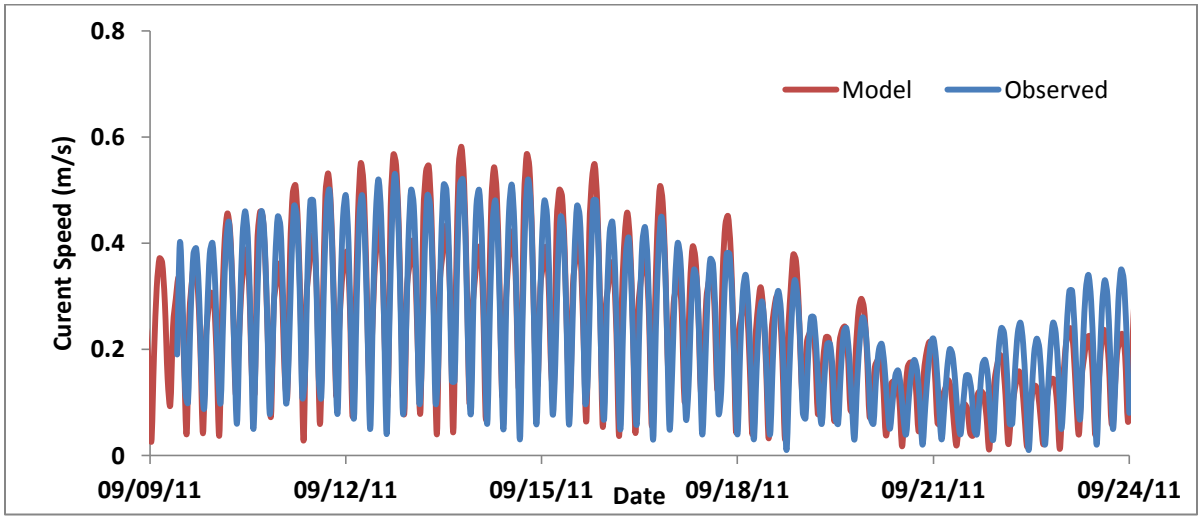

Figure 4.9. Observed and modeled current speed for the period 9th September to 24th September 2011

Figure 4.9 shows the comparison of the two weeks modeled and the observed current speed for the observed location. The results were obtained

after calibrating the model and setting the value of Chezy's roughness coefficient as 74 and 71 in x and y directions. The regression coefficient R-squared value 0.675 was obtained. The Root Mean Square Error of 0.099m.s^{-1} was achieved which shows good performance as the RMSE value is less than 0.1 for the tidal current speed predictions (Williams, J. and L. Esteves, 2017). They mentioned that the RMSE value provides quantitative measurement of accuracy of model prediction and RMSE value less than 0.2 demonstrate significant fit.

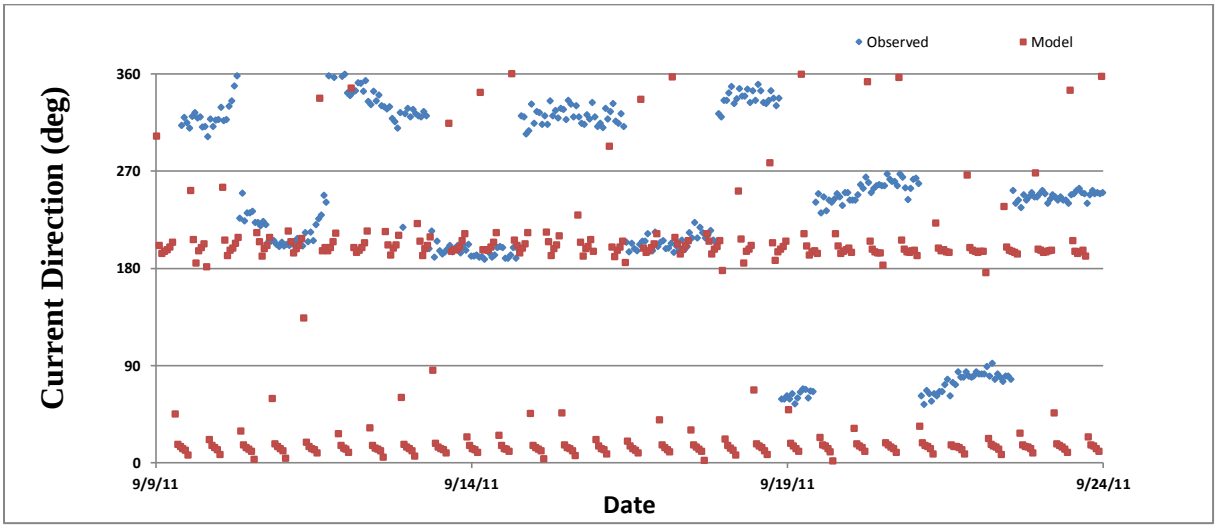

Figure 4.10. Observed and modeled current direction for the period 9th September to 24th September 2011.

Figure 4.10 shows the time series comparison of the modeled and observed current direction. The regression coefficient R^2 value obtained is 0.838. The disagreement between the modelled and computed current direction could not be reduced with variation of control parameters without affecting the current magnitude (which is agreeing reasonably well with the observation). Hence it was decided to move ahead with this combination. It was concluded that model is capable of simulating hydrodynamics of the bay with reasonable accuracy and can be used to simulate the morphodynamics for predicting the morphological development of bay.

4.4.2.2 Wave Model Validation

The numerical wave model Delft 3D-WAVE (SWAN) model was utilized for carrying out wave simulation for Kakinada Bay (Figure 4.5 and 4.6). The wave conditions from the offshore boundary of the model were propagated to the nearshore areas. The time-varying wave parameters like wave height, wave period and wave direction were taken as wave model boundary input specified in the Wavecon file. Wave model uses JONSWAP spectral shape for input, which uses a unimodal sea state. The Delft3D SWAN Model was calibrated by tuning JONSWAP bottom friction coefficient. Depth-induced breaking model of Battjes and Janssen (1978) was used to simulate wave dissipation. Depth induced breaking alpha and gamma parameters were investigated for calibration of model. The alpha breaking parameter controls the rate of dissipation and Gamma breaking parameter controls the ratio of wave height to water depth at which wave breaking occurs. In shallow waters predicted wave heights are sensitive to JONSWAP and gamma breaking parameters.

Wave model has been validated by comparing the observed wave data obtained from Kakinada Seaports for years 2006-2008 at the deeper ocean at 2310m depth with the waves generated from the NIOT Wave model. NIOT has published Wave Atlas for entire North Indian Ocean from 1988 to 2012, which has been utilized for wave simulation. The NIOT Model was used for Boundary input generation of wave boundary conditions and the wave parameters Wave Height, Wave Period and Wave Direction. NIOT model is of regional coverage (entire North Indian Ocean) and had been compared with number of locations with observed data. The results of NIOT atlas have been taken as basis for comparison in this work in the absence of other sources of data.

The comparison has been made between NIOT simulated waves with the observed data and presented in figure 4.11.

Wave parameter comparison of observed and Model data off Kakinada coast

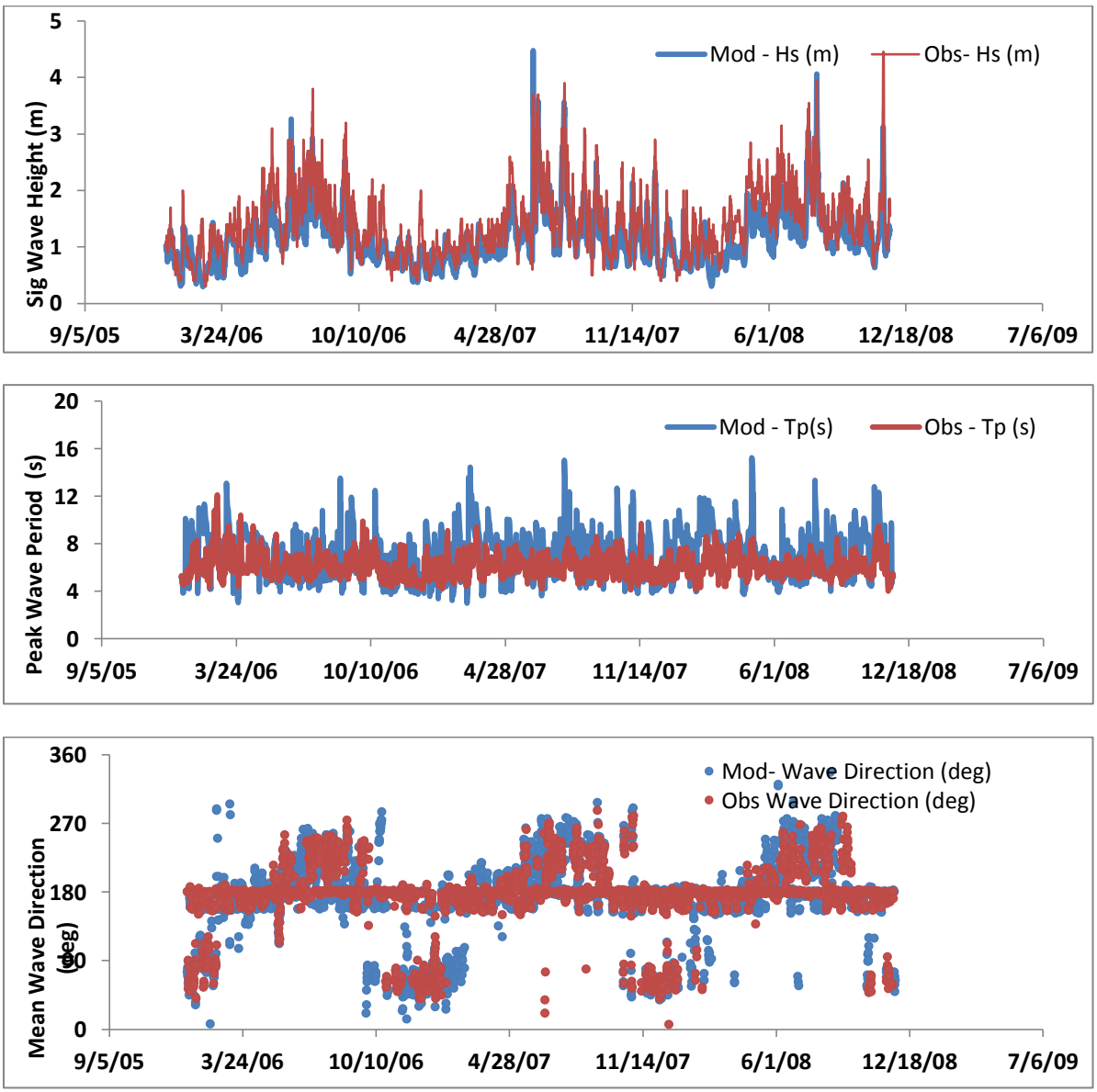

Figure 4.11. Comparison of Wave Height, Wave period and Mean Wave Direction between the observed and simulated wave data.

Figure 4.11 shows the comparison of wave height, wave period and mean wave direction between the simulated wave from NIOT Wave Atlas and

observed data obtained from Kakinada Seaports. From the figure 4.11, it was observed that wave parameters were in reasonable agreement.

After calibrating the wave model with the simulated waves, it was simulated using the NIOT simulated waves at the boundary for year 2011 (figure 4.12). Wave climate near the entrance of the bay and inside the bay (figure 4.13) were extracted from simulation results (figure 4.14).

Simulated wave data near model boundary

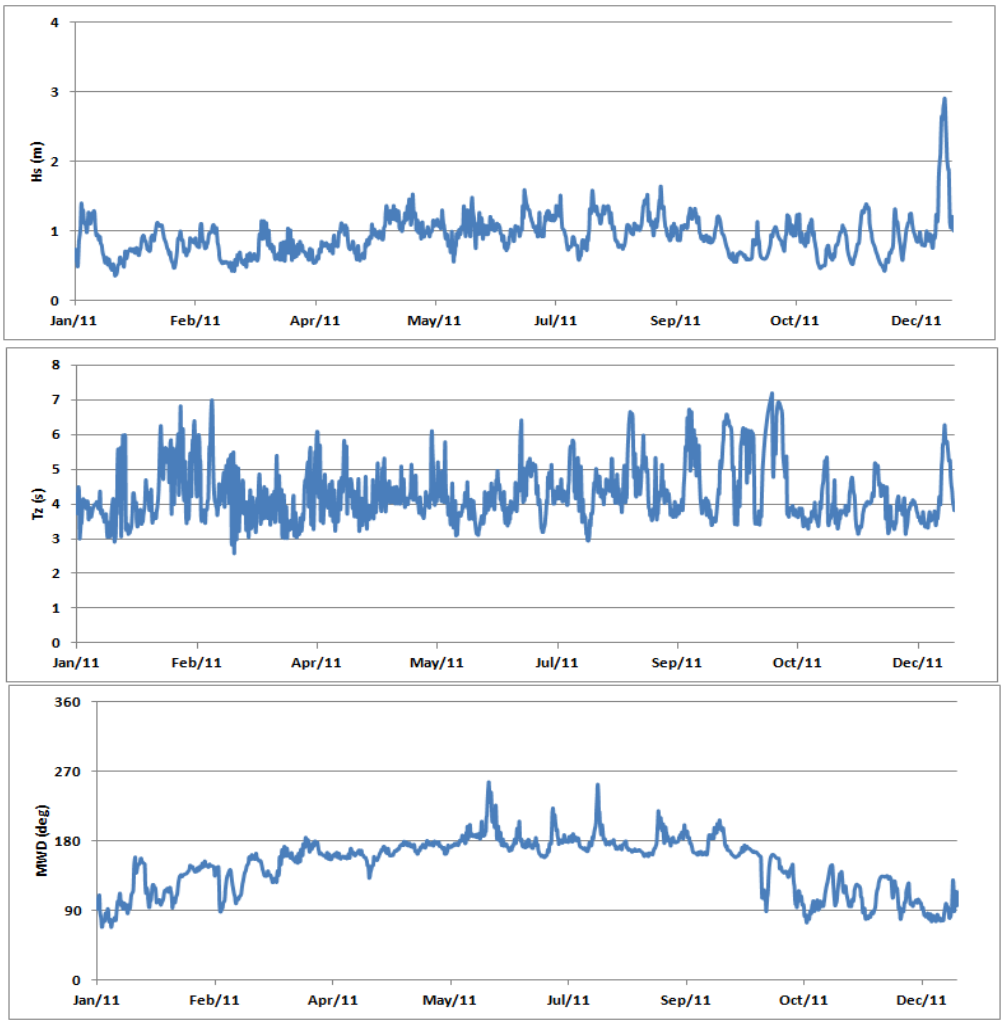

Figure 4.12. Time-series of year 2011 simulated significant wave height, wave period and mean wave direction near the model boundary.

Figure 4.12 shows the time-series of waves simulated near model boundary for year 2011. The simulated wave parameters show that the significant wave height near the model boundary range from 0.5 to 1.5m.

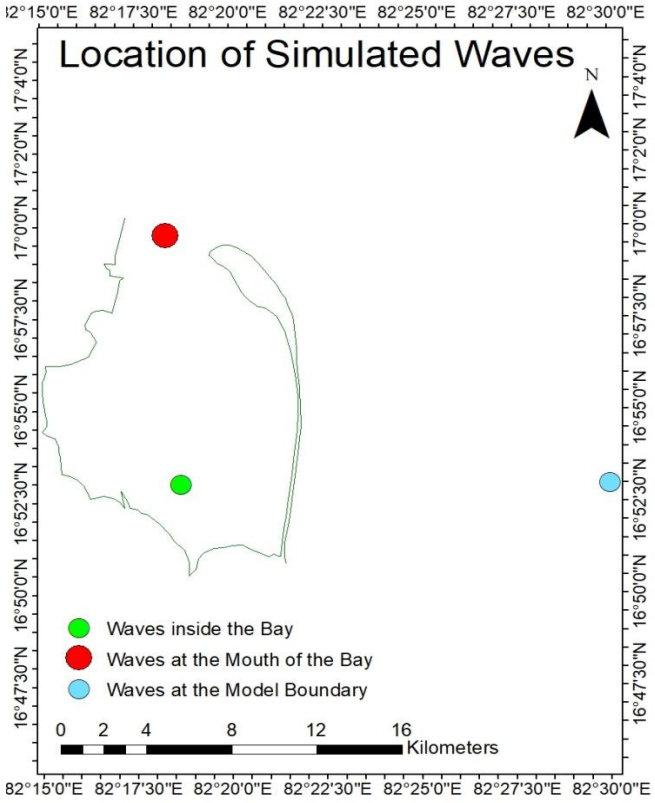

Figure 4.13. Location of simulated waves

Figure 4.13 describes the location of the simulated waves extracted near the model boundary, near the entrance of the bay and inside the bay. These locations are chosen to see how the significant wave heights from the model boundary change by the time it reaches the bay mouth and inside the bay.

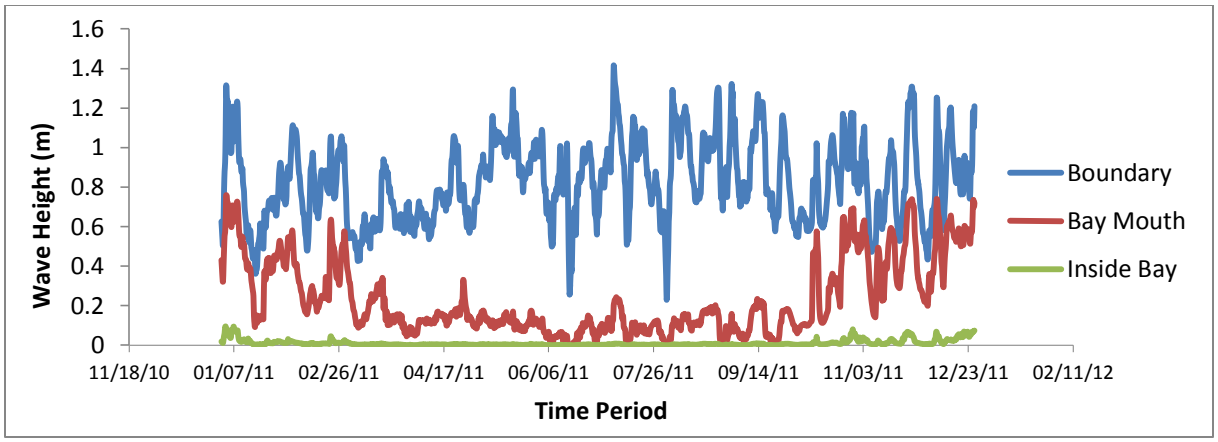

Figure 4.14. Simulated significant wave height time-series at the model boundary, mouth of the bay and inside the bay for year 2011.

Figure 4.14 shows the significant wave heights extracted from the simulated wave heights for the three locations inside the model. The waves are extracted near the model boundary, at the mouth of the bay and inside the bay. It is observed that the wave climate at the mouth and inside the bay is comparatively less than the boundary. It is observed from the figures that the approximate reduction of significant wave height inside the bay is 90%. This reduction shows that the wave influences inside the bay are very less and the sediment transport inside and near the southern end of the bay are more influenced by tide. Hence, waves were not included in the first set of morphological model.

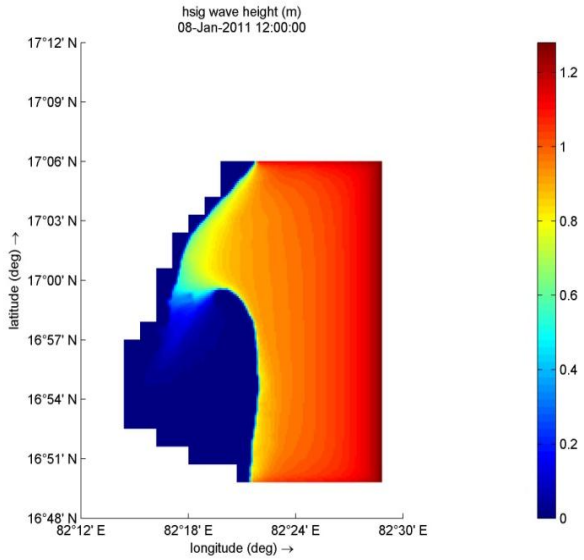

Figure 4.15 Significant Wave Height entering inside the Kakinada Bay

Figure 4.15 show that waves inside the bay are very less. The action of wave has been reduced considerably due to the presence of breakwater. With significant wave height observed at the model boundary around 2m, it has considerably reduced to 10% at the southern part inside the bay (about 20cm). The wave amplitude has lessened and with the gentle flow it may not affect sedimentation as no churning occurs inside the bay. Rajyalaxmi T. et al., 1986 stated that the bay is protected by the eastern edge of the sand spit from the action of waves thereby limiting its effects inside the bay. Bhavanarayana (1974) explained the wave mechanism inside the bay. He mentioned that as the waves enter the bay, they are refracted in such a way that they reach the southern and the south-western sides; but ultimately before reaching the shore, they lose much of their energy to produce significant long shore currents. Hence Model Reduction approach was followed computing simulation with tides alone and omitting waves, describing only the important physical processes.

4.4.2.3 Sediment Model Calibration

The sediment model was calibrated by getting closest agreement for the computed and observed suspended sediment concentration. The sediment transport largely depends on the sediment and grain size distribution of the seabed. Sediment model was run by giving sediment boundary conditions for cohesive silt sediments. For Bed shear stress calculation, Van Rijn (2007a) roughness predictor was used. Sediment in the Kakinada Bay is predominantly silty clay as reported by Reddy and Rao (1996) with a D50 size taken as 85 μm. The sediment substrate is highly cohesive due to presence of high percentage of silt, clay and organic matter. Specific sediment density was set as 2650 $kg.m^{-3}$ while dry bed density as 500$kg.m^{-3}$. Critical bed shear stress for sedimentation was given uniform value of 1000$N.m^{-2}$, and critical bed shear stress for erosion was uniform value of 0.5 $N.m^{-2}$. The value of critical bed shear stress for sedimentation is much higher than the maximum bottom shear stress induced by the waves and currents. This configuration has been proposed and widely used in engineering applications with low concentrations of suspended cohesive sediment (J.C. Winterwerp, W.G.M. van Kesteren, 2004; Santaro P. et. al., 2017).

The settling velocity was obtained as 0.1$mm.s^{-1}$. Minimum water depth value was given as 0.1m for sediment transport calculation. The transversal and longitudinal calibration factors for bed slope effects were chosen as 1.5 and 1 respectively. The modeled suspended sediment concentration was compared with observed data and the values were in reasonable agreement.

Sediment model has been run by giving sediment boundary conditions for cohesive silt sediments. Sediment data modeled was validated for suspended sediment concentration obtained from fieldwork (Figure 4.16).

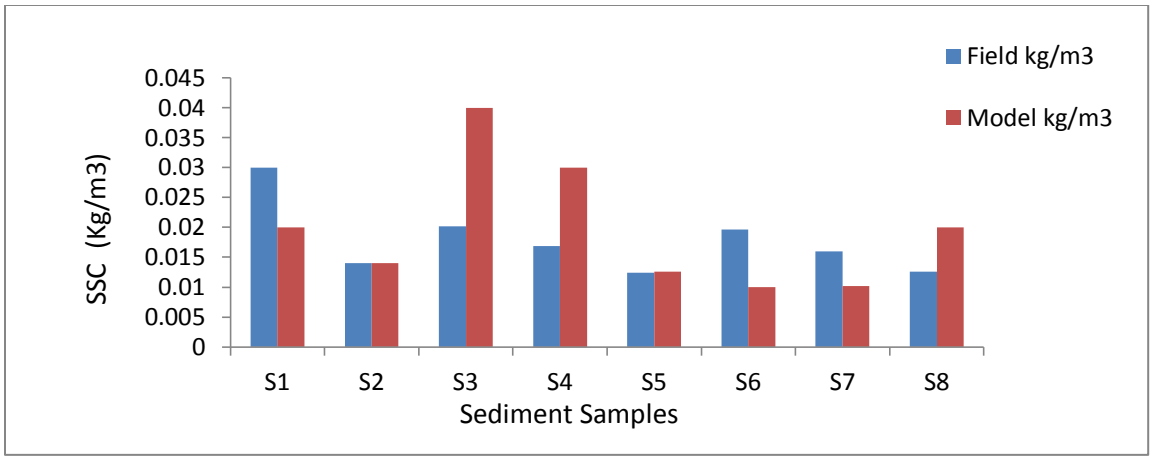

Figure 4.16. Comparison of Suspended Sediment Concentration (kg/m3) for field data with the modeled values inside Kakinada Bay.

The figure 4.16 shows the comparison of suspended sediment concentration between the observed and modeled data inside the Kakinada Bay. Variation has been observed in two locations S3 and S4 largely attributed to the widely spread suspended sediment concentration locations inside Kakinada Bay and the dynamic sediment discharge from the three tributaries made the variation of the field sediment concentration data with the model.

Thus, Hydrodynamics and sediment dynamics inside Kakinada Bay is studied and calibration and validation of flow and sediment models in Delft 3D performed with observational data.

CHAPTER 5

PREDICTION OF LONG-TERM MORPHOLOGICAL CHANGES

5.1 Introduction

In the present thesis, an attempt been made to assess the shoreline migration of Coringa Mangroves using remote sensing imageries and DSAS on GIS platform. The trend obtained showed the deposition and erosion pattern of the bay and their rates for the time period 1977-2019. Having assessed the trend of shoreline migration, this study further aimed to predict the morphological development of bay for next 100 years from year 2019 to 2119. Morphological modeling was done using flow model of DELFT 3D. The model was calibrated by validating the simulation results with the observed values.

Kakinada Bay being an enclosed bay from the three sides with only opening at the northern side with the presence of a breakwater; the action of waves inside the bay has been found to be negligible. With the negligible action of waves occurring inside the Kakinada Bay, the approach for adopting the model reduction technique by choosing only the most important physical process by eliminating action of waves from the model is adopted. As Lesser

(2009) stated the correct use of acceleration techniques as: "In order to use a morphological acceleration technique in a coastal situation it is essential to identify which coastal processes play a significant role in (residual) sediment transport patterns over the space and time scales of interest". While at the same time statement given by Roelvink (1999) and quoted by Dastgheib A. (2012) is "If you put enough of the essential physics into the model, the most important features of the morphological behavior will come out, even at the longer time scales" makes this study find which approach to adopt.

This study attempts to find out the essential processes and physics that are required for long-term simulation along with appropriate acceleration scheme. With reasonable confidence achieved after comparison, the forecast model to be extended for next 100 years with three combination of environmental forcings – (i) Tide only, (ii) Tide + Wave, (iii) Tide + Wave + MSL variation. The decadal volumetric changes are compared to understand the differences caused by incremental of addition of forcing.

5.2 Morphological Modeling with Tides only

The forecast model was formed with tides alone as the forcing for predicting morphological development of the bay for 100 years. In order to reduce the computational time and efforts for running simulations for longer time periods, morphological model was formed using input reduction method and acceleration method. Morphological tide was formed using constituents M_2 and C_1 and morphological acceleration factor was chosen using sensitivity analysis by comparing the accelerated and non-accelerated simulation results. The morphological model was validated by performing hindcast simulation for 30 years from 1988 to 2019 and the resultant shoreline was compared with the satellite derived shoreline. The DSAS results were used to compare the trend of accretion and erosion obtained by morphological modeling. Once morphological model was validated, forecast simulation was performed for 100 years from 2019 to 2119.

5.2.1 Morphological Tide Formation

Morphological model was formed in Flow model of Delft 3D. For prediction of long-term changes in morphological model, running model for long time period is difficult due to computational facility and time constraint. Thus morphological study has used Input Reduction process and morphological acceleration factor (Morfac). Input reduction method is applied by creating

the morphological tide comprising of tidal constituents M_2 and C_1. Here M_2 is principal lunar semi-diurnal constituent and C_1 is fictitious constituent formed by following equation 5.1 and 5.2:

C_1 Amplitude- $C_1=\text{sqrt}(2K_1O_1)$ (5.1)

C_1 Phase- $\text{Ø}C_1= (\text{Ø}O_1+ \text{Ø}K_1)/2$ (5.2)

The interaction of tidal constituents M_2, O_1, and K_1 for inducing sediment transport is applicable for the areas where the relation presented in eq. 5.3 holds good as suggested by Hoitink et al., (2003).

$$2\times O_1\times K_1 > M_2\times M_4 \quad (5.3)$$

The above condition was checked at two locations A and B at the open boundaries as shown in figure 5.1 in order to verify the inclusion of the tidal constituents O_1 and K_1 in the morphological tide.

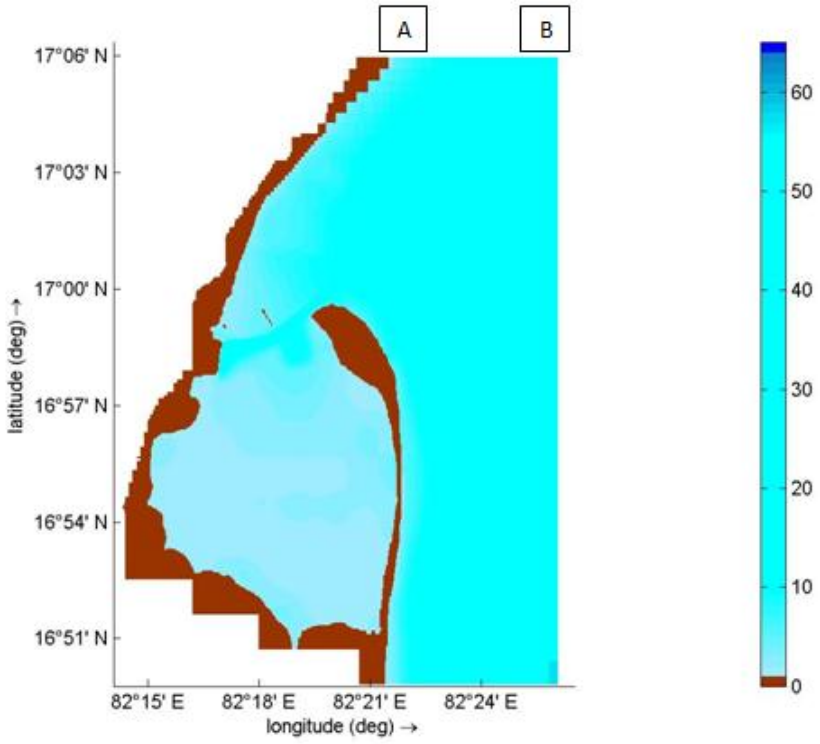

Figure 5.1. Location of offshore Tidal constituents

Amplitudes for the tidal constituents M_2, M_4, O_1 and K_1 at A and B points (Figure 5.1) were generated from Global Tide model and these values were given in the equation 5.3 for computing the relation required for inclusion of O_1 and K_1 tidal constituents in the morphological tide.

Table 5.1. Amplitude for Tidal constituents at model boundary A and B

Tidal Constituents	**Amplitude for Kakinada (A)**	**Amplitude for Kakinada (B)**
M_2	0.42752053	0.42798
M_4	0.00220777	0.00222
O_1	0.03898091	0.03902
K_1	0.10773287	0.10782
$2\ O_1K_1$	0.00839905	0.00841
M_2M_4	0.00094386	0.00095

For both the locations A and B, the value of $2O_1K_1$ was found greater than the value obtained by M_2M_4; hence the tidal constituents O_1 and K_1 were included in the morphological tide.

Morphological tide with tidal constituents M_2 and C_1 was formed, where C_1 is combination of O_1 and K_1 tidal constituents. The M_2 and C_1 period was set to 745 and 1490 minutes respectively. This was done for obtaining same residual sediment transport during interaction of C_1 with M_2 while using tidal components O_1 and K_1 with what would have been obtained using the astronomical tide.

5.2.2 Scaling Factor for the morphological tide

An amplification factor was introduced to the tidal constituents to improve the results by preserving total energy by multiplying scaling factors to M_2 and/or C_1 constituents suggested by Lesser (2009). Applying this scaling factor will bring up energy level to conserve and overstate the residual transports to required level due to interaction of M_2, O_1 and K_1. Scaling factor helps in conserving the total tidal energy.

Lesser gave following equations 5.4 and 5.5 for calculation of scaling factors for multiplying the tidal constituents:

1. F1, when scaling factor is applied to both M_2 and C_1:

$$f1 = \text{sqrt}[(M_2^2 + N_2^2 + S_2^2 + K_1^2 + O_1^2) / (M_2^2 + C_1^2)] \quad (5.4)$$

2. F2, when scaling factor is applied only to M_2

$$f2 = \text{sqrt}[(M_2^2 + N_2^2 + S_2^2 + K_1^2 + O_1^2) - C_1^2 / (M_2^2)] \quad (5.5)$$

The scaling factor values were obtained as f1=1.125 and f2=1.119. These values were multiplied with (M_2+C_1) and M_2 tidal constituents and simulations were run but cumulative sedimentation and erosion obtained were not matched with the simulation results obtained using astronomical tides. This could be attributed to the introduction of error to the M_2+O_1+K_1 residual due to the usage of scaling factors. When scaling factor is introduced to both the M_2 and C_1 constituents, error becomes proportional to the cube of amplification factor, while when applying only to the M_2 component, error introduced into the M_2+O_1+K_1 residual will be linear with the amplification factor (Lesser, 2009). Deriving correct spatially and time varying F2 factor using any analytical expression would be complicated hence a pragmatic method would be required for determining an optimum scaling factor. Hence a trial and error comparison method was adopted as suggested by Lesser (2009) for a range of scaling factors like 1.02, 1.09, 1.1, 1.2 and 1.3 applied on the basis of the residual transport representation

of a full spring-neap cycle of the astronomical tide. The cumulative sedimentation and erosion matched well using scaling factor 1.3 for various points when compared with the astronomical tides.

The final morphological tide comprising harmonic tidal constituents M_2, O_1 and K_1, with M_2 multiplied by scaling factor 1.3 was formed. The harmonic water level boundary conditions used at the boundary points are shown in Table 5.2.

Table 5.2. Harmonic tidal boundary conditions for the morphological tide

Tidal constituent	Frequency (Deg/hr)	Amplitude Begin (m)	Phase Begin (Deg)	Amplitude End (m)	Phase End (Deg)
C_1	14.496	0.09164633	246.97626	0.091741	247.0007
M_2	28.993	0.42752053	79.216638	0.424308	78.905544

The frequency of C_1 diurnal constituent was set as 14.496 deg/hour which indicates a 24h 50min time period. The M_2 frequency has been set as 28.993 deg/hour, which indicates a 12 h 25 min time period.

5.2.3 Calibration of Morphological Tide

Water level has been compared for model with the harmonic morphological tide including M_2 and C_1 as input boundary condition and run with full astronomical tide for month of September 2011 (Figure 5.2). Current velocity has been validated comparing astronomical tide with morphological tide with tidal constituents M_2 and C_1 (Figure 5.3).

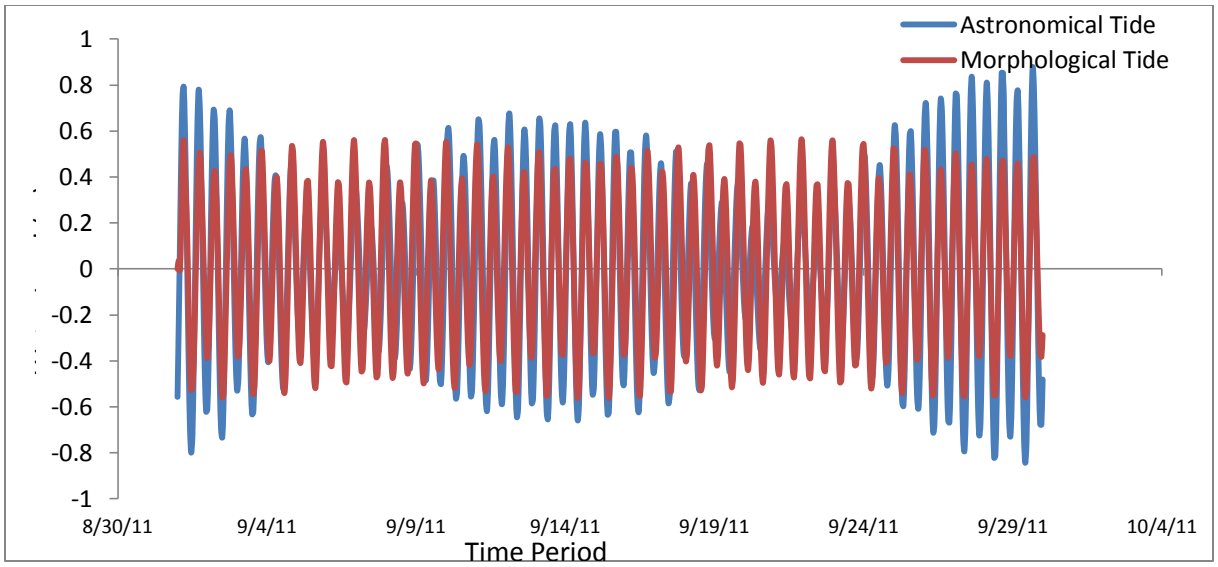

Figure 5.2. Time-series of water level comparing astronomical tide and morphological tide.

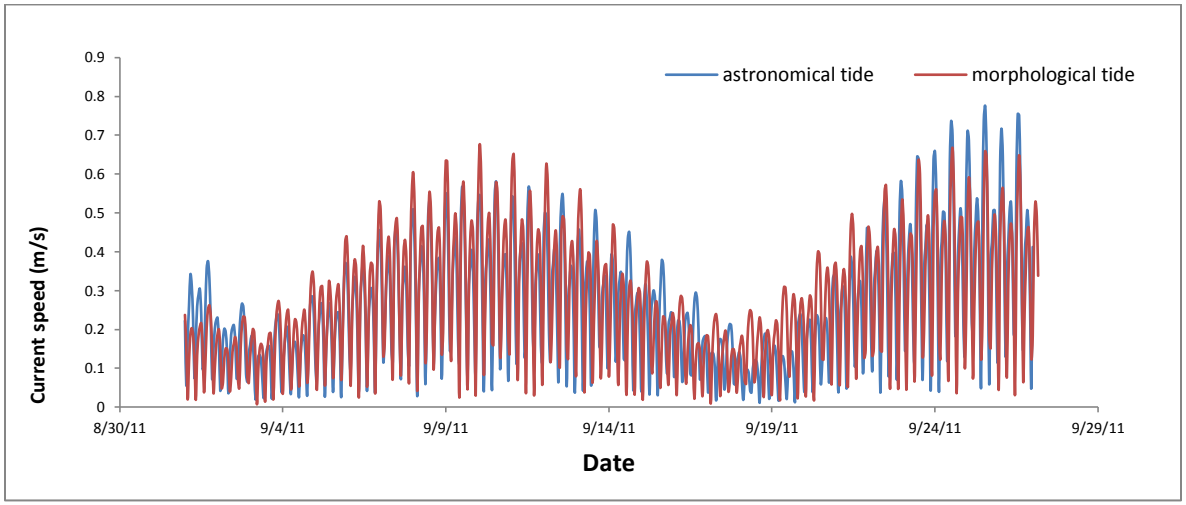

Figure 5.3. Time-series of current speed comparing astronomical tide and morphological tide.

The time-series graphs obtained comparing the water level and current speed using astronomical tide and morphological tide (figures 5.2 and 5.3). The graphs show the morphological model with the reduced morphological tide has been calibrated.

5.2.4 Sensitivity Analysis of Morphological Acceleration Factor

Sensitivity analysis of morphological acceleration factor was carried out. Morphological models were run for a month using morfac values 10, 20, 30 and 40. To arrive at an optimal morfac value, the sedimentation and erosion results were compared with model run with no acceleration factor, that is - with morfac 1.

The optimal morfac value was decided on the basis of sensitivity analysis of morphological factor carried out with the Brier Skill Score (Sutherland et al., 2004). They mentioned that BSS provides quantitative analysis of skill of model, where skill is accuracy of prediction by model relative to baseline prediction. Formulation of BSS is represented in Eq. 5.6.

$$BSS = 1 - \frac{<(Y-X)^2>}{<(B-X)^2>} \tag{5.6}$$

Where Y is predicted value, X is observed value; B is the baseline prediction for evaluating the model prediction and < > indicates the arithmetic mean. BSS with value 1 implies the morphological change predicted by model is perfectly identical to the benchmark simulation.

Morphological models were run with morfac values 10, 20, 30 and 40 predicting one month bed level morphological evolution. Bed level results were compared with benchmark simulation results with morfac 1 for six transects casted in North-South and West-East directions as shown in figure 5.4. BSS score for simulation with morfac 20 and 30 was greater than 0.9 for all transects as presented in table 5.3. In order to run morphological model for less time for simulating larger time period, morfac value was chosen as 30; as higher the acceleration factor, lesser the computational time. Hence morfac 30 was chosen as morphological acceleration factor for further hindcast and forecast simulations.

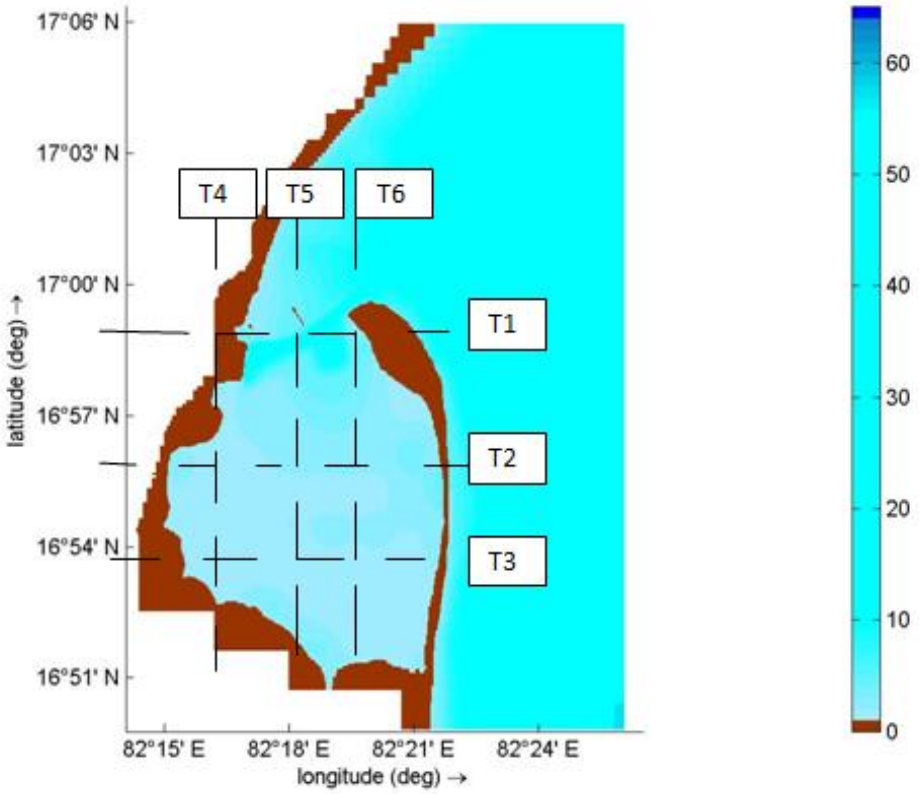

Figure 5.4. Transects casted for validation of hindcast model results

Table 5.3. BSS for various Morfac values at the transects

Transects	BSS for Morfac 20	BSS for Morfac 30	BSS for Morfac 40
T1	0.94	0.93	-2.15
T2	0.97	0.99	-3.45
T3	0.94	0.94	-3.55
T4	0.95	0.98	-3.38
T5	0.86	0.89	-2.61
T6	0.94	0.95	-2.75

Validation of morphological model was done by comparing the accelerated long-term morphological simulation with brute force simulation as a reference (Wilmink, 2015). Brute force model incorporates the harmonic morphological tide with morphological factor one run for one month, while morphological model was run with acceleration factor thirty for one day (plus spin time of 720minutes). The morphological acceleration factor thirty was validated by comparing both non-accelerated brute force and accelerated morphological simulations at 30days time period. The resultant water depth was compared for six transects casted in horizontal and vertical directions and it was found that the results were in good agreement.

Table 5.4. Statistical results for comparing Bathymetry along Transects for brute force and accelerated morphological model simulation

Transects	Regression Coefficient	Bias (m)	Standard Deviation (m)
T1	0.9999	-0.062	0.036
T2	0.9980	0.0197	0.019
T3	0.9997	0.037	0.038
T4	0.9999	-0.05	0.097
T5	0.9996	-0.05	0.088
T6	0.9997	-0.029	0.059

The statistical results Regression Coefficient values, Bias and Standard Deviation as shown in table 5.4 obtained after comparing the resultant water depth for the transects show that the brute force simulation and accelerated morphological model are in reasonable agreement and morphological model can be used further for forecasting for long-term morphological development.

5.2.5. Validation of Morphological prediction with Remote Sensing Data

In order to develop confidence in morphological model, the model was validated by tuning the model parameters for obtaining good agreement between the predicted results of morphological model and remote sensing data. The morphological development results from the model were used to extract the predicted shorelines to compare with the shorelines extracted from the satellite imageries of that year. For this the Landsat imageries were

used to delineate the shoreline and superimpose on the image with the model predicted shoreline.

5.2.5.1 Calibration of Morphological model

The calibration of morphological factor as suggested by Lesser (2009) has many degrees of freedom approach available to adopt with many potential possibilities to tune the morphological model by calibrating the underlying process models. The morphological model is composed of flow model and sediment transport model is calibrated and validated by tuning the calibration settings for the individual process models like Chezy bed roughness, eddy diffusivity, sediment grain size, bed slope factors, morphological tide which affect the resultant morphology.

Another approach adopted for calibrating the morphological model was qualitatively measuring the morphological changes captured by the hindcast simulation for a defined period using the morphological tide and morphological acceleration factor on the calibrated process model. Morphological model was calibrated by comparing the shoreline obtained from the hindcast modeling simulation resultant bathymetry with the shoreline delineated from the satellite shoreline. Both the satellite derived shoreline and simulate shoreline were superimposed on the satellite imagery of resultant year and the morphological changes were compared.

5.2.6. Hindcast Modeling

Hindcast simulation was performed using morphological tide and morphological acceleration factor for time period 1988-2019 for calibrating the morphological model by assessing the accuracy of long-term morphological simulation by comparing the simulated and satellite imagery derived shoreline. For running this morphological simulation, the initial bathymetry of initial year 1988 was given as input and model was run for

one year with morfac 30 to predict the morphological development of next 30 years resulting into morphology of year 2019. The obtained hindcast results were used to extract the predicted bathymetry and further from the extracted resultant bathymetry, land-water shoreline was delineated. This model delineated simulated shoreline was compared with the satellite shoreline by superimposing them together on the satellite imagery of the year the prediction was done for. The resultant simulated shoreline was validated with the satellite imagery derived shoreline of year 2019 by superimposing them on the satellite imagery of the resultant year 2019 as shown in figure 5.5.

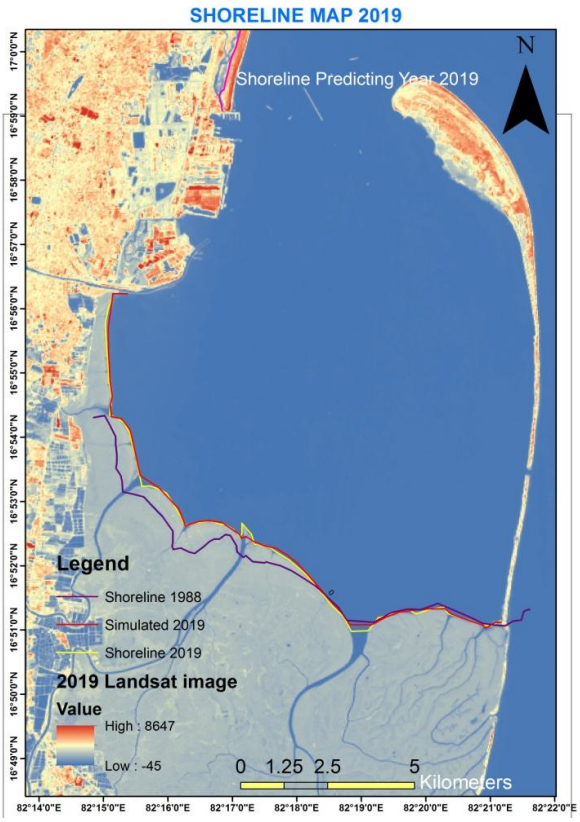

Figure 5.5. Simulated Shoreline as result of hindcast simulation predicted for year 2019

Figure 5.5 shows the satellite shorelines for years 1988 and 2019 and simulated shoreline for year 2019 obtained after hindcast simulation

superimposed on landsat satellite image of year 2019. The satellite and simulated shorelines for year 2019 have matched well. The figure shows there has been considerable accretion from year 1988 to 2019 at the western side of the bay which is in accordance with the satellite imageries and is well simulated by the morphological model. While at the eastern side of the bottom of the bay, morphological changes are very less.

5.2.7. Validation of Hindcast Model

The hindcast model result was quantified using Brier Skill Score (BSS). For validating the morphological simulation results obtained using input reduction and morphological acceleration factor, Lesser (2009) suggested the set up of BSS as:

$$\text{BSS} = 1 - \frac{<(\text{Y}-\text{Z})^2>}{<(\text{Z})^2>} \qquad (5.7)$$

Where Y is the prediction model result and Z is the benchmark brute-force simulation result. This sets the baseline result B the same as initial bathymetry or baseline model with no morphological changes.

BSS was calculated for six transects casted in North-South and East-West directions as shown in figure 5.6.

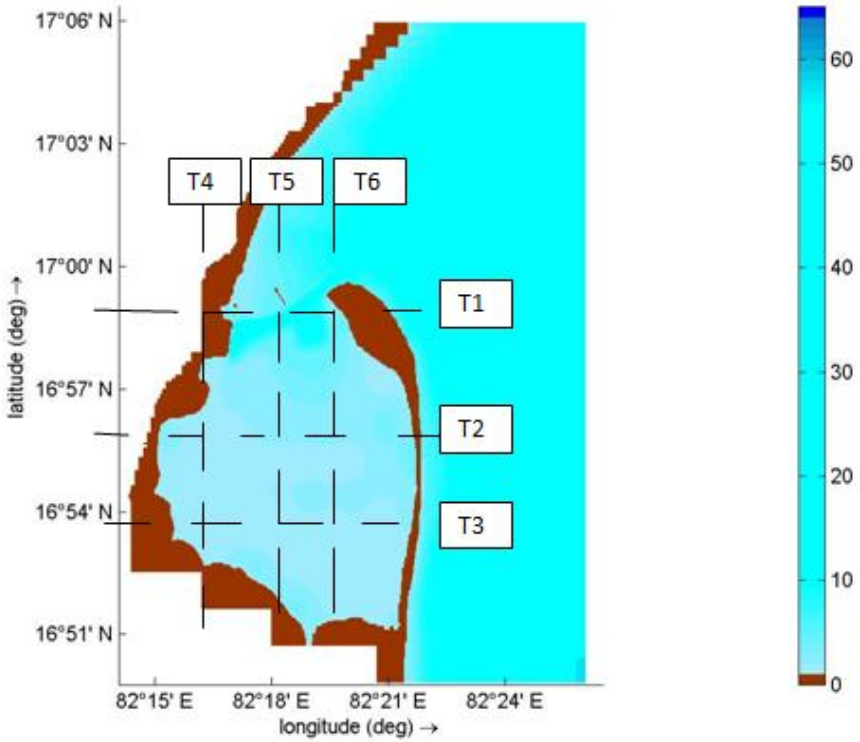

Figure 5.6. Transects casted for validation of hindcast model results

The hindcast result was quantified using Brier Skill Score equation 5.6. Total six transects were casted; three in the West-East direction and other three in the North-South direction. The resultant bathymetry was compared with observed bathymetry and the baseline prediction.

Table 5.5. Brier Skill Score for Hindcast Results

Transects	BSS
T1	0.9411
T2	0.9863
T3	0.9144
T4	0.9511
T5	0.9837
T6	0.9783

Table 5.5 shows the Brier Skill Score for the six transects casted in the North-South and West-East direction. The BSS obtained for all 6 transects show good agreement obtained between the hindcast results and the brute-force simulation. Morphological model is validated well as hindcast simulated morphological results are reasonably matching well with the satellite imageries. Morphological model is used for forecasting development of bay for the next 30years from year 2019 to 2049.

Thus obtaining the reasonable simulation results and comparing the predicted morphological changes, the morphological model was reasonably calibrated and validated.

5.2.8. Forecast modeling

Forecast model was simulated using the reduced morphological tide and morphological acceleration factor thirty. It was run for one year to simulate the morphological development for thirty years from year 2019 to 2049. Shoreline was delineated from the resultant bathymetry of forecast simulation predicting for year 2049 and superimposed with shoreline of year 2019 on Landsat satellite imagery of year 2019 as shown in figure 5.7.

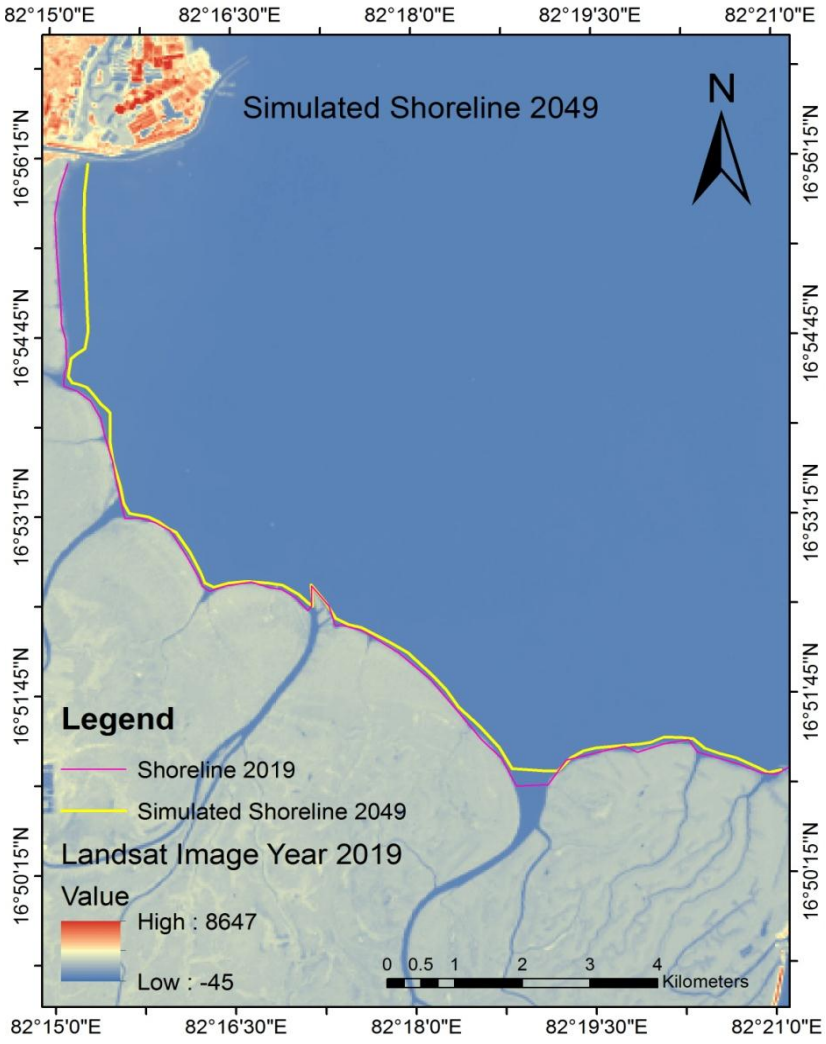

Figure 5.7. Simulated shoreline forecasted for year 2049

The figure 5.7 shows that there has been considerable accretion from year 2019 to 2049 at the western part of the bay. There is slight shoreline movement towards sea at the bottom of the bay in eastern side. Accretion has occurred southwards of the groins of the Kakinada channel which is in similar pattern with trend shown in past satellite images. Major accretion has occurred at the western part of bay and this forecasting simulation predicts shoreline movement in same direction. There is very slight progradation towards sea at the eastern side of the bottom of the bay. It gives insight that sediments getting deposited below the Kakinada channel are not getting

washed out. This will lead to development of land towards sea and formation of mudflats subsequently. While in the centre of the bay, there is not much change observed. Forecasting simulation gives similar accretion trend as was found from hindcast simulations and satellite imageries. Both simulations and satellite imageries show accretion at the western part of the bay.

After this, the action of tides alone on the morphological development of bay over 100 years has been studied upto year 2119. The result of longshore sediment transport as action of waves over the period of 100 years needs to be studied which may bring out the complete scenario of morphological modeling of long-term period. Hence second set of simulation is run with the combined action of tides and waves.

5.3. Forecast Modeling with Tides and Waves

The second simulation was run by incorporating waves with the tidal forcing. The flow model takes wave forcing into account and develops wave stirring and wave-induced currents. Once the individual wave and flow models are calibrated, they can be coupled together. The coupled model simulation can be run online or offline. In online coupling, the wave simulation runs with the initial boundary forcing conditions and then the wave generated forcing output is communicated to the flow model. This flow model runs for the specified time step period with the resulting waves generated forces and then after this computation, updated bathymetry and water levels are taken as input by the Wave model. While in offline coupling, the wave related parameters are computed first and then they are taken as initial values throughout the flow model simulation. The online coupling is better and more accurate as the model takes the updated bathymetry every time step and hence the errors are reduced. The individually calibrated flow model and wave model were coupled online.

5.3.1. Wave Schematization

For simulating the long-term morphodynamic evolution, input reduction is required for preventing high computational time while using the full time data (Latteux, 1995). Input reduction is used for tidal and wave input boundary conditions validated by comparing the reduced input simulation results with the brute-force simulation results.

Wave Schematization is the input reduction technique for the long-term morphological model where full time wave series are schematized into the representative wave classes which represent the full time wave series and reproduces the similar residual sediment transport rates and pattern.

A wave climate is the wave condition at a particular region for a time period. It varies temporally with short variations depending on the meteorological conditions; hence wave schematization is required. This is done with the goal for reduction of wave classes while maintaining reliability of morphological changes as compared to the real time data.

Methods of Wave Schematization

There are various methods followed for wave schematization like Fixed Bins Method, Opti-Routine Method, Energy Flux Method, Potential Sediment Transport Method, CERC Method, etc (Dobrochinski J.P.H., 2009). Wave Schematization follows division of wave climate time series composed of Wave Height, Mean Wave Period and Wave Direction into the wave height directional bins and then calculating the representative wave classes. The criterion on which the division of wave classes is based is different for each wave schematization method like wave energy flux, sediment transport, or selecting waves which contribute to more residual sediment transport and the bottom change. This study uses the Energy Flux Method to schematize the wave climate.

5.3.1.1 Energy Flux Method

Energy flux method divides real time wave data into the representative wave classes based on the Wave Energy Flux of each record of the wave climate in the time series. It uses the following equation 5.8.

$$E_f = (\rho\ g\ H_s^2 / 8)\ C_g \qquad (5.8)$$

where, E_f is Energy flux, ρ is water density ($1025 kg.m^{-3}$), g is the acceleration due to gravity ($9.81 m.s^{-2}$), H_s is the significant wave height and C_g is the group wave celerity ($m.s^{-1}$) of the deep water.

Where, T is the wave period (s).

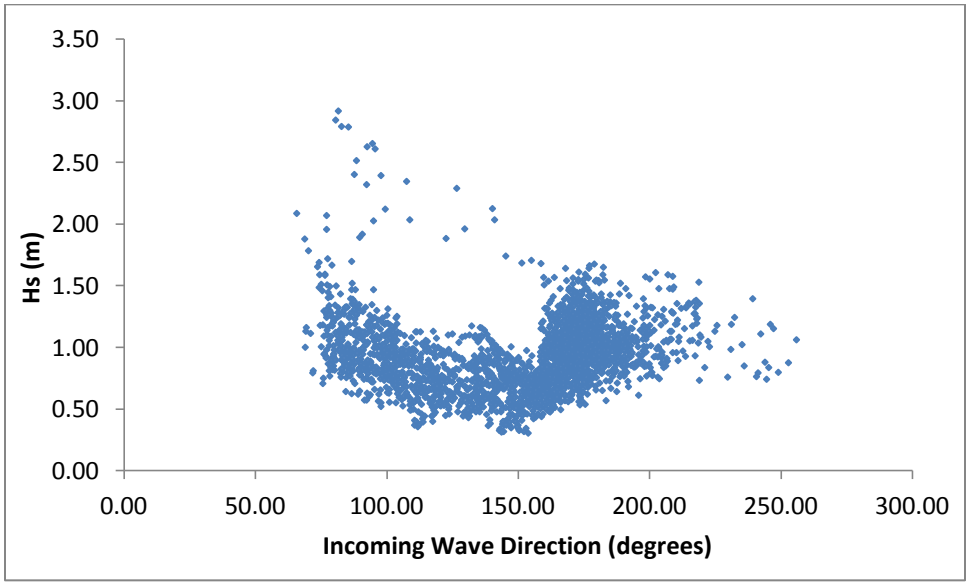

Figure 5.8. Scatter plot of Incoming Wave Direction versus Significant Wave Height with the wave data time series for year 2011 to be schematized.

The time-series of year 2011 year wave data was schematized using Wave Heights and Wave Directions. The figure 5.8 shows the scatter plot with distribution of wave parameters of year 2011. It shows the incoming wave direction versus significant wave height of the time series wave data of year 2011. Energy Flux for whole time-series wave data was calculated using the

equation 5.8. The number of directional bins and wave heights are decided to be 3 each. The range of the bins is defined in order to generate the same energy holding bins and representative wave classes. The incoming wave direction is used to delimit the wave classes with the same total energy flux of each wave class. The wave energy flux was divided into 3 directional bins as 1/3 of the total energy for each bin as shown in figure 5.9. The 3 obtained directional bins were further sub-divided into 3 wave height classes each as shown in figure 5.10. The resultant 9 representative wave classes obtained have 1/9 of total energy flux (sum of wave energy flux of all the wave cases).

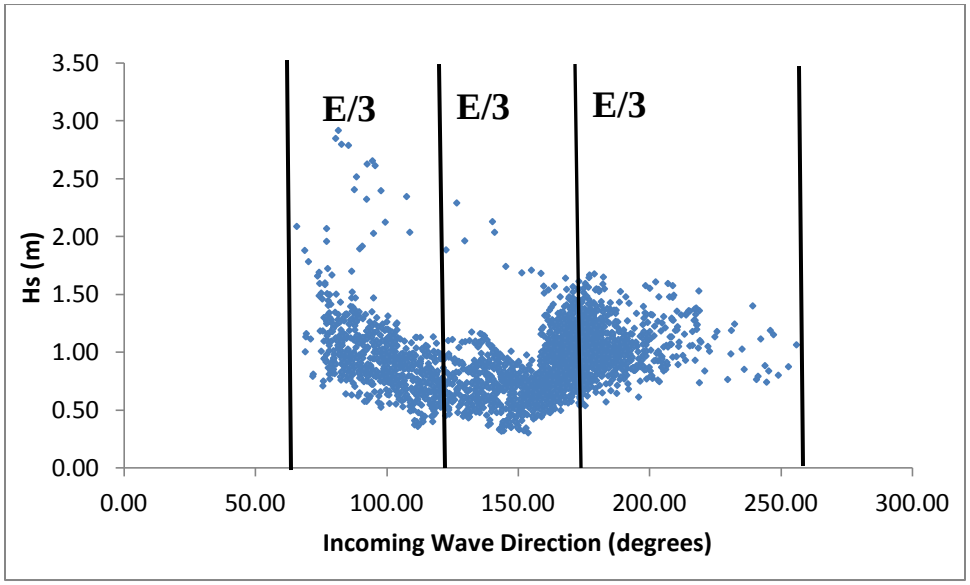

Figure 5.9. Formation of Directional Classes using Energy Flux Method.

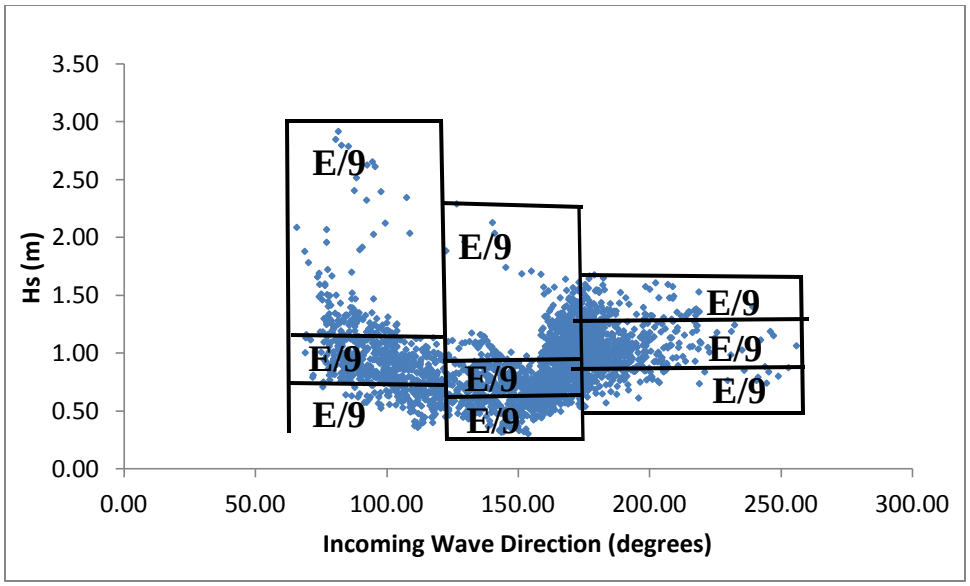

Figure 5.10. Nine representative wave classes selected using Energy Flux Method. Number of directional bins set to 3, number of wave height bins per directional group set to 3.

Final wave classes generated are each a case with representative wave parameters (table 5.6). The representative wave classes calculated using Energy Flux method has Wave Height, wave direction and wave time period obtained as per the mean energy flux, direction and wave period of the class respectively.

5.3.1.2 The Potential Sediment Transport Method

This method divides wave data manually into a number of wave classes and directional bins on the basis of potential sediment transport of the representative wave conditions. The representative wave height is calculated using the CERC formula (Eq 5.9) which has the same potential sediment transport as the whole wave data.

$$H_{rep}.^{2.5}\sum P_i = \sum P_i H_i^{2.5} \quad (5.9)$$

$$H_{rep} = (\sum P_i H_i^{2.5} / \sum P_i)^{1/2.5} \quad (5.10)$$

Where

H_i is the significant wave height in the bin "i" and P_i is the probability of wave height in the class.

The representative wave direction and period are calculated using equations 5.11 and 5.12 respectively.

$$Dir_{rep} = mean\ (dir_i) \quad (5.11)$$

$$T_{rep} = mean\ (T_i) \quad (5.12)$$

Where,

dir_i is the wave direction and T_i is the wave period in bin i calculated based on the statistical analysis.

The representative wave classes formed using the Potential Sediment Transport Approach is presented in table 5.9.

Season-Wise Wave Climate Schematization

The wave climate is schematized season-wise where wave classes are formed on basis of their occurrence in two seasons. The wave climate in Kakinada coast and Bay of Bengal is characterized by South-West Monsoon and North-East Monsoon. Waves predominantly approach from the South West during March-October and from the North East during November to February. The longshore transport is towards the northeast during the months March to October and southwest during the months November to February (Chandramohan et al., 1988). The representation of wave classes selected differed with the seasons. The probability of occurrence was given for each wave class for morfac calculation.

For the period March-October, wave climate for year 2011 was assessed and wave direction was found varying from 74° to 256° in this period. While for the period November-February, wave direction was found varying from 72° to 180°. The wave climate was divided into 5 directional wave classes for

March-October and 4 directional wave classes for period November-February. The wave climate for March-October period was divided into 5 classes with a difference of 36degrees between each class. While the wave climate for November-February period was divided into 4 classes with a difference of 28 degrees between each class.

Representative Wave Height for each wave class was calculated using equation 5.12 and representative wave direction and wave period were calculated using equation 5.13 and 5.14 respectively. The season-wise representative wave classes for Energy Flux Method are presented in the tables 5.7 and 5.8. The season-wise representative wave classes for Potential Sediment Transport Approach are presented in tables 5.10 and 5.11 for both the seasons.

5.3.1.3. Application of Schematized Wave Classes with Morphological Acceleration Factor

The schematized wave classes obtained as input reduction technique must be collaborated with the acceleration factor irrespective of the method used to schematize the waves. The schematized wave classes are combined with the acceleration factor to turn the simulation into the morphological simulation for the desired time period (Lesser, 2009 and Dastgheib A., 2012).

The representative wave classes were combined with the morphological tide using Variable Morfac approach. The random phasing between tide and wave is accounted by simulating each wave condition with the fixed hydrodynamic duration of morphological tide which is 12hours 25 minutes =745minutes. Morphological acceleration factor definite for each representative wave class matching their duration with their occurrence probability is applied. Morfac thus helps to accelerate the morphological development occurring during one tide to the development which would happen during the complete time

period of the specific wave condition in a year. Hence 9 morphological tides are needed to simulate the morphological development for one year where each tide attributes to one wave condition. The morphological acceleration factor was varied for each wave class as per the occurrence of the representative wave class in the wave data time-series. Each wave class has specific morphological acceleration factor calculated using Eq. 5.13.

$$Morfac = (Pc * T)/T_{mor.tide} \quad (5.13)$$

Where, Morfac is morphological acceleration factor, Pc is Probability of occurrence, T is the time period of the morphological simulation and $T_{mor.tide}$ is hydrodynamic duration of morphological tide. Probability of occurrence is the number of days the representative wave height occurs in the particular year.

The morfac calculation for a representative wave period that occurs for few days in a year is calculated as per equation 5.13(a) (Lesser, 2009)

Morfac = (No.of Days X 24 X 60) / 745 (5.13(a))

The morfac calculation for a representative wave period that occurs for only few hours in a year is calculated as per equation 5.13(b) (Lesser, 2009).

Morfac = (No.of hours X 60) / 745 (5.13(b))

The advantage of this approach as quoted by Lesser, 2009 is higher acceleration factor is applied to the wave conditions which are more common and smaller and where morphological changes are less; while lower acceleration factor is applied to the highly active morphological changes occurring larger wave conditions.

Table 5.6. Schematized Wave Classes using Energy Flux Method without seasons

Wave Classes	Rep Wave Height (m)	Rep Wave Period (s)	Rep Wave Direction (deg)	Pc Duration (Days)	Morfac
1	0.66	4.3	133	18	1.45
2	0.80	3.7	148	30	2.41
3	0.81	4.3	170	24	1.93
4	0.95	4.4	120	25	2.01
5	1.08	4.5	172	25	2.01
6	1.09	3.8	164	19	1.53
7	1.10	4.4	114	7	0.56
8	1.29	4.6	174	7	0.56
9	1.60	4.4	139	1	0.08

Table 5.7. Representative Wave Classes for South-West Monsoon (March-October) using Energy Flux Method

March-October	Rep Wave Height (m)	Rep Wave Period (s)	Rep Wave Direction (deg)	Pc Duration (Days)	Morfac
1	0.70	4.5	151	16	1.28
2	1.08	4.9	151	25	2
3	0.91	4.3	173	14	1.12
4	1.26	4.4	174	12	0.96
5	1.03	3.8	192	2	0.16

Table 5.8. Representative Wave Classes for North-East Monsoon (November-February) using Energy Flux Method

November-February	Rep Wave Height (m)	Rep Wave Period (s)	Rep Wave Direction (deg)	Pc Duration (Days)	Morfac
1	0.87	3.5	86	11	0.88
2	1.57	4.4	88	7	0.56
3	0.58	4.1	132	10	0.8
4	1.02	4.3	117	3	0.24

Table 5.9. Schematized Wave Classes using Potential Sediment Transport Approach without seasons

Wave Classes	Rep Wave Height (m)	Rep Wave Period (s)	Rep Wave Direction (deg)	Pc Duration (Days)	Morfac
1	0.87	4.1	122	24	1.45
2	0.80	3.7	148	30	2.41
3	0.81	4.3	171	24	1.93
4	0.95	4.4	120	25	2.01
5	1.08	4.6	172	25	2.01
6	1.09	3.8	164	19	1.53
7	1.10	4.4	114	7	0.56
8	1.29	4.6	174	7	0.56
9	1.60	4.4	139	1	0.08

Table 5.10. Representative Wave Classes for South-West Monsoon (March-October) using Potential Sediment Transport Approach

March-October	Rep Wave Height (m)	Rep Wave Period (s)	Rep Wave Direction (deg)	Pc Duration (Days)	Morfac
1	0.99	3.8	97	16	7.73
2	0.74	4.5	135	14	6.76
3	0.96	4.5	168	17	8.21
4	0.99	3.7	193	16	7.73
5	1.03	3.2	234	17	8.21

Table 5.11. Representative Wave Classes for North-East Monsoon (November-February) using Potential Sediment Transport Approach

November-February	Rep Wave Height (m)	Rep Wave Period (s)	Rep Wave Direction (deg)	Pc Duration (Days)	Morfac
1	1.063	3.8	88	22	10.63
2	0.76	3.8	115	17	8.21
3	0.66	4.2	128	17	8.21
4	0.68	3.1	172	17	8.21

5.3.2. Comparison between the approaches of wave schematization

The wave schematization method for forecast simulation was selected by comparing the bruteforce simulation results with the hindcast results of Energy Flux Method (EFM) and Potential Sediment Transport Approach (PSTA) Method with and without seasons.

5.3.2.1. Flow Wave Coupled Hindcast Modeling

The flow and wave coupled model was validated using Hindcast modeling. The model was simulated for 30years from 1988 to 2019 using morphological tide, schematized waves and variable morphological factors. The representative waves were formed using EFM and PSTA method with and without seasons.

Hindcast simulation was performed for period 1988-2019 using the schematized waves obtained from both the methods. The results were compared by resultant shoreline superimposition, Brier Skill Score and change in volume of the bay. The shoreline comparison was made by superimposing the shorelines obtained from hindcast simulation from both the wave schematization methods and the observed shoreline for year 2019. Brier Skill Score was calculated using the predicted simulation result with the benchmark simulation result using equation 5.7. The volume of the bay was compared for hindcast simulation results obtained from both wave schematization methods with the brute force simulation. For brute force hindcast simulation, the model was run with the full yearly wave climate for period 1988-2019. The resultant volume of the bay for year 2019 was compared with the simulation results as presented in figure 5.12 and table 5.13. The resultant shorelines for year 2019 were compared with the observed shoreline for year 2019 as shown in figure 5.11.

Shoreline Changes

The shoreline comparison was made by superimposing the shorelines obtained from hindcast simulation from all four set of wave schematization method simulations and the observed shoreline for year 2019 (by Satellite Remote sensing imageries). For brute force hindcast simulation, the model was simulated for one year with the observed wave data for during the

period 1988-2019. The resultant shorelines for year 2019 were compared with the observed shoreline for year 2019 (Figure 5.11).

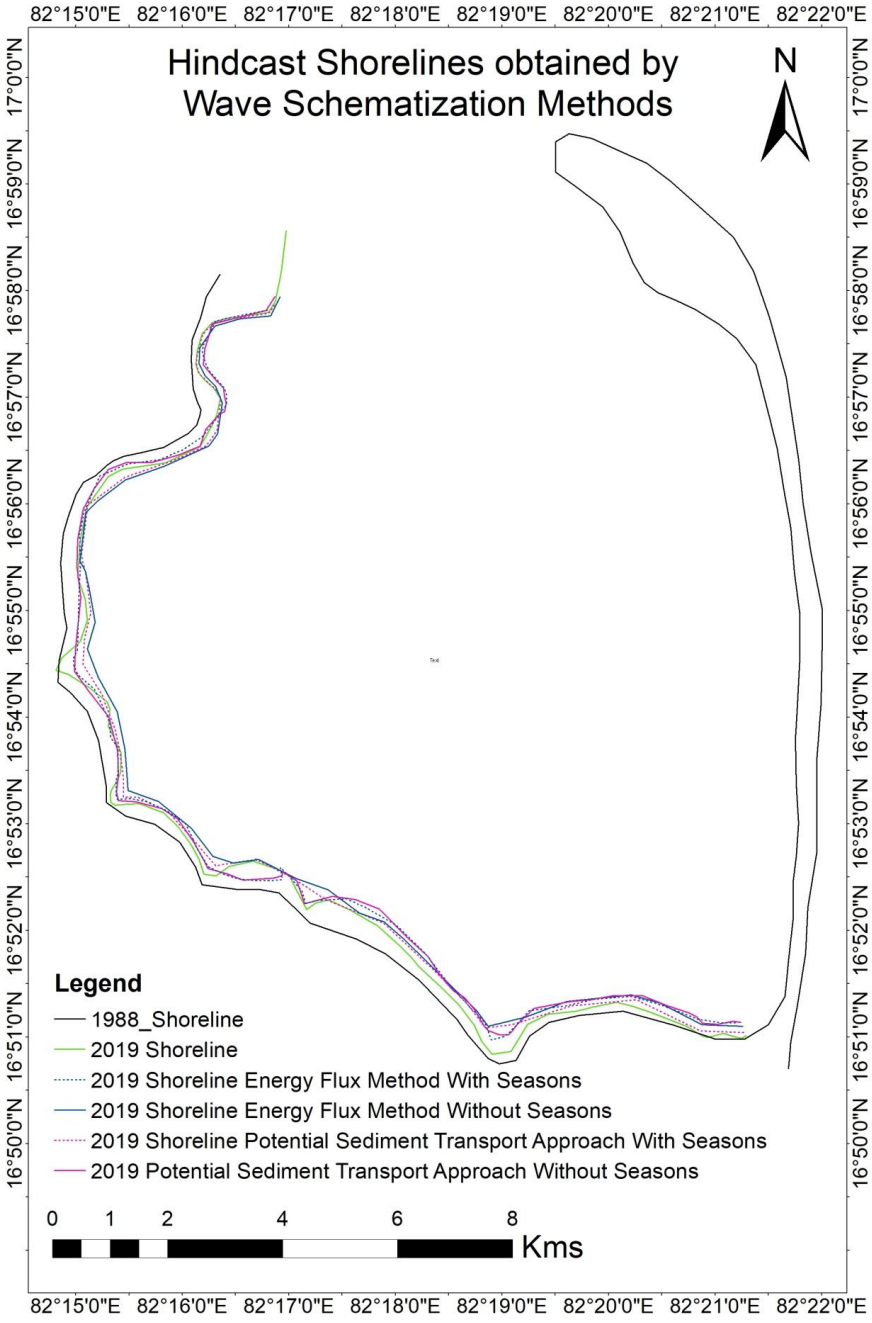

Figure 5.11. Comparison of hindcast shorelines using different wave schematization methods

The figure 5.11 shows the shorelines obtained for year 2019 as result of hindcast simulation results comparing the EFM and PSTA wave schematization methods with and without applying seasonality. The figure shows migration of shoreline from year 1988 to 2019. The 2019 hindcast resultant shorelines are compared with the satellite derived 2019 shoreline. The results show that though both the schematization methods have generated good results, the shoreline obtained from Potential Sediment Transport Approach is matching reasonably well with the observed shoreline. At the same time application of seasonality in wave schematization resulted in better results. The inclusion of seasons seem to moderate the end quantity as both EFM and PSTA methods seems to over predict in the absence of seasonal variation

5.3.2.2 Brier Skill Score

BSS provides quantitative analysis of the skill of model, where skill is the accuracy of prediction by model relative to baseline prediction (Sutherland et al., 2004). The BSS varies in a scale of 0.0-1.0 with higher values indicating better match.

The wave schematization methods were compared by calculating Brier Skill Score for the hindcast simulation results. The bathymetry obtained using both the methods was used to calculate the Brier Skill Score using equation 5.7. Six transects were casted in North-South and East-West Direction as shown in figure 5.6.

Table 5.12. Brier Skill Score computed for hindcast results obtained using Energy Flux and Potential Sediment Transport wave schematization Methods with and without seasons.

Transects	BSS EF without seasons	EF with seasons	PSTA without seasons	PSTA with seasons
T1	0.9555	0.9906	0.9181	0.9415
T2	0.9100	0.9883	0.8884	0.9063
T3	0.9199	0.9760	0.9259	0.9700
T4	0.9281	0.9550	0.9090	0.9100
T5	0.9822	0.9911	0.9632	0.9914
T6	0.9783	0.9836	0.9681	0.9702

Table 5.12 shows the comparison of BSS values for hindcast modeling simulation results obtained using EFM and PSTA wave schematization methods with and without seasons. Both the methods have resulted in good reasonable BSS values. The Flow-Wave Coupled model is reasonably validated. The results showed that application of seasonality in forming representative wave class has improved the wave schematization results.

5.3.2.3. The Bay Volume Comparison

The water volume of the bay at MSL as top datum obtained from simulations with both the wave schematization approaches with and without seasons was compared with the bruteforce simulation taking full yearly wave climate as input (Table 5.13).

Table 5.13. Comparison of Bay volume obtained from Hindcast Simulation using Wave Schematization Methods with the Brute Force Hindcast Simulation

Hindcast Simulation For period 1988-2019	Volume of the Bay Mm^3 Predicted Year (2019)
Brute-Force	303.76
Energy Flux Method (EF) Without Seasons	371.37
Energy Flux Method (EF) With Seasons	328.21
Potential Sediment Transport Approach (PSTA) Without Seasons	328.19
Potential Sediment Transport Approach (PSTA) With Seasons	300.11

The table 5.13 shows the volume of the bay obtained after hindcast simulation using wave schematization methods. The result shows that the Potential Sediment Transport Approach with seasons has yielded the closest match of volume with the brute-force simulation. The results also show that adding seasonality while forming the representative waves, the results have improved. Figure 5.12 shows the graphical representation of the volume comparison of all the methods with the brute-force simulation.

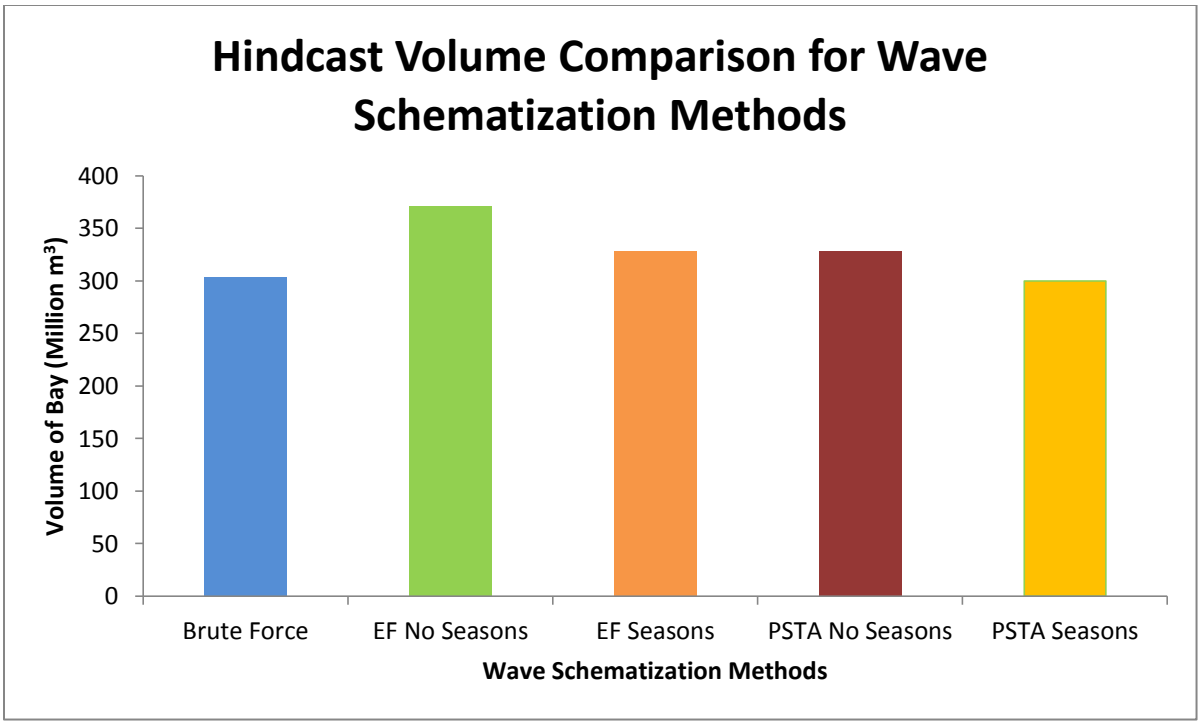

Figure 5.12. The hindcast volume comparison for year 2019 obtained from EFM and PSTA wave schematization methods with the Brute Force hindcast simulation for period 1988-2019.

Figure 5.12 shows that the volume obtained for year 2019 from Energy Flux Method and Potential Sediment Transport Approach are compared with and without seasons with the Brute-Force hindcast Simulation. The volume results show that the simulation with waves schematized using Potential sediment Transport Approach with seasons has yielded better results. The volume of the bay obtained with the simulation with Potential sediment Transport Approach matches closely with the Brute Force simulation. Overall comparison of all the methods suggests that the inclusion of seasonality in the wave schematization improves the result.

From the shoreline migration results, Brier Skill Score and the volume of the bay result, it was concluded that the potential sediment transport approach has yielded better results. Thus for further morphological simulations

predicting evolution of bay for next 100 years, the representative waves schematized using the Potential Sediment Transport Approach was used.

5.3.3 River Discharge Schematization

There are four creeks in the Kakinada Bay discharging water into the Kakinada Bay. Kakinada Channel, Matlapalem Creek, Corangi River and Gaderu River are four main source of water discharge into the bay. The discharges from these sources vary very less and slowly over a year, hence contributing not much to the morphological changes of the mouth of the creek and the surroundings. These discharges are not affected by the action of waves as they are located at the southern bottom of the bay, very far from the mouth of the bay and enclosed from the three sides. Hence very simple schematization method has been used for input reduction of river discharges. The mean level of the river discharge is taken as constant source input condition (Lesser, 2009).

Table 5.14 Schematized River Discharge Data

Source of Discharge	Flow ($m^3.s^{-1}$)	Sediment ($Kg.m^{-3}$)
Gaderu	1.5	0.01
Corangi	0.6	0.01
Mattlapalem Creek	0.4	0.01
Kakinada Channel	0.2	0.01

These discharge values mentioned in table 5.14 was given as input in the morphological model as discharge source into the bay.

5.4 Forecast Modeling with Tides, Waves and Mean Sea Level Rise

The third simulation was run by incorporating decadal mean sea level rise in the flow and wave coupled model. The NASA sea level projection tool was

used to download the sea level rise data from the 6th Assessment Report (AR6) of International Panel of Climate Change (IPCC). These sea level predictions have considered processes specifically with which predictions can be done with the medium confidence (Chen D., et al., 2021). There are 5 Shared Socioeconomic Pathway Scenarios (SSPs) out of which SSP3-7.0 case was selected to project sea level rise for this study. SSPs3-7.0 is a medium to high reference case with no added climate policy. It refers to high aerosols emissions.

The decadal data was available for Kakinada region. The value of mean sea level rise was added in the input bathymetry of the model. Total Sea Level Rise for each decade is presented in the table 5.15.

Table 5.15. Total Sea Level Rise for each Decade

Year	Sea Level Rise (m)
2029	0.09
2039	0.13
2049	0.19
2059	0.25
2069	0.25
2079	0.25
2089	0.52
2099	0.63
2109	0.63

The decadal mean sea level rise was added in the bathymetry as input for every decade simulation in the flow and wave online coupled model. The forecast morphological model was simulated for 100 years from 2019 to 2119 with tides, waves and decadal mean sea level rise as the inputs.

5.5 Development of the Bay over 100 years

The morphological development of the bay is studied for the bay for 100 years. Three scenarios were studied with different forcing:

a) Tides only

b) Tides and Waves coupled

c) Decadal MSL changes with coupled Tides and Waves model

Morphological development of the bay was predicted using the calibrated and validated morphological model for 100 years from year 2019 to 2119 with three scenarios: Tides alone, tides and waves combined and decadal sea level rise with combined tides and waves. The morphological results obtained with these three variants were compared studying Planimetric Variations, Volumetric variations, Shoreline changes, Suspended sediment concentration and depth variations.

5.5.1 Planimetric Changes of the bay

The planimetric changes of the bay were analyzed comparing the resultant water depth obtained for all three scenarios after long-term morphological modeling for 100 years (Figures 5.13, 5.14, 5.15 and 5.16).

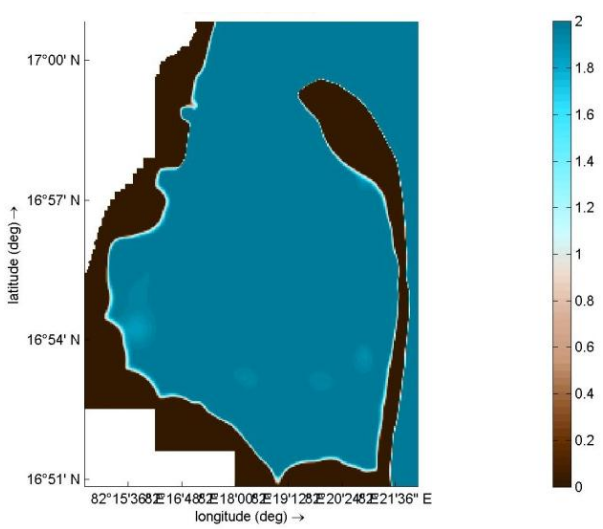

Figure 5.13. Initial Bathymetry (Year 2019)

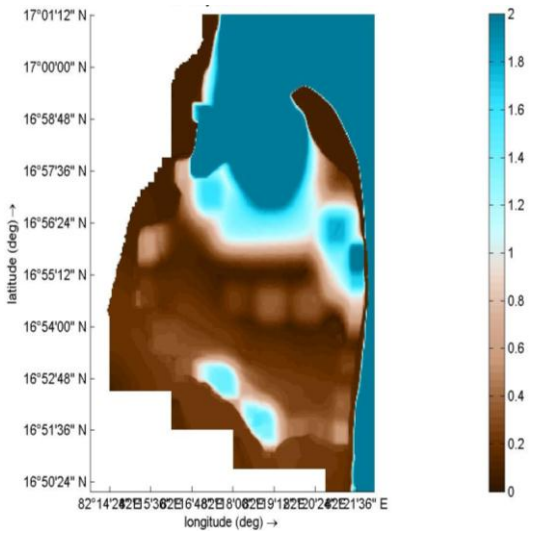

Figure 5.14. Simulated Bathymetry (Year 2119) Tides alone as forcing

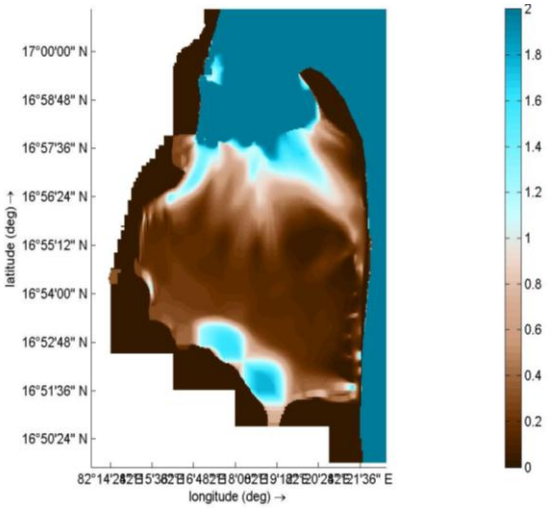

Figure 5.15. Simulated Bathymetry (Year 2119) Tides and Waves

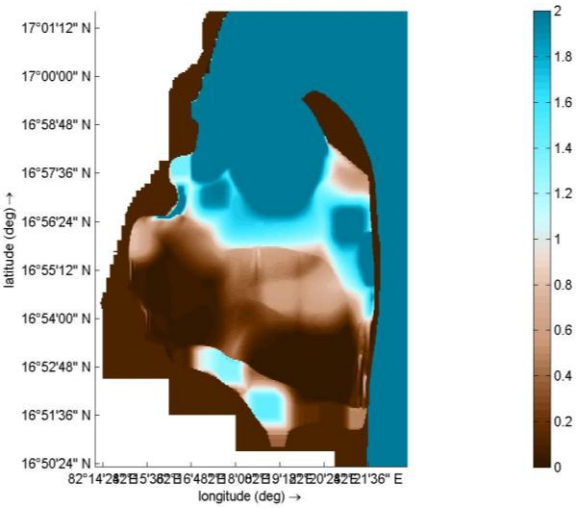

Figure 5.16. Simulated Bathymetry (Year 2119) Tides, Waves and MSL

The figures 5.13, 5.14, 5.15 and 5.16 show the planimetric variation of the bay with effect of tides, the combined effects of waves and tides and decadal mean sea level rise with combined effects of waves and tides. The figures show the simulated depth of the bay of year 2119 obtained from morphological simulation with the three variants of forcing.

The difference between the initial and the final simulated bed level is presented in figures 5.17, 5.18 and 5.19.

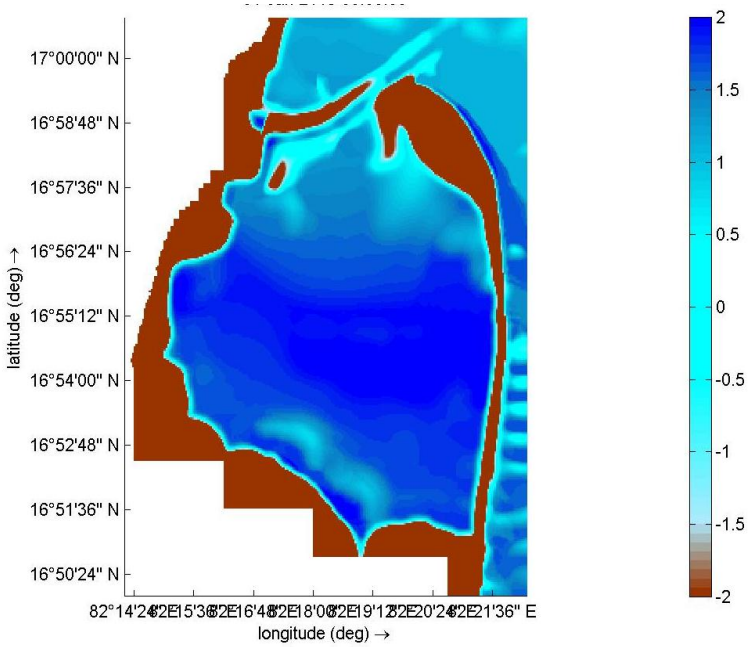

Figure 5.17. Difference between the initial year 2019 and final predicted 2119 year bathymetry. (Tides alone)

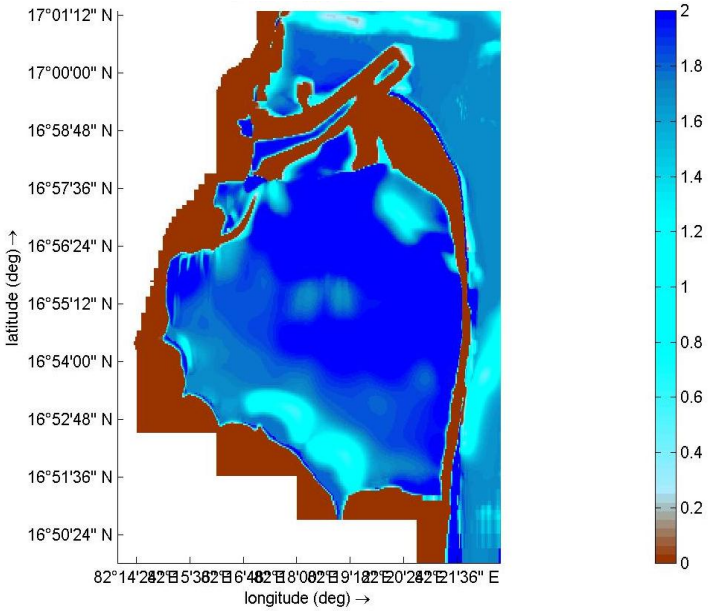

Figure 5.18. Difference between the initial year 2019 and final predicted 2119 year bathymetry (Tides and Waves combined)

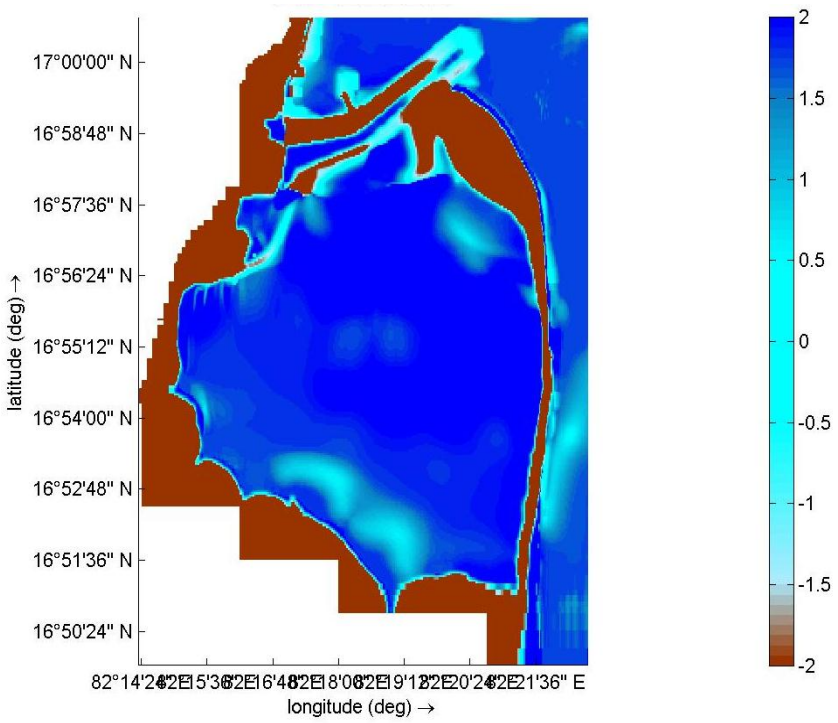

Figure 5.19. Difference between the initial year 2019 and final predicted 2119 year bathymetry (Tides and Waves combined with MSL effects)

It is observed that with the addition of waves, considerable sedimentation has occurred inside the bay and below the head of the spit. The change in geometry of the bay is highly determined by the tidal propagation inside the bay as suggested by Escoffier (1940). The morphology of bay is highly governed by the longshore sediment transport as the combined action of tides and waves as wave induced longshore currents bring sediments along. Waves induced radiation stresses lead to the wave orbital motion which initiates the sediment movement in suspension. Waves increase the bed shear stress which leads to the stirring of sediments from the seabed bottom and leads to the sediment remobilization and littoral transport. This longshore sediment transport from the Godavari River to the mouth of the Kakinada Bay is due to the wave action. Waves bring the longshore sediment transport from the Southern direction towards North and from northern direction towards south. The net transport attributed to the predominant flow of sediment transport towards the northeast

(Chandramohan et al., 1988). Thus, considerable sedimentation has occurred inside the Kakinada bay.

It is observed that with the coupled action of tides, waves and mean sea level, there is widening of the mouth of the bay and a shift of the Kakinada Spit towards offshore as compared with the initial bathymetry and simulated bathymetry with tides alone. The offshore extension of bay is the result of the wave-induced longshore current leading to the net longshore drift (Dastgheib A., 2012), pushing the spit in the direction of the wave-induced current as suggested by Sha and Van den Berg (1993). With offshore shift of spit, there has occurred deepening parallel to the spit at the eastern side of the bay. The morphological changes as observed in the figures suggest that the shift is limited towards offshore direction, while there is stability inside the bay. Since Kakinada Bay is highly tide-dominated energy regime, the residual sediment transport only reshapes the morphology inside while the overall shape of the bay remains the same.

The depth profiles obtained after 100 years of morphological simulations with the three variants are compared. Three transects were casted inside the bay for depth profile comparison. Two transects T1 and T2 in the West-East direction (from the western side of the bay to the eastern side of the bay) and one transect T3 in the North-South direction were casted inside the bay (figure 5.20).

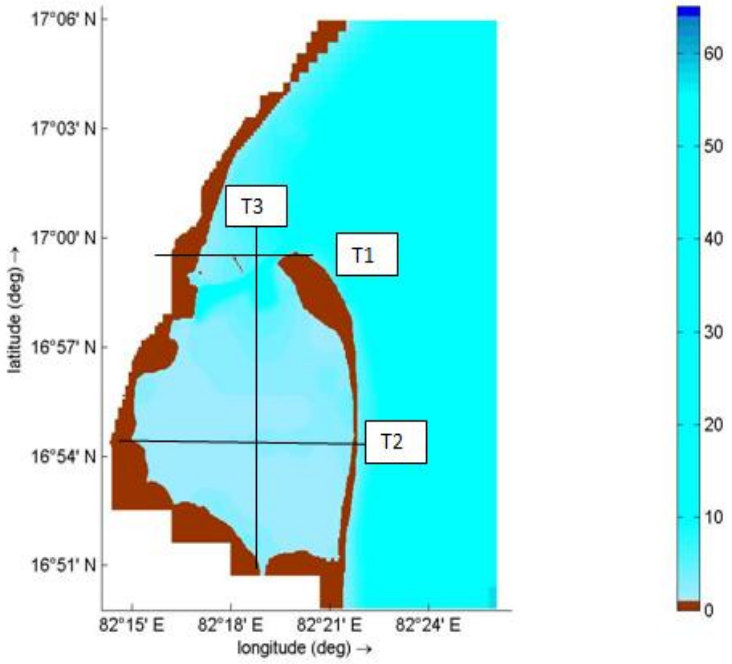

Figure 5.20. Transects casted for comparison of morphological simulation results obtained from the three variants.

5.5.2 Depth variation across the Cross-Sections of the bay

Transect 1 is the cross-section at the mouth of the bay in the West-East-direction. The length of this transect is nearly 5km.

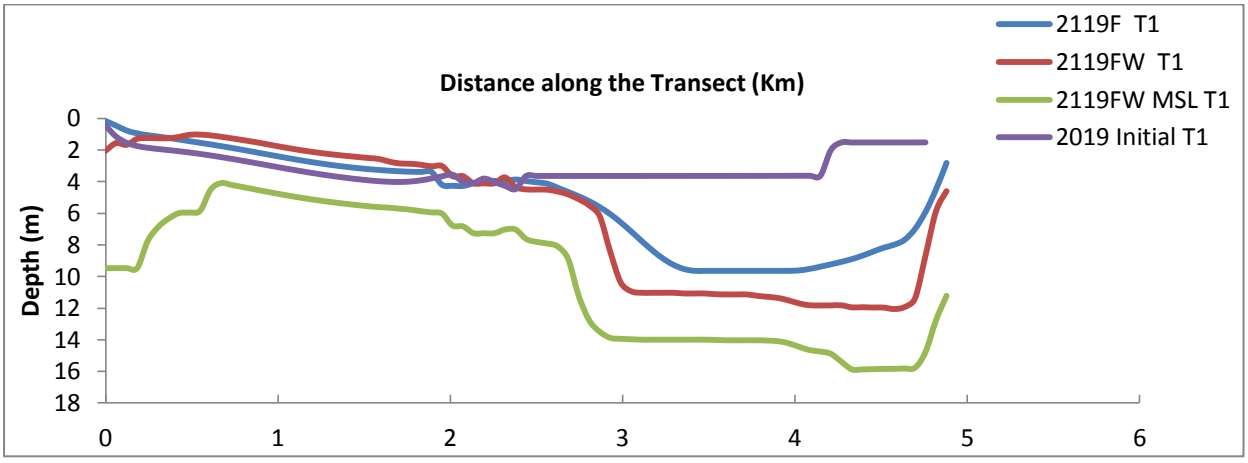

Figure 5.21. Resulting cross-section of year 2119 comparing Tides alone, Tides and Waves combined and sea level rise with combined tides and waves along Transect 1.

The figure 5.21 shows the depth result of year 2119 of all three simulations compared with the initial depth of the cross-section of year 2019. F in the graph denotes tides alone, FW denotes tides and waves combined and FW MSL denotes tides and waves combined with increase in mean sea level. The figure 5.21 suggests that the curves show the depth change at the mouth of the bay in the West-East direction. The overall graph suggests there is high increase in depth with the mean sea level rise as compared to tides alone and tides and waves combined. While with tides and waves combined, the depth of the cross-section is slightly more than with only tides in action which suggests erosion has occurred. The initial part of the curve shows that there is a slight decrease in the depth with tides and tides and waves combined simulation from the initial bathymetry which suggests that deposition has occurred. While in the centre of the curve, there is similar pattern of depth variation is observed. The right side of the curve shows there is increase in the depth due to the deepening of channel. The last part of the curve shows that the mouth of the bay has widened when compared with the initial depth. This suggests the offshore extension of spit over a period of 100 years with the combined action of three forcing.

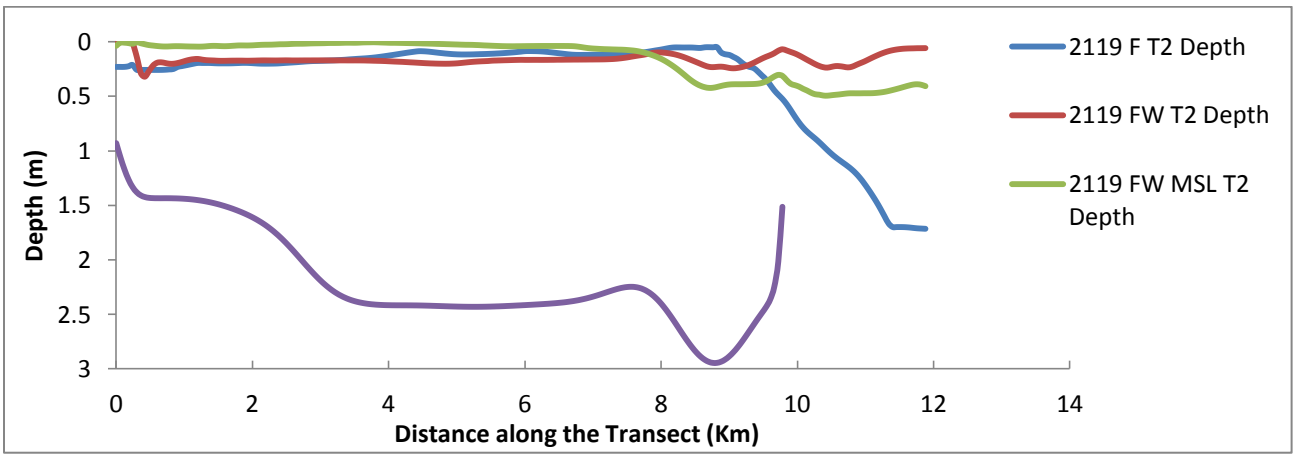

Figure 5.22. Resulting cross-section of year 2119 comparing Tides alone, Tides and Waves combined and sea level rise with combined tides and waves along Transect 2.

The figure 5.22 shows the change in depth along the transect 2 inside the bay for year 2119 comparing the three forcing with the initial depth. Transect 2 is casted in the West-East direction in the middle of the bay. The graph suggests that considerable amount of sedimentation has occurred inside the bay resulting into decrease in the depth from the initial conditions. The right side of the curve in the graph suggests the offshore extension of the spit. With tides alone, at the right branch of the curve, the increase in depth suggests the deepening near the spit that has taken place with 100 years of morphological evolution. While with the combined action of tides and waves and with MSL rise, there is comparatively lesser increase in depth near the spit which suggests that with wave action and MSL rise, the sedimentation has counteracted the occurrence of deepening near the spit.

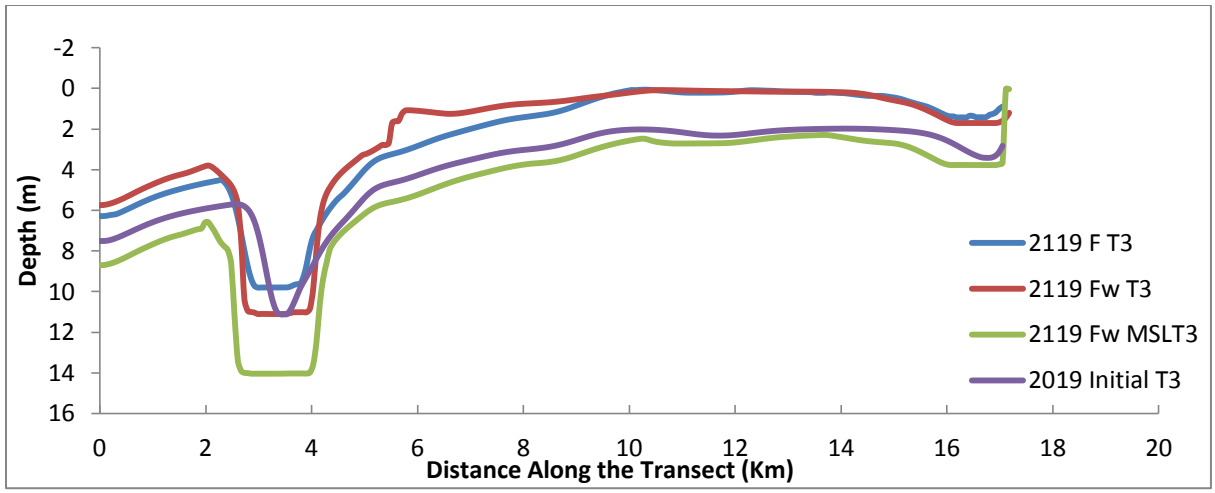

Figure 5.23. Resulting cross-section of year 2119 comparing Tides alone, Tides and Waves combined and sea level rise with combined tides and waves along Transect 3.

The figure 5.23 shows the change in depth along the transect 3 inside the bay for year 2119 comparing the three forcing with the initial depth. Transect 3 is casted in the North-South direction (figure 5.20). Left part of the curve shows the deepening of the mouth of the bay with rise in sea level as compared to the initial bathymetry. The centre part of the curve denotes

the changes in the middle portion of the bay. The figure shows that with the action of tides alone and combined waves and tides, lot of sedimentation has occurred resulting into the reduction of the depth. While the depth obtained with sea level rise with combined action of tides and waves, depth of the bay has increased. The right side of the curve shows the change in the depth of the southern bottom of the bay. This also has shown the similar trend of considerable sedimentation leading to lowering of depth in the centre and the southern part of the bay, while simulation with rise in sea level shows the increase in the depth.

5.5.3 Shoreline changes

The change in the shoreline boundary of the bay including the western side mangroves, southern portion and the spit has been compared for the three variant simulations. Shorelines were delineated for morphological prediction of Kakinada Bay from 2019 to 2119 for all three variants: Tides alone, Tides and Wave and Tides and Wave with decadal Mean Sea Level Rise. The figures 5.24, 5.25, 5.26 and 5.27 show the change in bay from year 2019 to 2119.

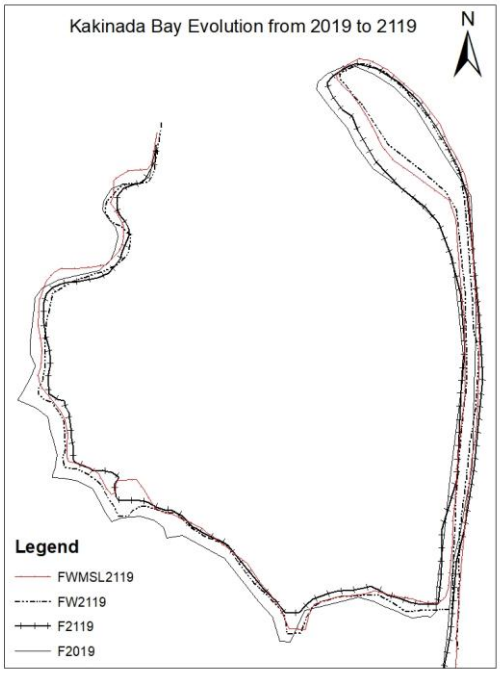

Figure 5.24. Resulting shorelines of Kakinada Bay for year 2119 comparing Tides alone, Tides and Waves combined and sea level rise with combined waves and tides.

Figure 5.24 illustrates the simulated shorelines of Kakinada Bay for year 2119 obtained after 100 years of the morphological simulation comparing three different forcing models: Tides alone, Tides and Waves combined and Decadal Mean sea level rise with the combined tides and waves with the initial shoreline of year 2019. F in the figure denotes tides alone, FW denotes tides and waves combined and FW MSL denotes tides and waves combined with increase in mean sea level. The figure shows that the Spit has moved slightly towards offshore from year 2019 to 2119 for all three variants. There is thinning of head of spit with addition of waves over 100 years as compared to the tides alone.

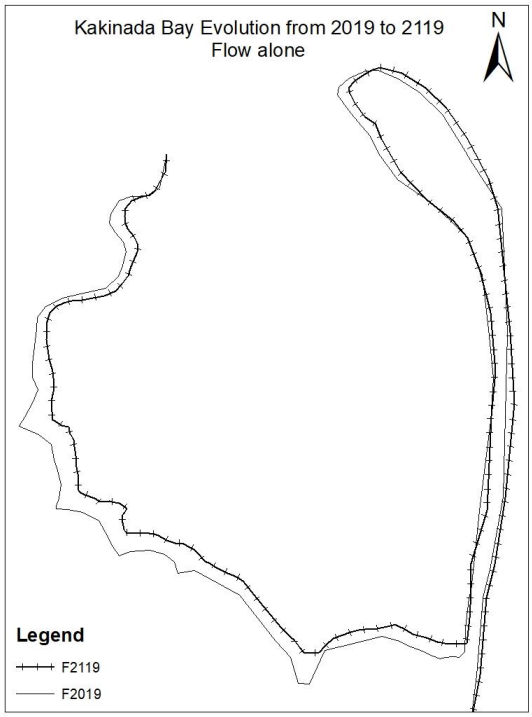

Figure 5.25. Resulting Shoreline of Kakinada Bay for year 2119 with Tides alone as forcing.

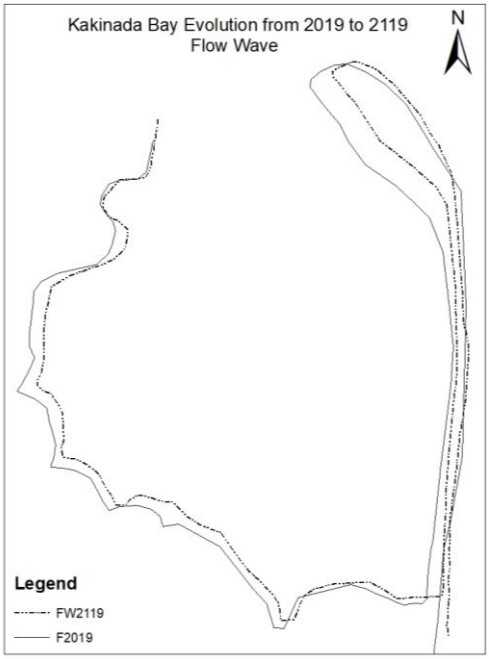

Figure 5.26. Resulting Shoreline of Kakinada Bay for year 2119 with tides and waves as forcing.

Figure 5.27. Resulting Shoreline of Kakinada Bay for year 2119 with tides and waves with MSL Rise as forcing.

The figures 5.25, 5.26 and 5.27 show the bay evolution after 100 years with tides alone, tides and wave combined and decadal mean sea level rise with tides and wave combined as forcing respectively. It shows that in figure 5.25 with tides alone as forcing, there is considerable accretion at the western side and southern part of the bay. There is very slight migration of head of the spit towards offshore direction. The figure 5.26 shows that with the combined action of tides and waves, there is considerable accretion at the western part of the bay, but very slight accretion at the south-eastern part of the bay. The change in spit morphology as obtained shows there is thinning of the spit at the head and in the spit length. The spit has extended offshore at the eastern side. The extension of spit is attributed as the result of the net longshore drift caused by the wave-induced longshore current (Dastgheib A., 2012) pushing the spit in the direction of the wave-induced current as suggested by Sha and Van den Berg (1993). Figure 5.27 illustrate

the effect of rise in mean sea level on the morphology of the bay. It is observed that at the north-west part of the bay, shoreline has moved towards the land suggesting the submergence of land due to land erosion under the effect of sea level rise. While at the rest part of the western side of the bay, considerable accretion has occurred. At the southern part of the bay, there is a slight shift of the mouth of the Gaderu River towards the right side. At the eastern corner of the spit near its foot, accretion of land is observed alongwith the offshore extension of spit. With rise in sea level, the offshore extension of spit head and the spit length has occurred leading to the widening of the mouth of the spit.

5.5.4 Suspended Sediment Concentration across the Cross-Sections of the bay

Transect 1 is the cross-section at the mouth of the bay in the West-East direction (figure 5.20). The distance of this transect is nearly 5Km.

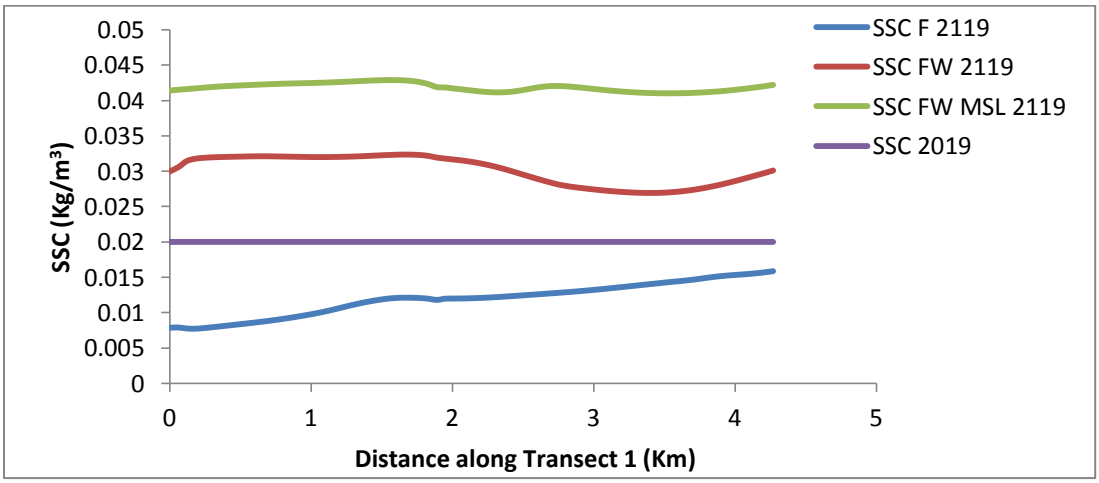

Figure 5.28. Resulting Suspended Sediment Concentration for year 2119 comparing Tides alone, Tides and Waves combined and sea level rise with combined tides and waves along Transect 1.

The figure 5.28 shows the resultant sediment concentration for year 2119 obtained from three simulations at transect 1 from West-East direction of

the bay compared with the initial sediment concentration of year 2019. The figure suggests that the curves show the sediment concentration change at the mouth of the bay from the western part of the bay to the eastern part of the bay. The figure 5.28 suggests there is high increase in sediment concentration for the simulation with combined effect of tides and waves as well as the simulation with added effect of mean sea level rise. The results show that with addition of waves, in comparison with the 2019 SSC, almost uniform increase in SSC is seen. This shows that the wave induced current have brought sediments along by the action of longshore sediment transport.

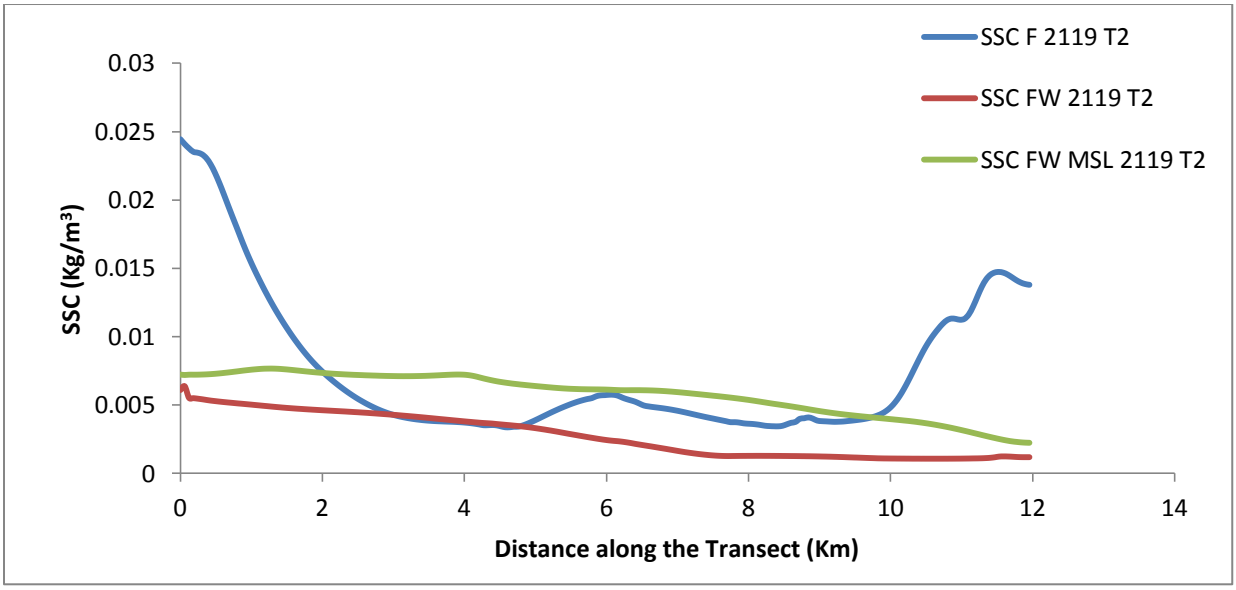

Figure 5.29. Resulting Suspended Sediment Concentration for year 2119 comparing Tides alone, Tides and Waves combined and Mean sea level rise with combined tides and waves along Transect 2.

The figure 5.29 shows the resultant sediment concentration for year 2119 obtained from three simulations at transect 2 casted in West-East direction compared with the initial sediment concentration of year 2019. Transect 2 is casted in West-East direction at the centre of the bay (figure 5.20).

The figure 5.29 shows that overall sediment concentration in the centre of the bay has decreased considerably as compared to the initial sediment concentration. The figure suggests the sediment concentration in the centre of the bay is comparatively higher for the simulation with combined action of MSL rise with waves and tides. The left branch of the curve with tides alone as forcing shows high sediment concentration at the western part of the bay which is decreasing along transect in the centre of the bay. While the right branch of the same curve with tides alone as forcing shows the sediment concentration increases as the transect moves near the spit. The figure shows that with addition of waves along with tides, the sediment concentration at the centre of the bay is quite less which decreases slightly further towards the right side of the transect moving towards the spit. The decrease in sediment concentration with waves and tides as forcing suggest action of wave induced currents in stirring and eroding the sediments from the bay.

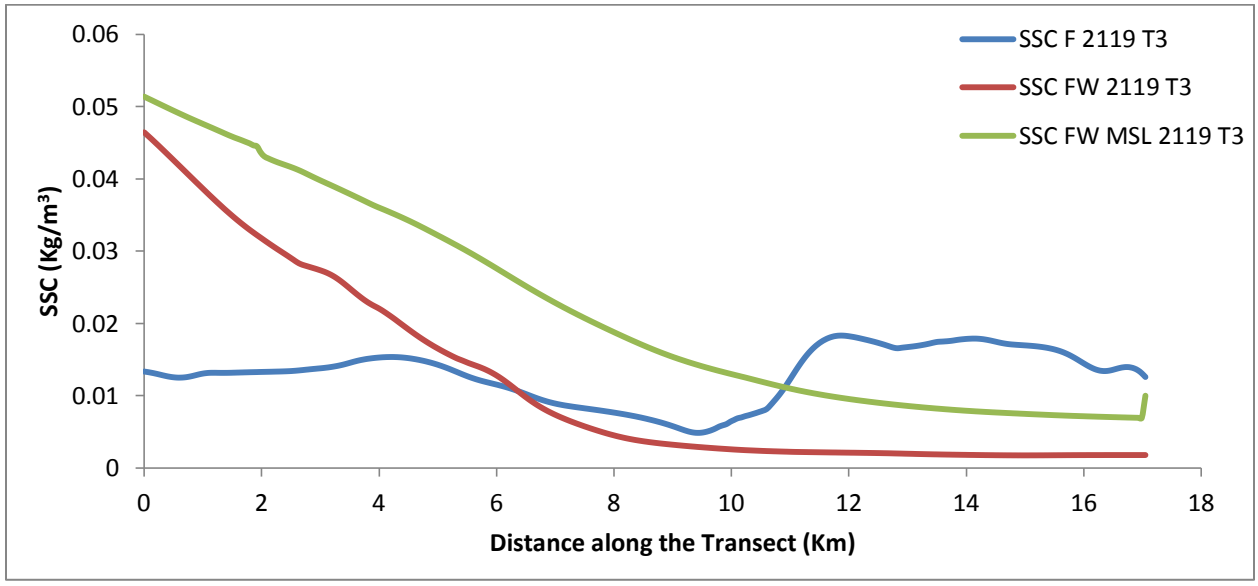

Figure 5.30. Resulting Suspended Sediment Concentration for year 2119 comparing Tides alone, Tides and Waves combined and Mean sea level rise with combined tides and waves along Transect 3.

The figure 5.30 shows the resultant sediment concentration obtained for year 2119 from three variants as input forcing simulations at transect 3 casted in North-South direction (figure 5.20). The left branch of the curve denotes the northern part of transect at the mouth of the bay where with combined action of waves and tides and mean sea level rise with waves and tides have shown high sediment concentration. While as the transect moves down the bay in the centre and the southern part of the bay, the sediment concentration has considerably reduced. The sediment concentration with tides alone as forcing is changing very less throughout the transect distance. Sediment concentration at the mouth of the bay is nearly in equilibrium till its length across the centre of the bay, while a sudden drop in the concentration is observed at the centre, further increasing till the southern bottom of the bay.

The sediment concentration graphs suggest that the action of wave is highly concentrated at the mouth of the bay, where sediments are brought by the action of the longshore transport.

5.5.5. Volumetric Changes

The sand volume of the bay was computed for 100 years of morphological prediction of the bay. The volume was compared for three variants from year 2019 to 2119. The volume of the bay was computed using SURFER, where depth points over grid points were interpolated using Kriging interpolation method. The sediment volume of each year for all three variant simulation results were computed using positive or cut volume calculated for the space between the grid surface and arbitrarily chosen datum of Z=-20. The area of bay taken for volume calculation is shown in figure 5.31. The polygon defines the spatial boundaries for which volume was computed.

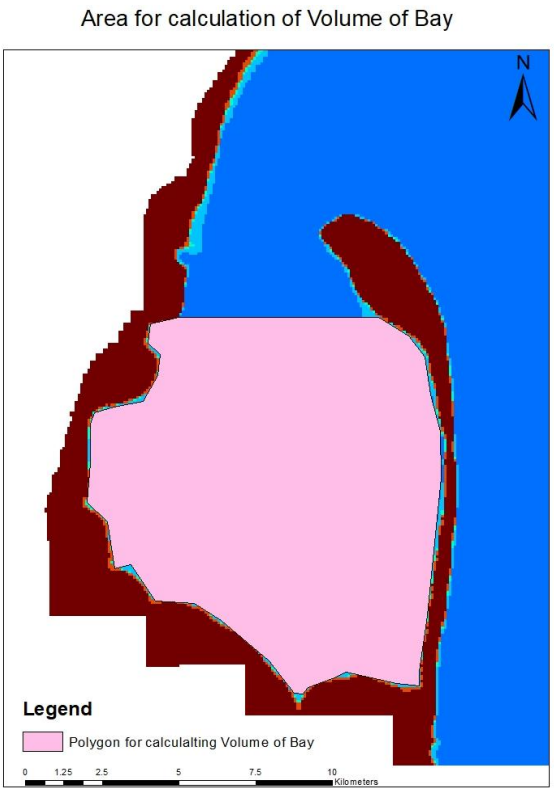

Figure 5.31. Polygon taken for calculation of volume of the bay

Table 5.16. Comparison of sediment volume of the bay from 2019 to 2119

Year	Sediment Volume Tides only (Million m^3)	Sediment Volume Tides & Waves (Million m^3)	Sediment Volume Tides & Waves with MSL changes (Million m^3)
2019	350	350	350
2029	339	318.72	320.89
2039	330	277.77	320.89
2049	324.58	273.33	318.21
2059	317.21	273.33	307.30

2069	312.78	271.83	304.31
2079	312.78	271.03	315.86
2089	309.17	269.87	312.86
2099	308.07	269.29	309.83
2109	307.70	270.60	307.66
2119	307.70	301.15	275.03

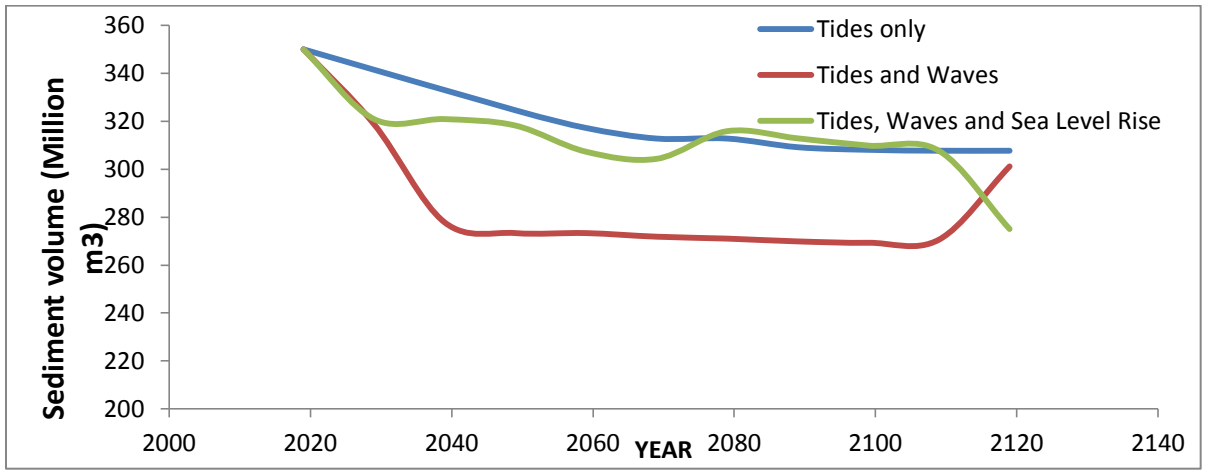

Figure 5.32. Sedimentation Volume of the Bay

The figure 5.32 shows that sediment volume of the bay has varied with different forcing. With tides alone, there is very slight decrease in the volume of the bay. Initially there is a steep slope but at the later branch of the curve, the curve is maintained. The branch of the curve from the beginning to the right in the figure can be referred as morphologically stable which happened because of the balance achieved due to the deposition of sediments The volume exchange with tides alone as forcing is nearly constant as mixing leads to flushing in the bay (Dyer, 1973).

When the flow-wave action is combined as forcing action, there is a steep decrease in the volume. After a swift adjustment to the slope profile, the volume has attained a quasi-equilibrium stage. With added waves, wave-

induced current and additional bed shear stresses come into action (Dastgheib, A., 2012). In the initial stages of evolution, the high water depth is lowering which leads to increase in the wave induced bottom shear stress. Hence the waves start resuspending the bottom sediments and lowers down the bottom elevation. The reduction of volume with addition of waves is explained by Dastgheib, A., (2012) as with larger tidal range, bed shear stress generated by waves becomes insignificant and leads to decreased sediment stirring. Further in the figure the volume has reached a dynamic equilibrium which attributes to the fact that there has been a balance achieved between the erosion and deposition occurring inside the bay. The figure shows that the tidal flat at the branch of the curve from the peak to the right has attained the dynamic equilibrium and has become morphologically stable. While at the end of the curve there is a sharp accretion peak obtained due to sediment deposition. The vertical peak achieved by the tidal flat is the result of the self-reinforced process with high accretion dynamics. The rise in volume is explained by the phenomenon that processes play part in filling up the basin as all elevations lower than the peak are not stable. Once maximum bottom shear stress is reached at low elevation, the maximum height of waves is limited by the dissipative processes like bottom friction, white capping and wave breaking (Fagherazzi, S., et al., 2007).

With Flow and Wave combined action and decadal MSL rise, the sedimentation volume curve as shown in the figure suggests that the volume of the bay for a larger time hasn’t varied much except for a dip in 2060 and 2070. After this to the right of the branch of the curve, there is very slight dip in the volume followed by a steep volume decrease at the end by 2119. The high sea level rise with combined effect of tides and waves led to sediment erosion. This phenomenon can be described as when the newly

deposited sediments show shallowing of bay as water volume decrease with time.

5.5.6 Statistical Analysis of Simulated Shoreline

To develop correlation between the DSAS statistical results and the morphological model results, the 2049 year predicted shoreline from tides alone simulation was given in the database (Figure 5.5). Statistical analysis was performed for calculating the rate of shoreline change from year 1977 to year 2049.

5.5.6.1 EPR and NSM of forecasted shoreline

The shoreline for year 2049 was extracted from the morphological model forecasting result. The shoreline was added in the DSAS database to calculate the shoreline change trend from year 1977 to 2049. There were 41 transects casted for 20km shoreline and End Point Rate and Net Shoreline Movement was calculated for a period of 72years. The average EPR accretion rate obtained was 10.6m.y^{-1} and the average EPR erosion rate 1.01m.y^{-1} for period 1977-2049. Net Shoreline Movement showed shoreline considerably accreted for more than 1km at transects 1 to 9, 20 to 22.

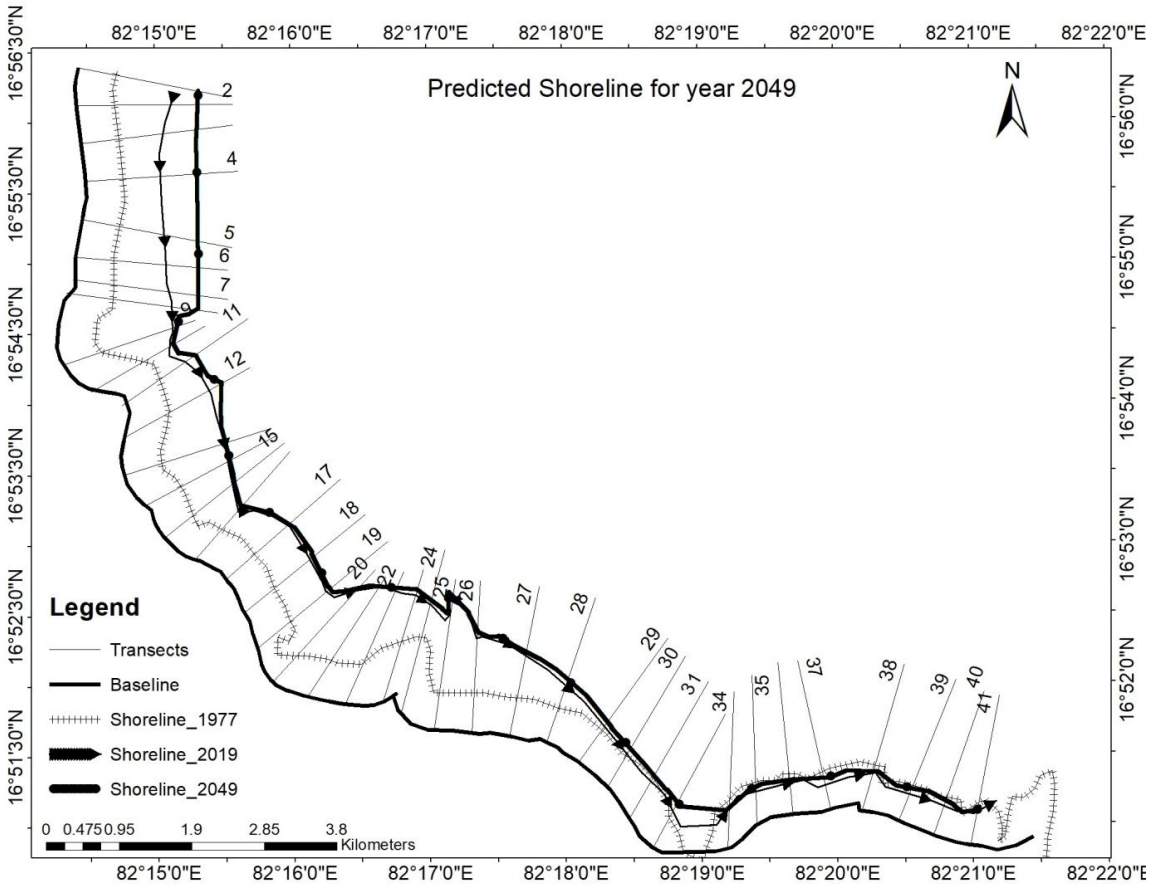

Figure 5.33. Simulated shoreline for year 2049 with satellite derived shorelines

Figure 5.33 shows the year 2049 simulated shoreline accreting considerably at the western side of the bay from year 1977 which in the similar trend as obtained by DSAS.

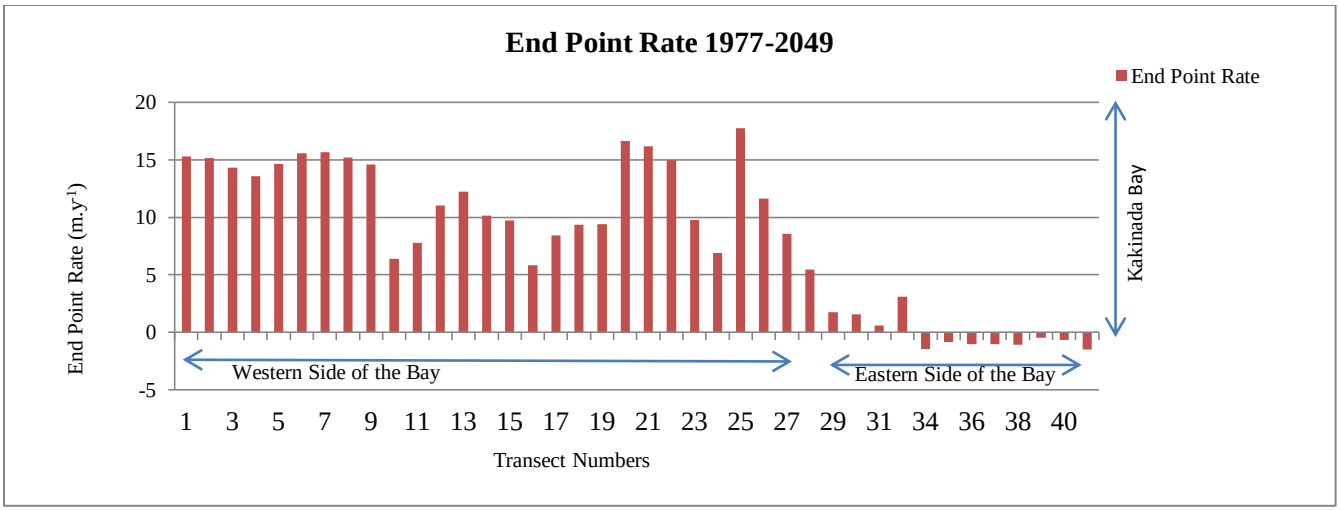

Figure 5.34. Transect wise End Point Rate ($m.y^{-1}$) for 1977-2049 for 20Km stretch.

EPR results (Figure 5.34) show considerable accretion predicted majorly from transects 1-26 from 1977-2049 at the western side of the bay. Shoreline movement obtained from DSAS and the morphological model are in the similar trend.

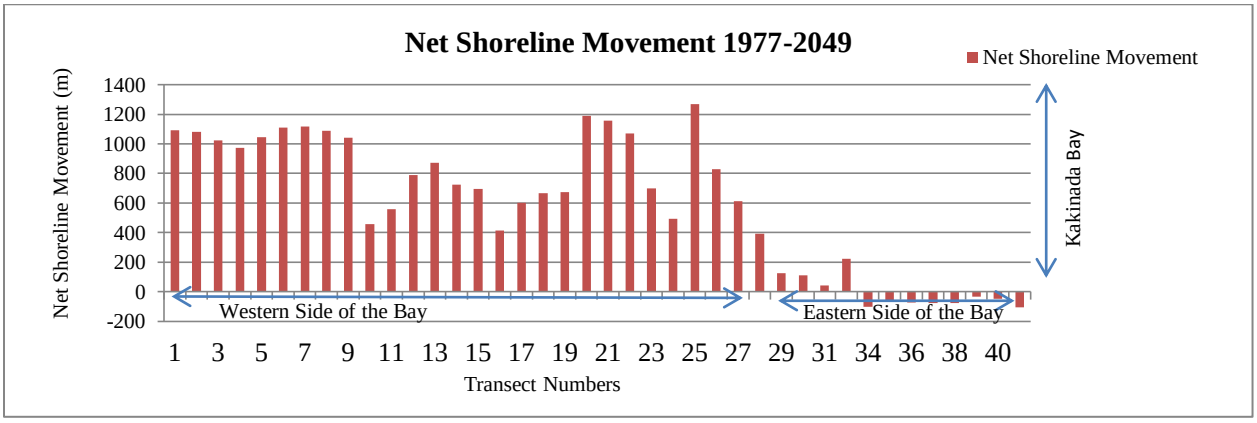

Figure 5.35. Transect wise Net Shoreline Movement (m) for 1977-2049 for 20Km stretch

Figure 5.35 shows the NSM from year 1977 to 2049 accreting majorly at the western side of the bay. Shoreline has accreted for more than 1km at

transects 1 to 9, and 21 to 23 in 72 years span of time while very slight erosion at the eastern side of the bottom of the bay.

The statistical results obtained after evaluating the trend obtained for shoreline migration from numerical modeling is in similar trend with the statistical results obtained using remote sensing and GIS on DSAS platform. The numerical modeling results show similar pattern of accretion and erosion as was found while assessing the shoreline migration using satellite shorelines incorporated in DSAS. The western side of bay has clearly been accreting while there is slight erosion occurrence at the southern bottom of the bay.

5.5.6.2 Statistical comparison of Shoreline obtained from Remote Sensing and Forecasted shoreline obtained from Numerical Modeling

The statistical comparison was made between the Remote Sensing and Numerical Modeling techniques. The shorelines derived from satellite imagery and the simulation results obtained using numerical modeling was compared. Both the shorelines were taken in DSAS and End Point Rate over a period 1977-2019 was compared presented in figure 5.36. The End Point Rate was compared for the hindcast simulated shoreline obtained for year 2019 with the satellite shoreline for year 2019.

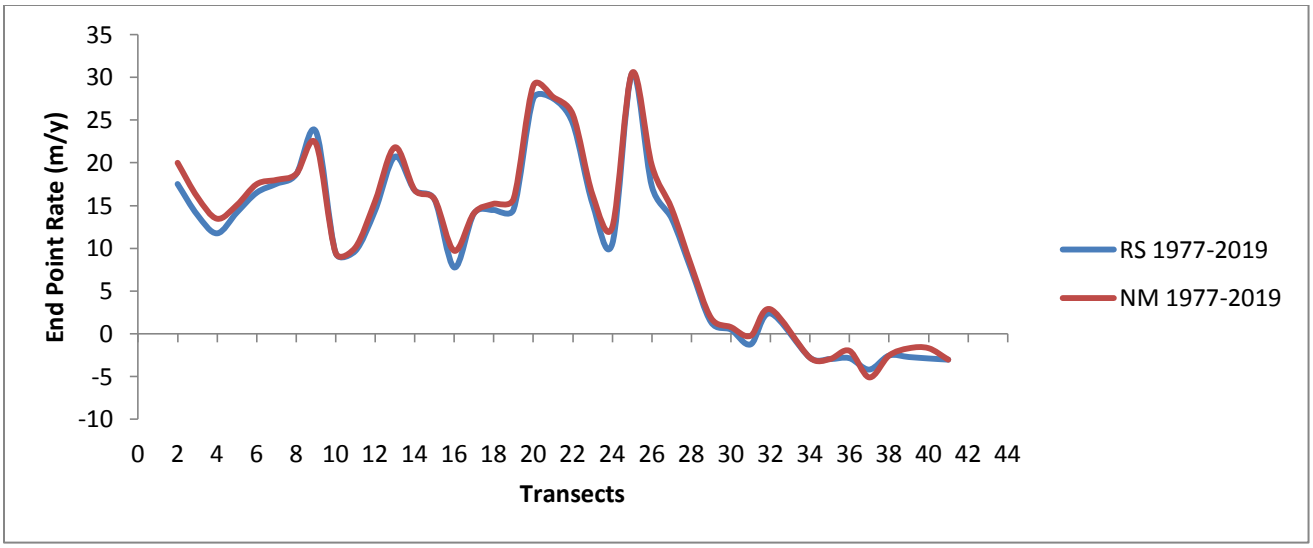

Figure 5.36. End Point Rate comparison for shoreline derived from remote sensing and numerical modeling for year 2019. (RS denotes Remote Sensing and NM denotes Numerical Modeling).

The figure 5.36 shows the End Point Rate figures obtained comparing the two shorelines. It shows that at the left branch of the curve representing the initial transects, the EPR is slightly higher for the hindcast numerical simulation result. The End point rates show that there is considerable shoreline movement at the western part of the bay while slight erosion is found in the southern part of the bay near the foot of the spit. Both the shorelines derived from the satellite imagery and numerical modeling are in close correlation. The Regression coefficient obtained was 0.9931. Thus the results develop good confidence in the numerical modeling results.

Thus the nexus of these two studies gives an exemplary integration of the available technologies that can be helpful for various coastal development modeling.

CHAPTER 6

SUMMARY AND CONCLUSIONS

The evolution of Kakinada Bay along with its morphological features like Coringa Mangroves, Kakinada Spit and Hope Island over a period of century is attributed to the action of physical forcing, hydrodynamics, wave action and sediment dynamics. The aim of this research to predict the long-term morphological development of Kakinada bay over spatial extent of kilometers and temporal scales of century has been successfully achieved.

6.1 Summary

This study has quantified the rate of change of the shoreline of Kakinada Bay using the Landsat imageries for years 1977, 1988, 2000, 2013 and 2019 in the DSAS. The trend of erosion and accretion occurring inside the bay was obtained for a mangrove shoreline length of 20.5 km. 41 transects were cast at an interval of 500 m for calculating the change and their migration distance using three statistical indices EPR, NSM and LRR. Results showed that there was considerable growth of mangroves in the bay leading to the seaward migration of the mangrove shoreline from the year 1977– 2019. The study observed the difference in the mangrove shoreline migration dynamics in the South-eastern (near the southern part of the spit) and the western part of the Kakinada Bay. The results help in identifying the regions prone to mangrove degradation and enable management planning for the protection of the eroding stretch of the mangrove shoreline.

Coringa Mangrove shoreline change analysis for 42 years from 1977 to 2019 enhanced by remote sensing, GIS and statistical analysis contributed a better understanding of the temporal and spatial rate of change of mangrove shoreline. Shoreline rate of change evaluated by the statistical methods EPR and LRR showed a strong correlation between the two. Quantitative

estimates of shoreline changes reported the higher average accretion rate along the mangrove shoreline stretch throughout the period of four decades. About two-thirds of the mangrove shoreline accreted at the western side of the bay, while shoreline recession at the eastern side of the bottom of the bay was observed. The forcing mechanism of the mangrove shoreline migration was out of the scope of the present study and the work can extend these results using numerical modeling techniques.

In the present study an attempt has been made to assess the shoreline migration of Coringa Mangroves using remote sensing imageries on DSAS platform. The trend obtained showed the erosion and accretion pattern inside the bay and their rates for the time period 1977-2019. Having assessed the trend of shoreline migration, this study further aimed to predict the morphological development of bay for next 100 years from year 2019 to 2119. Morphological modeling was done using flow model of DELFT 3D. The model was calibrated by validating the simulation results with the observed values. In order to reduce the computational time and efforts for running simulations for longer time periods, morphological model was formed using model reduction, input reduction method and acceleration method. Model reduction method was applied by taking only the most important processes as input, hence one simulation was performed with tides alone as input forcing. Input reduction method was followed by forming the morphological tide and representative schematized waves. Constant and variable morphological acceleration factors were formed applying acceleration method. For the combined action of tides and waves, online flow and wave coupled model was formed.

Morphological tide was formed using constituents M_2 and C_1 and morphological acceleration factor was chosen using sensitivity analysis by comparing the accelerated and non-accelerated simulation results. Representative waves were schematized using Potential Sediment Transport

Approach. The morphological model was validated by performing hindcast simulation for 30 years from 1988 to 2019 and the resultant shoreline was compared with the satellite derived shoreline. The DSAS results were used to compare the trend of accretion and erosion obtained by morphological modeling. Once morphological model was validated, forecast simulation was performed for 100 years from 2019 to 2119 for three variants. Three different simulations were performed with tides alone, tides and waves combined and decadal sea level rise with combined effect of tides and waves. The planimetric variations, shoreline changes, depth variations, suspended sediment variations and volumetric changes of the bay were compared for three simulation results.

6.2 Conclusions drawn to the research questions

In order to achieve the aim of this research, the study was done step wise with two objectives and few questions addressed. Conclusions derived reaching these objectives and addressing questions are summarized here.

a) To which extent the long-term morphological modeling results are reliable?

This study answers the question if these long-term morphological modeling can produce the reliable results by creating nexus of two techniques 'Remote Sensing and Numerical Modeling'. The morphological model is validated by running the hindcast model simulating the morphological development of bay for 30years from 1988 to 2019 with three sets of simulation. The hindcast simulated results were compared with the remote sensing satellite derived shoreline for simulation with tides only, tides and waves combined with waves schematized with Energy Flux Method and tides and waves with waves schematized with Potential Sediment Transport Method. The simulated and satellite derived shorelines for year 2019 were superimposed

together on satellite imagery of year 2019. The model predicted results were evaluated using Brier Skill Score (BSS) for six transects compared with benchmark shoreline and the results were found to be in close agreement with BSS value greater than 0.9 for all six transects. The validation of both models with tides alone and with tides and waves combined show that with addition of wave, model is validated better overall. Hence with the reasonably validated hindcast morphological model, the long-term morphological modeling results are considered reliable.

b) Which are the most crucial hydrodynamic forcing in the long-term morphological development of the region?

The long-term morphological modeling uses the process-based models which use various approaches like Model reduction where physical processes to be modeled are reduced; Input reduction where the input forcing are schematized to the representative input producing results similar with the full-time data. For long-term morphological modeling it is imperative to identify and distinguish the most crucial processes leading to the morphological development of the bay on larger spatial and temporal scales. This helps in understanding the effect of exclusion of less significant processes from the model over long-term morphological results of the bay. The study has made a successful attempt to answer the hypothesis made to choose the appropriate approach between the two statements issued by Lesser (2009) and Roelvink (1999). The approach for adopting model reduction following the correct use of acceleration techniques as stated by Lesser (2009): "In order to use a morphological acceleration technique in a coastal situation it is essential to identify which coastal processes play a significant role in (residual) sediment transport patterns over the space and time scales of interest". The second approach following the statement given by Roelvink (1999) and quoted by Dastgheib A. (2012) as: "If you put

enough of the essential physics into the model, the most important features of the morphological behavior will come out, even at the longer time scales".

This study investigated the morphological modeling results of two approaches incorporating the 'most important processes' and the 'essential physics'. Hence the morphological modeling for 100 years is performed over two sets of physical processes; one with tidal effects only and another with tides and waves. The forecast results were compared for both the simulations comparing the planimetric variations, shoreline variations, volumetric changes, suspended sediment concentration, depth changes. It was found that with addition of waves, the longshore transport was brought into the action bringing considerable amount of sediments at the mouth of the bay. Though wave action is less inside the bay, addition of wave as forcing brought improvement in the model results.

Addition of waves with tidal simulation has brought out wave-induced currents leading to longshore sediment transport bringing more sediment in the system. The study concludes that incorporating underlying processes in numerical simulation is the most appropriate approach as it gives more insight into the behavior of the system. Adding the effect of interaction of wave current on sediment transport brought out a relatively more complete mechanism of the long-term morphological evolution.

c) Can the climate change effects on the development of bay be predicted by the long-term morphological model?

The long-term morphological models can help in examining the anthropogenic activities leading to climate change effects like the sea-level rise. The third set of simulation brought out the morphological evolution of the bay over the decadal rise in mean sea level combined with waves and tides action. Since the morphological change and result of mean sea level rise on tidal bay takes long period of decades and century, this long-term

modeling has investigated the effects of human intervention led climate change on the long-term morphological modeling. Adding waves and sea level rise has a substantial effect on the bay. With the increase in mean sea level, there occurs decrease in frictional effects, tidal amplification alteration and dampening of shallow water effects. Adding all forcing like waves, tides, and sea level rise in the model brought out a more complete morphological development. The study shows that morphological model has reproduced the complete change in bay morphological features and has quantitatively assessed the sea level rise effect in the coastal system.

Thus the study has achieved its objectives as the long-term morphological model of Kakinada Bay is predicted using numerical simulation duly validated with remote sensing data. The numerical model shoreline results obtained with hindcast simulation are compared with the shoreline derived from the satellite imageries and performance of the models is evaluated using Brier Skill Score. With confidence achieved in the model results, 100 years of morphological development from year 2019 to 2119 is simulated and compared for three different scenarios. The incorporation of environmental forcing as model inputs is optimized by identifying their incremental effects over the morphological development over 100 years.

6.3 Utility/application of results in prediction of mangrove coverage

The nexus of remote sensing and numerical modeling is an efficient combination of two studies that help in studying the trend of spatial and temporal morphological development of the coastal forms and predicting their long-term future development. The scheme of coupling of satellite imageries and numerical modeling is rarely adopted for studying the coastal development and shoreline migration studies large time scales. This study has used remote sensing images for studying the trend of evolution of

mangrove shoreline of Kakinada Bay using the statistical indices of DSAS and used it to validate the morphological model results. The integration of remote sensing and numerical modeling helps in understanding the dynamics of the coastal environment and improving the coastal development monitoring capability by filling the spatio-temporal data gaps and predicting the short and long-term development of the coastal forms and effectively plan the coastal protection and their management strategies.

The remote sensing data provides large spatial coverage and temporal resolution, but it has certain limitations of cloud cover and satellite revisit time. Though numerical models are used to simulate the shoreline migration based on the action of hydrological parameters, it needs validation for matching the simulation results with the actual shoreline migration. Concurrently, a hindcast model was established to calibrate the numerical model result with the satellite data. The simulated mangrove shoreline obtained by the hindcast modeling in this study showed alike pattern with the satellite derived mangrove shoreline. The remote sensing analysis and numerical modeling results showed that the mangrove shoreline migration and bay development is basically based on the tidal currents and the sediment transport.

Hence, both the methods have their own advantages. Nexus of these two can efficiently use their respective advantages like longer time series and high resolution data collaborated with the high computational power techniques and platforms. Thus it becomes a crucial method for monitoring the shoreline migration and predicting the evolution and development of the coastal area over large areas and longer time period.

6.4 Scope for future study

The study has tried out an approach on how remote sensing and numerical modeling can integrate to model a coastal ecosystem and help in predicting

the future development of the coastal area. The validation of numerical model results with the remote sensing data can very well build up the confidence in the simulation performed. The well calibrated and validated model simulation results can predict both the short and long-term evolution of the coastal forms. Hence it will give an insight in identifying the potential area susceptible to erosion and reduction of size of the landforms. Phenomenon like erosion and accretion leading to shoreline migration can be identified and measures for protection of the coast can be taken. Thus the conservation measures for the predicted endangered ecosystems can be well planned for their better management.

The incorporation of all possible physical processes in long-term morphological modeling brings out more complete dynamics of evolution. Simple schematization techniques for input reduction and acceleration of morphological modeling will help in reducing the long computational timing and effort. A sensitivity analysis for each additional forcing parameter on the overall evolution could be helpful to optimize the computational efforts.

REFERENCES

Alemayehu, F., Onwonga Richard, Mwangi James Kinyanjui and Wasonga Oliverv, 2014. Assessment of shoreline changes in the period 1969-2010 in Watamuarea, Kenya. Global Journal of Science Frontier Research: H Environment & Earth Science, 14 (6), 19-31.

Alongi, D.M., 2002. Present state and future of the world's mangrove forests. Environmental Conservation, 29 (3), 331-349.

Awang, Nor., 2010. Hydrodynamic modelling for mangrove afforestation at Haji Dorani, west coast peninsular Malaysia.

Balke, T., Bouma, T.J., Horstman, E.M., Webb, E.L. Erftemeijer P.L.A. and Herman P.M.J., 2011. Windows of opportunity: thresholds to mangrove seedling establishment on tidal flats. Marine Ecology-Progress Series, 440, 1-9.

Barman, N.K., Chatterjee, S. and Khan, A., 2015. Trends of Shoreline Position: An Approach to Future Prediction for Balasore Shoreline, Odisha, India. Open Journal of Marine Science, 5, 13-25.

Bhavnarayana P.V., 1974. Some observations on the Benthic faunal distribution in the Kakinada Bay. Recent researches in Estuarine Biology. (Ed.) R. Natarajan. Hindustan Publishing Corporation, Delhi, 146-150.

Booij, N., Ris, R. and Holthuijsen, L., 1999. A third-generation wave model for coastal regions, Part I, Model description and validation. Journal of Geophysical Research, 104 (C4), 7649– 7666.

Chandramohan, P., Nayak, B.U. and Raju V.S., 1988. Application of longshore transport equations to Andhra coast, East Coast of India. Coastal Engineering, 12, 285-297.

Chandramohan, P. and Nayak, B.U. 1991. Long shore sediment transport along the Indian coast. Indian Journal of Marine Sciences, 20, 110–114.

Chandramohan, P., Jena, B.K. and Sanil Kumar, V., 2001. Littoral drift sources and sinks along the Indian coast. Current Science, 81(3), 292-297.

Chandramohan, P., Nayak, B.U. and Raju, V.S., 1989. Distribution of deep corter wave power around the Indian coast based on ship observations. Journal of coastal Research, 5(4), 829-844.

Chandrasekar, N., V.Viviek, J. and Saravanan, S., 2013. Coastal vulnerability and shoreline changes for southern tip of India-remote sensing and GIS approach. Journal of Earth Science & Climatic Change, 04(4), 144.

Chen, D., M. Rojas, B. H. Samset, K. Cobb, A. Diongue Niang, P. Edwards, S. Emori, S. H. Faria, E. 8 Hawkins, P. Hope, P. Huybrechts, M. Meinshausen, S. K. Mustafa, G. K. Plattner, A. M. Tréguier, 2021, 9 Framing, Context, and Methods. In: Climate Change 2021: The Physical Science Basis. Contribution of 10 Working Group I to the Sixth Assessment Report of the Intergovernmental Panel on Climate Change 11 [Masson-Delmotte, V., P. Zhai, A. Pirani, S. L. Connors, C. Péan, S. Berger, N. Caud, Y. Chen, L. Goldfarb, 12 M. I. Gomis, M. Huang, K. Leitzell, E. Lonnoy, J.B.R. Matthews, T. K. Maycock, T. Waterfield, O. Yelekçi, 13 R. Yu and B. Zhou (eds.)].

Cook, P.L.M., Butler E.C.V. and Eyre B.D., 2004a. Carbon and nitrogen cycling on intertidal mudflats of a temperate Australian estuary. I. Benthic metabolism. Marine Ecology Progress Series, 280, 25–38.

Cowell, P.J. and Thom, B.G., 1994. Morphodynamics of coastal evolution. In: Carter R.W.G., Woodroffe C.D. (Eds.), Coastal Evolution: Late Quaternary Shoreline Morphodynamics. Cambridge University Press, Cambridge, 33-86.

Dam, G., Van Der Wegen, M., Roelvink, D., Labeur, R.J. and Bliek, Bram, B., 2015. Simulation of long-term morphodynamics of the Western Scheldt. In: 36st IAHR Congress, The Hague, Netherlands.

Dastgheib, A., 2012. Long-term process-based morphological modeling of large tidal basins. PhD thesis UNESCO-IHE/DUT. CRC Press/Balkema.

Deltares (2011a). User manual Delft3D-FLOW, Deltares, Delft.

Deltares (2014). User manual Delft3D-FLOW, Deltares, Delft.

De Vriend, H.J., 1991. Mathematical modelling and large-scale coastal behaviour, Part 1: Physical processes. Journal of Hydraulic Research, 29, 727-740.

De Vriend, H. J., and Ribberink, J. S. 1996. Mathematical modeling of meso-tidal barrier island coasts. Part II: Process-based simulation models. Advances in Coastal and Ocean engineering, P. L.-F. LIU, ed., World Scientific Publishing Company, Singapore, 150-179.

Deltares. The morphological model of the Rhine-Meuse Delta. 1205961-001-ZWS-0005, 31 December 2012.

Deltares. (2013). Delft3D-FLOW: Simulation of multi-dimensional hydrodynamic flows and transport phenomena, including sediments: User Manual. (Vol. Version: 3.15 Revision: 26466). Delft, the Netherlands: Deltares.

Deltares. (2014). Delft3D workshop. New Orleans, LA.

Dobrochinski, J.P.H., 2009. Wave climate reduction and schematization for morphological modelling. MSc Thesis, Delft University of Technology, Delft, Univali University, Brazil.

Dolan, R., Hayden, B.P. and May, S., 1991. Erosion of the US shorelines. Journal of Remote Sensing, 6, 26-31.

Dyer, K.R., 1973. Estuaries- a Physical Introduction, John Wiley & Sons, New York, 140pp.

Elbagory, I.A., Heikal, E.M. and Koraim, A.S, 2019. Shoreline Changes Using Digitizing of Landsat Images at Miami to Montaza Beach, Alexandria, Egypt. International Journal of Civil Engineering and Technology, 10(05), 75-91.

Elnabwy, M.T.; Elbeltagi, E.; El Banna, M.M., Elshikh, M.M., Motawa, I. and Kaloop, M.R., 2002. An Approach Based on Landsat Images for Shoreline Monitoring to Support Integrated Coastal Management—A Case Study, Ezbet Elborg, Nile Delta, Egypt. ISPRS International Journal of Geo-Information, 9, 199.

Escoffier, F.F., 1940. The stability of tidal inlets. Shore and Beach 8 (4), 111 – 114.

Fagherazzi, S., Palermo, C., Rulli, M.C., Carniello, L. and Defina, A., 2007. Wind waves in shallow microtidal basins and the dynamic equilibrium of tidal flats. Journal of Geophysical Research, 112, F02024.

Fenster, M., Dolan, R. and Elder, J., 1993. A new method for predicting shoreline positions from historical data. Journal of Coastal Research, 9, 147-171.

Fletcher, C.H., Romine, B.M., Genz, A.S., Barbee, M.M., Dyer, Matthew, Anderson, T.R., Lim, S.C., Vitousek, Sean, Bochicchio, Christopher, and Richmond, B.M., 2012. National assessment of shoreline change: Historical shoreline change in the Hawaiian Islands: U.S. Geological Survey Open-File Report, 2011–1051, 55 p.

Frederick, Ato Armah, 2011. GIS-based Assessment of Short Term Shoreline Changes in the Coastal Erosion-Sensitive Zone of Accra, Ghana. Research Journal of Environmental Sciences, 5, 643-654.

Friess, D.A. and Oliver, G.J.H., 2013. Dynamic Environments of Singapore. McGraw Hill.

Friess, D.A., Krauss, K.W., Horstman, E.M., Balke, T., Bouma, T.J., Galli, D. and Webb E.L., 2012. Are all intertidal wetlands naturally created equal? Bottlenecks, thresholds and knowledge gaps to mangrove and saltmarsh ecosystems. Biological Reviews, 87(2), 346-366.

Furukawa, K., Wolanski. E. and Mueller H., 1997. Currents and sediment transport in mangrove forests. Estuarine, Coastal and Shelf Science, 44(3), 301-310.

George, D.A., Gelfenbaum, G., Lesser G. and Stevens, A.W., 2006. Deschutes Estuary Feasibility Study: Hydrodynamics and sediment transport modeling. United States Geological Survey, Open File Report 2006-1318.

Himmelstoss, E.A., Farris, A.S., Henderson, R.E., Kratzmann, M.G., Ergul, Ayhan, Zhang, Ouya, Zichichi, J.L., and Thieler, E.R., 2018, Digital Shoreline Analysis System (version 5.0): U.S. Geological Survey software release, https://code.usgs.gov/cch/dsas.

Hoitink, A.J.F., Hoekstra, P., and Van Maren, D.S., 2003. Flow asymmetry associated with astronomical tides: Implications for the residual transport of sediment. Journal of Geophysical Research, 108(C10), 3315.

Horstman, E., Dohmen-Janssen, C.M., and Hulscher, S.J.M.H., 2013. Modeling tidal dynamics in a mangrove creek catchment in Delft3D. In P. Bonneton, & T. Garlan (Eds.), Coastal Dynamics, Arcachon, France, 833-844.

Jagers, H.R.A., 2003. Modeling planform changes of braided rivers: University of Twente.Jickells, T.D. and Rae, J.E. (eds), 1997. Biogeochemistry of intertidal sediments. 9, Cambridge University Press, Cambridge.

Jonah, F.E., Boateng, I., Osman, A., Shimba, M.J., Mensah, E.A., Adu-Boahen, K., Chuku, E.O. and Effah, E., 2016. Shoreline Change Analysis Using End Point Rate and Net Shoreline Movement 2 Statistics: an application to Elmina, Cape Coast and Moree Section of Ghana's Coast.

Kannan, R., Kanungo, A., Murthy, M.V.R., 2016. Detection of Shoreline Changes Visakhapatnam Coast, Andhra Pradesh from Multi-Temporal Satellite Images. Journal of Remote Sensing and GIS, 5, 157.

Kankara, R., Selvan, S.C., Markose, V.J., Rajan, B. and Arockiaraj, S., 2015. Estimation of long and short-term shoreline changes along Andhra Pradesh coast using remote sensing and GIS techniques. Proceedia Engineering, 116, 855–862.

Kraus, N.C., Larson, M. and Kriebel, D.L., 1991. Evaluation of beach erosion and accretion predictors. Proceedings of Conference Sediments 1991, ASCE, Seattle, 527-587.

Latteux, B., 1995. Techniques for long-term morphological simulation under tidal action. Marine Geology, 126, 129-141.

Lesser, G.R., Roelvink, Dano J.A., Van Kester, Jan and Stelling, G., 2004. Development and Validation of a Three-Dimensional Morphological Model. Coastal Engineering, 51, 883-915.

Lesser, G.R., 2009. An approach to medium-term coastal morphological modelling. PhD thesis, UNESCO-IHE & Delft Technical University, Delft. CRCPress/Balkema. ISBN 978-0-415-55668-2.

Li, H.; Jia, M.; Zhang, R.; Ren, Y.; Wen, X., 2019. Incorporating the Plant Phenological Trajectory into Mangrove Species Mapping with Dense Time Series Sentinel-2 Imagery and the Google Earth Engine Platform. Remote Sensing, 11, 2479.

Joesidawati, M.I. and Suntoyo, 2016. Shoreline change in Tuban district, East Java using geospatial and Digital Shoreline Analysis System (DSAS) techniques. International Journal of Oceans and Oceanography, 235-246.

Mageswaran, T., Mohan, V.R., Selvan, S.C., Arumugam, T., Usha, T. and Kankara, R.S., 2015. Assessment of shoreline changes along Nagapattinam coast using geospatial techniques. International Journal of Geomatics and Geosciences, 5(4), 555-563.

Mahadevan, C. and B. Prasad Rao., 1956. Growth of the sand bar north of the Godavari Confluence. Current Science, 25(12), 385–87.

Mary Divya Suganya, G., Rajakumari, S., Deepika, B., Mahumitha, R., Manonmani, R., Thulasi Bai, P.D., Anantha Kamatchi, G., Purvaja, R. and Ramesh, R., 2017. Spatio temporal change analysis of mangroves along the Krishna and Godavari Deltaic region using IRS satellite images. User Interface Meet (UIM), Hyderabad.

Massel, S.R., Furukawa, K. and Brinkman, R.M., 1999. Surface wave propagation in mangrove forests. Fluid Dynamics Research, 24, 219-249.

Mazda, Y., Magi, M., Nanao, H., Kogo, M., Miyagi, T., Kanazawa N. and Kobashi, D., 2002. Coastal erosion due to long-term human impact on mangrove forests. Wetlands Ecological Management, 10, 1-9.

Michiel, A.F., Knappen and Joustra, R., 2012. Morphological Acceleration Factor: usability, accuracy and run time reductions. XIXth TELEMAC-MASCARET User conference proceedings.

Moerman E., 2011. Long-term morphological modeling of the mouth of the Columbia River. Delft University of Technology, Delft, The Netherlands, Masters thesis.

Morton, R.A., Miller, T.L. and Moore, L.J., 2004. National assessment of shoreline change, Part 1: Historical shoreline changes and associated coastal land loss along the U.S. Gulf of Mexico, US Geological Survey Open File Report 2004-1043, US Geological Survey, USA, 44.

Mukhopadhyay, A., Mukherjee, S., Mukherjee, S., Ghosh, S., Hazra, S. and Mitra, D., 2012. Automatic shoreline detection and future prediction: A case study on Puri Coast, Bay of Bengal, India, European Journal of Remote Sensing, 45(1), 201-213.

Murty, M.R., Kumar, C.R., Reddy, K.M. and Ramasubramanian, R., 2011. Geospatial analysis of Coringa-Marine Protected Area, Andhra Pradesh, India. International Journal of Earth Sciences and Engineering, 4(8), 24-38.

Nageswara Rao, K., Sadakata, N., Hema Malini, B. and Takayasu, K., 2005. Sedimentation Processes and asymmetric development of the Godavari Delta, India. Society for Sedimentary Geology, ISBN 1-56576-113-8, 433–449.

Nageswara Rao. K., 2006. Coastal morphodynamics and asymmetric development of the Godavari delta: Implications to facies architecture and reservoir heterogeneity. Journal of the Geological Society of India. 67, 609-617.

Nair, S., 2017. Assessment and Vulnerability Modeling of Vanuatu's Mangroves using GIS and Remote Sensing. Master of Science Thesis, Central European University, Budapest.

Nayak, S., 2002. Use of Satellite Data in Coastal Mapping. Indian Cartographer, 147-156.

Oyedotun, Temitope D. Timothy., 2014. Shoreline geometry: DSAS as a tool for Historical Trend Analysis. Geomorphological Techniques. Chapter 3(2.2), British Society for Geomorphology, 1-12.

Pandey, A. and Nayak, G.N., 2013. Understanding distribution and abundance of metals with space and time in estuarine mudflat sedimentary environment. Environmental Earth Science, 70, 2561-2575.

Quartel, S., Kroon, A., Augustinus, P., Van Santen, P. and Tri, N.H., 2007. Wave attenuation in coastal mangroves in the Red River Delta, Vietnam. Journal of Asian Earth Sciences, 29(4), 576-584.

Rajyalaxmi, T., Maheswarudu, G., Reddy, D.M. and Joshi, H.C., 1986. An approach to environmental impact study in the Kakinada Bay. Environmental Biology Coastal Ecosystem, 125-140.

Ramasubramanian, R., and Ravishankar, T., 2004. Mangrove forest restoration in Andhra Pradesh, India. Chennai: M.S.Swaminathan Research Foundatio).

Ramasubramanian, R., Gnanappazham, L., Ravishankar T. and Navamuniyammal, M., 2006. Mangroves of Godavari – Analysis Through Remote Sensing Approach. Wetlands Ecology and Management, 14, 29-37.

Ranasinghe, R., Swinkels, C., Luijendijk, A., Roelvink, D., Bosboom, J., Stive, M. and Walstra, D., 2011. Morphodynamic upscaling with the Morfac approach: Dependencies and sensitivities. Coastal Engineering, 58, 806-811.

Rao, V.R., Reddy, B.S.R., Raman, A.V., Murthy, M.V.R., 2003. Oceanographic features of the Bay-Mangrove waterways of Coringa, east coast of India. Proceedings of AP Academy of Sciences, 7, 135–142.

Raut, D., Ganesh, T., Murty, N.V.S.S. and Raman, A.V., 2005. Macrobenthos of Kakinada Bay in the Godavari delta, East coast of India: comparing decadal changes. Estuarine Coastal Shelf Science, 62, 609–620.

Ravishankar, T. and Ramasubramanian, R., 2004. Manual on Mangrove Nursery Techniques. M.S. Swaminathan Research Foundation, Chennai.

Reddy, N.P.C. and Rao, K., 1996. Sedimentological and clay mineral studies in Kakinada Bay, east coast of India. Indian Journal of Marine Sciences, 25, 12-15.

Reshma, N.K. and Mani Murali, R., 2018. Current status and decadal growth analysis of Krishna - Godavari delta regions using remote sensing. Journal of Coastal Research. Special Issue No. 85: Proceedings of the 15th International Coastal Symposium, Haeundae, Busan, 13-18 May 2018, 1416-1420.

Reyns, J., Dastgheib, A., Ranasinghe, R., Luijendijk, A., Walstra, D.J. and Roelvink, D., 2014. Morphodynamic upscaling with the Morfac Approach in Tidal conditions. Coastal Engineering, 1-8.

Roelvink, D. and Reniers, A., 2012. A Guide to Modeling Coastal Morphology. World Scientific, Singapore.

Roelvink, J.A., 2006. Coastal morphodynamic evolution techniques. Coastal Engineering, 53(2), 277-287.

Rönnbäck, P., Troell, M., Zetterström, T., Babu, D.E., 2003. Mangrove dependence and socio-economic concerns in shrimp hatcheries of Andhra Pradesh, India. Environmental Conservation, 30, 344–352.

Sahu, Akash., 2019. Numerical Modeling of Shoreline Response to Storm Tides and Sea Level Rise. Master of Science (MS), Thesis, Civil &

Environmental Engineering, Old Dominion University, DOI: 10.25777/cbqn-0431.

Sanders, C.J., Smoak, J.M., Naidu, A.S., Araripe, D.R., Sanders, L.M. and Patchineelam, S.R., 2010b. Organic carbon burial in a mangrove forest, margin and intertidal mud flat. Estuarine, Coastal and Shelf Science, 90, 68-172.

Santoro, P., Fossati, M., Tassi, P., Huybrechts, N., Bang, D. P. V., Piedra-Cueva, J. C. I., 2017. A coupled wave-current-sediment transport model for an estuarine system: Application to the Río de la Plata and Montevideo Bay. Applied Mathematical Modelling, 52, 107-130.

Satyanarayana, B., Raman, A.V., Dehairs, F., Kalavati, C. and Chandramohan, P., 2002. Mangrove floristic and zonation patterns of Coringa, Kakinada Bay, East coast of India. Wetland Ecological Management, 10(1), 25–37.

Satyanarayana, B., Koedam, N., De Smet, K., Di Nitto1, D., Bauwens, M., Jayatissa, L.P., Cannicci, S. and Dahdouh- Guebas, F., 2011. Long-term mangrove forest development in Sri Lanka: early predictions evaluated against outcomes using VHR remote sensing and VHR ground-truth data. Mar. Ecol.-Prog. Ser., 443, 51–63.

Satyanarayana, B., Raman, A.V., Mohd-Lokman, H., Dehairs, F., Sharma V.S. and Dahdouh-Guebas Farid, 2009. Multivariate methods distinguishing mangrove community structure of Coringa in the Godavari Delta, East coast of India. Aquatic Ecosystem Health and Management, 12(4), 401-408.

Selvam V., Ravichandran K.K., Gnanappazham L., Navamuniyammal M., 2003. Assessment of community-based restoration of Pichavaram mangrove wetland using remote sensing data. Current Science India, 85, 794–798.

Sha, L.P. and Van den Berg, J.H., 1993. Variation in ebb-tidal delta geometry along the coast of The Netherlands and the German Bight. Journal of Coastal Research, 9 (3), 730–746.

Sharmila , R. Venkatachalapathy, R.S. Kankara, M. Mugilarasan and K. Gurumoorthi, 2015. Wave Characteristics of Kakinada Coast During South-West and North-East Monsoon: Statistical and Spectral Approach. International Journal of Oceanography and Marine Ecological System, (4) 16-30.

Souza-Filho, P.W.M., Martins, E.S.F. and Costa, F.R., 2006. Using Mangroves as a geological indicator of coastal changes in the Bragança macrotidal flat, Brazilian Amazon: A remote sensing data approach. Ocean & Coastal Management, 49, 462-475.

Sreenivas, N.V., 1998. Zooplankton composition and distribution in mangrove habitat of Godavari Estuary – Kakinada. PhD thesis, Andhra University, Andhra Pradesh.

Stark, J., 2012. The influence of dredging activities on the morphological development of the Columbia River Mouth. M.Sc. Thesis, Delft University of Technology.

Sutherland, J., Peet, A. and Soulsby, R., 2004. Evaluating the performance of morphological models. Coastal Engineering - COAST ENG, 51, 917-939.

Temitope D. Timothy Oyedotun, Arturo Ruiz-Luna & Alma G. Navarro-Hernández, 2018. Contemporary shoreline changes and consequences at a tropical coastal domain, Geology, Ecology, and Landscapes, 2(2), 104-114.

Thieler, E.R., Himmelstoss, E.A., Zichichi, J.L., and Ergul, Ayhan, 2009. Digital Shoreline Analysis System (DSAS) version 4.0 — An ArcGIS extension

for calculating shoreline change: U.S. Geological Survey Open-File Report 2008-1278. *current version 4.3

Thinh, N. and Hens, L., 2017. A Digital Shoreline Analysis System (DSAS) applied on mangrove shoreline changes along the Giao Thuy Coastal area (Nam Dinh, Vietnam) during 2005-2014. Vietnam Journal of Earth Sciences, 39, 87-96.

Thom, B.G., 1967. Mangrove ecology and deltaic geomorphology: Tabasco, Mexico. Journal of Ecology, 55(2), 301-343.

Thulsi Rao K., 2013. Biodiversity Management Plan for Coringa Wildlife Sanctuary, Andhra Pradesh 2013-2023.

Tomlinson, P.B., 1986. The botany of mangroves. Cambridge University Press, NY.

Toorman, E.A., 2001. Suspension capacity of uniform shear flows. Report HYD/ET/00/4, Hydraulics Laboratory, Katholieke Universiteit Leuven.

Tran Thi, V., Tien Thi Xuan, A., Phan Nguyen, H., Dahdouh-Guebas, F., and Koedam, N., 2014. Application of remote sensing and GIS for detection of long-term mangrove shoreline changes in Mui Ca Mau, Vietnam, Biogeosciences, 11, 3781–3795.

Valchev, N., P. Eftimova, and Andreeva N., 2018. Implementation and validation of a multi-domain coastal hazard forecasting system in an open bay. Coastal Engineering, 134, 212-228.

Van der Werf, J., Van Oyen, T., De Maerschalck, B., Nnafie, A., Van Rooijen, A., Taal, M., 2015. Modeling the morphodynamics of the mouth of the Scheldt estuary. In E-proceedings of the 36th IAHRWorld Congress, The Hague, 80–86.

Van Rijn, L.C., 2008. Principles of fluid flow and surface waves in rivers, estuaries, seas and oceans. Aqua Publications, The Netherlands.

Vriend, de H.J., Zyserman, J., Nicholson, J., Roelvink, J.A., Pechon, P. and Southgate, H.N., 1993. Medium-term 2DH coastal area modelling. Coastal Engineering, 21, 193-224.

Watson, J.G., 1928. Mangrove forests of the Malay Peninsula. Malayan Forest Records No. 6. Federated Malay States Government, Kuala Lumpur.

Williams, J. and Esteves, L., 2017. Guidance on Setup, Calibration, and Validation of Hydrodynamic, Wave, and Sediment Models for Shelf Seas and Estuaries. Advances in Civil Engineering, 1-25.

Wilmink, R.J.A., 2015. Accelerated Morphological Modelling: A schematized case study into the medium- and long-term morphological acceleration techniques Morfac and Mormerge. M.Sc. Thesis. Arcadis and University of Twente.

Wilton, K. and Saintilan, N., 2000. Protocols for mangrove and saltmarsh habitat mapping, Unit Technical Report 2000/01, Coastal Wetlands Unit, Australian Catholic University, Australia.

Winterwerp, J. C., and van Kesteren W. G. M. (2004). Introduction to the physics of cohesive sediment in the marine environment.

Wolanski, E., 1995. Transport of sediment in mangrove swamps. Hydrobiologia, 295, 31–42.

Wolanski, E., Mazda, Y., Ridd, P., 1992. Mangrove hydrodynamics. In: Robertson, A.I., Alongi, D.M. (Eds.), Tropical Mangrove Ecosystems. Coastal and Estuarine Studies no. 41. American Geophysical Union, 329.

Woodroffe, C.D., 1982. Geomorphology and development of mangrove swamps, Grand Cayman Island, West Indies. Bulletin of Marine Science, 32(2), 381-398.

Woodroffe, C.D., 1995. Response of tide-dominated mangrove shorelines in Northern Australia to anticipated sea-level rise. Earth Surface Processes and Landforms, 20, 65–85.

Zeinali, S., Talebbydokhti, N., Jandaghian, M. and Tavvakol, S., 2014. Coastal morph dynamics and long-term morphological modeling. Research Journal of Environmental and Earth Sciences, 6(11), 493-499.

PAPERS PUBLISHED

International Journal:

1.)Garima Sharma & K.V.K.R.K. Patnaik (2020): Assessment of Coringa Mangrove shoreline migration using geospatial techniques, Journal of Operational Oceanography.
DOI: 10.1080/1755876X.2020.1840245

International Conference:

1.)Garima Sharma, K.M. Sivakholundu & K.V.K.R.K. Patnaik (2019): Predicting Long-Term Morphological Development of Kakinada Bay. Proceedings of 1st Maritime International Conference (MARINCO 2019)

Indian Journal:

1.)Garima Sharma, K.M. Sivakholundu & K.V.K.R.K. Patnaik (2020): Long-Term Morphodynamic Evolution of Kakinada Bay using Upscaling Methods. Marine Engineers Review. Volume 14.

APPENDICES

Table 1. R^2 value for various flow model calibration parameter values

S.No.	Chezy Coefficient (Horizontal)	Chezy Coefficient (Vertical)	Eddy Diffusivity	Eddy Viscosity	R^2 Water Level	R^2 Current Velocity
1	67	67	0.5	0.5	0.5489	0.612
2	71	71	0.8	0.8	0.9658	0.6697
3	72	71	0.8	0.8	0.9397	0.772
4	74	71	1	0.8	0.9359	0.617
5	74	71	1	1	0.9452	0.675
6	74	74	1	1	0.9422	0.7028

Table 2. Delft3D WAVE (SWAN) Model Parameters

Wave Model Parameters	Range	Default	Best Run Parameter
Wave generation model			3rd generation SWAN
Rate of dissipation due depth induced breaking (Battjes & Janssen, 1978)			1
Breaking Parameter Gamma (Hb/db)	0.55-1.2	0.73	0.73
Breaking Parameter Alpha	0.1-10	1	1
Collin's bottom friction coefficient			0.016
JONSWAP Friction Value ($m^2.s^{-2}$)	-	0.067	0.067

Triads-Energy Transfer from low to high frequencies in shallow water	-	Off	On
Dissipation due to white-capping			Komen et al, 1994
Diffraction Smoothing Coefficient	0-1	0.2	0.2
Diffraction Smoothing Steps	1-999	5	5
Wind Growth	-	On	On
JONSWAP Peak Enhancement Factor	-	3.3	3.3
Wave Induced Set Up			Yes
Refraction			Yes

Table 3. Delft 3D FLOW Model Definitions

Model Definitions	**Default Value**	**Model Value**
Number of Layers	1	1
Horizontal Eddy Viscosity	1	1
Vertical Eddy Viscosity	1	1
Model for 3D Turbulence	k-epsilon	
Gravity ($m.s^{-2}$)	9.81	9.81
Water Density ($Kg.m^{-3}$)	1025	1025
Chezy Coefficient (Roughness value)	65	74 in x direction, 71 in y direction

Table 4. Morphological Model Parameter Settings

Parameter	Description	Value
FLOW		
Grid cell size		10-50 m
Δt	Computational time step	30 seconds
$TPeriod$	Simulation period	15 Days
C	Chézy roughness coefficient	U=74; V=71 √m/s
$\vec{\tau}b,2D$	Stress formulation	Fredsøe (1984)
lrov	Slip condition	Free
vv	Horizontal eddy viscosity	1 $m^2.s^{-1}$
vd	Horizontal eddy diffusivity	1 $m^2.s^{-1}$
MOR		
$TSPIN$	Spin up time	720 minutes
$fMORFAC$	Morphological scale factor	30
SED	Type of sediment	Cohesive
$c0$	Initial sediment concentration	0.02 $kg.m^{-3}$
$CREF$	Density for hindered settling	1600 $kg.m^{-3}$
ρs	Specific density	2650 $kg.m^{-3}$
$CDryB$	Dry bed density	500 $kg.m^{-3}$
ws	Sediment settling velocity	0.1 $mm.s^{-1}$
τe	Critical bed sheer stress for erosion	0.5 $N.m^{-2}$
τd	Critical bed sheer stress for deposition	1000 $N.m^{-2}$
M	Erosion parameter	0.002$Kg.m^{-2}.s^{-1}$
Δzs	Initial sediment layer thickness	0.2 m
Effect of sediment on	No	

density

Table 5. Schematized Wave Classes using Energy Flux Method

Wave Classes	Rep Wave Height (m)	Rep Wave Period (s)	Rep Wave Direction (deg)	Pc Duration (Days)	Morfac
1	0.66	4.3	133	18	1.45
2	0.80	3.7	148	30	2.41
3	0.81	4.3	171	24	1.93
4	0.95	4.4	120	25	2.01
5	1.08	4.5	172	25	2.01
6	1.09	3.8	164	19	1.53
7	1.10	4.4	114	7	0.56
8	1.29	4.6	174	7	0.56
9	1.60	4.4	139	1	0.08

Table 6. Representative Wave Classes for South-West Monsoon (March-October) using Energy Flux Method

March-October	Rep Wave Height (m)	Rep Wave Period (s)	Rep Wave Direction (deg)	Pc Duration (Days)	Morfac
1	0.70	4.5	151	16	1.28
2	1.08	4.9	151	25	2
3	0.91	4.3	173	14	1.12
4	1.26	4.4	175	12	0.96
5	1.03	3.8	193	2	0.16

Table 7. Representative Wave Classes for North-East Monsoon (November-February) using Energy Flux Method

November-February	Rep Wave Height (m)	Rep Wave Period (s)	Rep Wave Direction (deg)	Pc Duration (Days)	Morfac
1	0.87	3.5	86	11	0.88
2	1.57	4.4	88	7	0.56
3	0.58	4.1	132	10	0.8
4	1.02	4.3	117	3	0.24

Table 8. Schematized Wave Classes using Potential Sediment Transport Approach

Wave Classes	Rep Wave Height (m)	Rep Wave Period (s)	Rep Wave Direction (deg)	Pc Duration (Days)	Morfac
1	0.87	4.0	121	24	1.45
2	0.80	3.7	148	30	2.41
3	0.81	4.3	170	24	1.93
4	0.95	4.4	120	25	2.01
5	1.08	4.5	172	25	2.01
6	1.09	3.8	164	19	1.53
7	1.10	4.4	114	7	0.56
8	1.29	4.6	174	7	0.56
9	1.60	4.4	139	1	0.08

Table 9. Representative Wave Classes for South-West Monsoon (March-October) using Potential Sediment Transport Approach

March-October	Rep Wave Height (m)	Rep Wave Period (s)	Rep Wave Direction (deg)	Pc Duration (Days)	Morfac
1	0.99	3.8	97	16	7.73
2	0.74	4.5	134	14	6.76
3	0.96	4.5	168	17	8.21
4	0.99	3.7	193	16	7.73
5	1.03	3.2	234	17	8.21

Table 10. Representative Wave Classes for North-East Monsoon (November-February) using Potential Sediment Transport Approach

November-February	Rep Wave Height (m)	Rep Wave Period (s)	Rep Wave Direction (deg)	Pc Duration (Days)	Morfac
1	1.063	3.8	88	22	10.63
2	0.76	3.8	115	17	8.21
3	0.66	4.2	128	17	8.21
4	0.68	3.2	172	17	8.21

Table 11. Sample R Calculation for Morfac Values

S.No.	Morfac	R^2
1	MOR 10	0.8400
2	MOR 20	0.8612
3	MOR 30	0.9081
4	MOR 40	0.8344

The table 11 shows the R^2 value for shoreline distance obtained for the transects casted from each morfac value compared with the bruteforce simulation with no morfac.

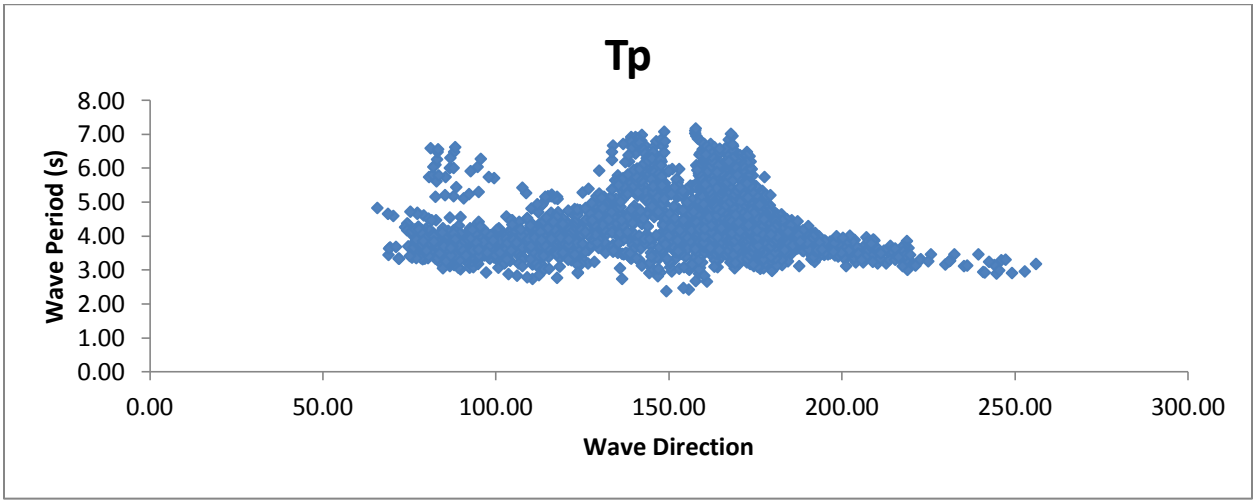

Figure 1. Scatter Plot of Incoming Wave Direction versus Wave Period with the wave data time series for year 2011 to be schematized.

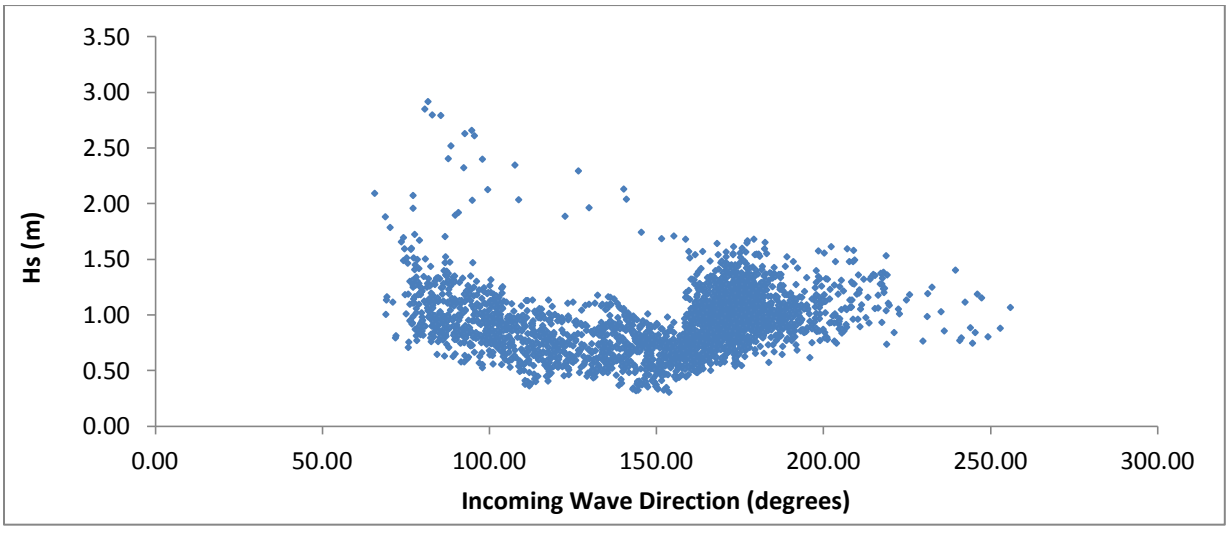

Figure 2. Scatter plot of Incoming Wave Direction versus Significant Wave Height with the wave data time series for year 2011 to be schematized.